

DEVELOPMENT OF 3D METAL CATALYSTS FOR REDOX REACTIONS

Cumulative Dissertation

to acquire the academic degree
doctor rerum naturalium (Dr. rer. nat.)
of the Faculty of Mathematics and Natural Sciences
at the University of Rostock

Submitted by David Leonard, born on 18th November 1995 in Rutherglen, UK
Rostock, 16.08.2021

The present work was accomplished at the Leibniz Institute for Catalysis e. V. at the University of Rostock, at the chair for Applied Catalysis in the work group of Prof Dr Matthias Beller during the period from August 2018 to August 2021.

Reviewer #1: Prof Dr Matthias Beller
Leibniz-Institut für Katalyse e. V.
Reviewer #2: Prof Dr Shoubhik Das
University of Antwerp

David Leonard: *Development of 3d Metal Catalysts for Redox Reactions*,
Cumulative Dissertation, *doctor rerum naturalium* (Dr. rer. nat.)

Year of submission to the faculty: 2021
Year of oral defense: 2021

STATEMENT OF AUTHORSHIP

I hereby affirm that I have written the present work by myself without outside assistance. No other resources were utilised than stated. All references as well as verbatim extracts were quoted and all sources of information were specifically acknowledged.

Ich versichere hiermit an Eides statt, dass ich die vorliegende Arbeit selbstständig angefertigt und ohne fremde Hilfe verfasst habe. Dazu habe ich keine außer den von mir angegebenen Hilfsmitteln und Quellen verwendet und die den benutzten Werken inhaltlich und wörtlich entnommenen Stellen habe ich als solche kenntlich gemacht.

Rostock, August 2021

David Leonard

Dedicated to the loving memory of my grandfather,
George Laursen Docharty

1930 – 2020

PUBLICATIONS

Some ideas and figures have appeared previously in the following publications:

1. Li, W.; Liu, W.; Leonard, D. K.; Rabeah, J.; Brückner, A.; Junge, K.; Beller, M. Practical Catalytic Cleavage of C(sp³)-C(sp³) Bonds in Amines. *Angew. Chem., Int. Ed.* **2019**, *58*, 10693–10697.
2. Leonard, D. K.; Li, W.; Junge, K.; Beller, M. Improved Bimetallic Cobalt–Manganese Catalysts for Selective Oxidative Cleavage of Morpholine Derivatives. *ACS Catal.* **2019**, *9*, 11125–11129.
3. Leonard, D. K.; Li, W.; Rockstroh, N.; Junge, K.; Beller, M. Aerobic Site-Selective C(sp³)-C(sp³) Bond Cleavage in *N*-Heterocycles. *Catal. Commun.* **2021**, *157*, 106333.
4. Leonard, D. K.; Ryabchuk, P.; Junge, K.; Beller, M. A Convenient and Stable Heterogeneous Nickel Catalyst for Hydrodehalogenation of Aryl Halides Using Molecular Hydrogen. *Submitted Manuscript* **2021**.

ACKNOWLEDGEMENTS

First, I would like to thank my supervisor Prof Dr Matthias Beller for allowing me to join his research group where I was given the wonderful opportunity to indulge in my own scientific curiosities. I owe you many thanks for your expert guidance and for welcoming me into your outstanding institute. Your kindness, good humour, and far-reaching knowledge of all aspects of chemistry has made it a pleasure to be your student.

To my group leader Dr Kathrin Junge, I thank you for your encouragement, fairness, and kindness. It has been a pleasure to work in your group for the past three years.

I am indebted to the board of trustees of the *Fonds der Chemischen Industrie* for their financial support (*Kekulé-Stipendium* n. 103231).

I would like to thank my laboratory colleagues, Dr Thomas Leischner, Dr Pavel Ryabchuk, and Dr Veronica Papa, for it has been a pleasure to work closely with such talented individuals. Their sense of humour and camaraderie made coming to work consistently joyful and brilliantly entertaining.

A great deal of appreciation goes to all my other colleagues in the *Nachhaltige Redoxreaktionen* group. Thank you Dr Dario Formenti, Dr Weiping Liu, Dr Wu Li, Dr Marcel Garbe, Dr Jacob Schneekönig, Dr Peter McNeice, Dr Ruiyang Qu, Dr Svenja Budweg, Dr Julian Hervochon, Johannes Fessler, Shuxin Mao, Florian Bourriquen, Dennis Verspeek, Saskia Lange, Niklas Heinrich, Leandro Duarte de Almeida and Helen Hornke.

I also owe thanks to my brilliant colleagues Dr Reni Grauke, Dr Nils Rockstroh, Dr Alexander Léval, Dr Sergey Tin, Christoph Wulf, Thibault Tannoux, and Andrea Dell'Acqua for their friendship.

Lastly I would like to thank my family for all their support. In particular, I would like to thank my sister Sarah for her encouragement and for always looking out for me. A very special thanks goes to my parents, Morris and Lynne, whose love, kindness and generosity has been greatly appreciated, especially during my time here in Germany away from home. I cannot thank you enough for everything.

Thank you.

SUMMARY

This dissertation reports the application of diverse non-noble metal-based catalytic systems for the homogeneous oxidation of organic substrates using air, specifically in amines and *N*-heterocycles. Specifically, simple 3d metal salts have been used, in combination with *N*-ligands, to facilitate the oxidative cleavage of C(sp³)-C(sp³) bonds in a selective manner. These reactions have been studied, with the aid of spectroscopic methods, to propose plausible mechanistic pathways. We believe such deconstructive strategies can enable late-stage functionalisation of pharmaceuticals, the synthesis of drug metabolites, and may in future provide a means of biomass valorisation. Additionally, a nickel-based catalytic system for the heterogeneous hydrodehalogenation of industrially relevant substrates, including environmentally persistent fire retardants, highly toxic polybrominated diphenyl ethers (PBDE), and 1,2,4,5-tetrachlorobenzene is described.

Gegenstand der vorliegenden Dissertation ist die Anwendung verschiedener katalytischer Systeme auf Basis von Nichtedelmetallen für die homogene Oxidation organischer Substrate an Luft, insbesondere von Aminen und *N*-Heterocyclen. 3d-Metallsalze wurden in Kombination mit *N*-Liganden verwendet, um die selektive oxidative Spaltung von C(sp³)-C(sp³)-Bindungen zu erleichtern. Mit Hilfe von spektroskopischen Methoden wurden die Reaktionen auf ihre zugrundeliegenden Mechanismen untersucht. Zukünftig könnten solche dekonstruktiven Strategien eine späte Funktionalisierung von Pharmazeutika und die Synthese von Arzneimittelmetaboliten ermöglichen und ein Mittel zur Aufwertung von Biomasse sein. Darüber hinaus wird ein katalytisches System auf Nickelbasis für die heterogene Hydrodehalogenierung von industriell relevanten Substraten beschrieben, einschließlich umweltschädliche Flammenschutzmittel, hochgiftige polybromierte Diphenylether (PBDE) und 1,2,4,5-Tetrachlorbenzol.

LIST OF ABBREVIATIONS

δ	chemical shift
DDQ	2,3-dichloro-5,6-dicyano-1,4-benzoquinone
equiv	equivalents
Et	ethyl
HFIP	1,1,1,3,3,3-hexafluoropropan-2-ol
J	coupling constant
Me	methyl
NMR	nuclear magnetic resonance
ppm	parts per million
TEMPO	2,2,6,6-tetramethylpiperidinyloxy
TFA	trifluoroacetic acid
TMS	trimethylsilane

UNITS OF MEASUREMENT

The International System of Units (SI) is utilised throughout this work to measure experimental of theoretical quantities. All derived units and their expression in terms of the SI base units are given below.

quantity	unit	name	conversion to SI base units
pressure	bar	bar	$1 \text{ bar} = 10^5 \text{ Pa}$
temperature	$^{\circ}\text{C}$	degrees celsius	$T/\text{K} = T/^{\circ}\text{C} - 273.15$
volume	mL	millilitre	$1 \text{ mL} = 1 \text{ cm}^3 = 10^{-6} \text{ m}^3$

CONTENTS

1	TARGET AND MOTIVATION	1
2	INTRODUCTION	2
	2.0.1 Chemistry and Catalysis	2
	2.0.2 Homogeneous vs. Heterogeneous Catalysis	4
2.1	Copper	5
2.2	Manganese	6
2.3	Iron	7
2.4	Cobalt	7
2.5	Oxidations	9
2.6	C–C Single Bond Cleavage	10
	2.6.1 Applications	10
	2.6.2 Traditional Methods	11
	2.6.3 State-of-the-Art	12
2.7	Multivariate Optimisation	14
3	RESULTS AND DISCUSSION	17
3.1	Copper-Catalysed Cleavage of Amines	17
	3.1.1 Mechanistic Investigations	19
3.2	Improved Cobalt–Manganese Catalysts	21
	3.2.1 Reaction Scope	23
	3.2.2 Mechanistic Investigations	27
3.3	A Simple Iron Catalyst	28
3.4	Nickel-Catalysed Hydrodehalogenation	32
4	SUMMARY AND OUTLOOK	40
5	SELECTED PUBLICATIONS	41
5.1	Practical Catalytic Cleavage of C(sp ³)–C(sp ³) Bonds in Amines	42
5.2	Improved Bimetallic Cobalt–Manganese Catalysts for Selective Oxidative Cleavage of Morpholine Derivatives	48
5.3	Aerobic Iron-Catalyzed Site-Selective C(sp ³)–C(sp ³) Bond Cleavage in <i>N</i> -Heterocycles	54
5.4	A Convenient and Stable Heterogeneous Nickel Catalyst for Hydrodehalogenation of Aryl Halides Using Molecular Hydrogen	60
A	APPENDIX: EXPERIMENTAL SECTION	69
A.1	General experimental details	69
A.2	Synthetic Procedures Used in Section 5.1	70
	A.2.1 Synthesis of Morpholines and Piperazines	70
	A.2.2 Synthesis of Amines	70
	A.2.3 Copper-Catalysed Oxidations	71
A.3	Synthetic Procedures Used in Section 5.2	71

A.3.1	Cobalt–Manganese-Catalysed Oxidations	72
A.4	Synthetic Procedures Used in Section 5.3	72
A.4.1	Iron-Catalysed Oxidations	72
A.5	Synthetic Procedures Used in Section 5.4	73
A.5.1	Synthesis of the Ni-Phen@TiO ₂ -800 Catalyst	73
BIBLIOGRAPHY		75

LIST OF FIGURES

Figure 1	Trends in human population and nitrogen use throughout the twentieth century. Source: <i>Nat. Geosci.</i> ^[9]	4
Figure 2	The Mutanda Mine in the DRC. Source: <i>Bloomberg</i>	8
Figure 3	OFAT study: two sequential studies, first exploring T, then <i>p</i>	15
Figure 4	Full-factorial study: one study exploring T and <i>p</i> at the same time.	15
Figure 5	2^2 design.	16
Figure 6	2^3 design.	16
Figure 7	2^{3-1} design.	16
Figure 8	C–C bond cleavage in natural product derivatives and drugs.	20
Figure 9	STEM HAADF image of the precipitate formed during the reaction. Iron oxide particles are visible (see the bright spots).	33
Figure 10	STEM ADF image of the precipitate formed during the reaction. Iron oxide particles are visible (see the dark spots).	33
Figure 11	Contour plots illustrating the interactions between temperature and catalyst loading, and base and catalyst loading.	35

LIST OF SCHEMES

Scheme 1	Rare examples of C–C oxidative additions.	11
Scheme 2	(i) Criegee and (ii) Malaprade oxidations.	12
Scheme 3	Allylic C(sp ³)–C(sp ³) cleavage using azide/DDQ/TFA (Jiao group 2017). . .	12
Scheme 4	Deconstructive fluorination using SelectFluor.	13
Scheme 5	C(sp ³)–C(sp ³) cleavage using NaNO ₂ /HCl (Liu group 2021).	13
Scheme 6	Photoinduced C(sp ³)–C(sp ³) cleavage (Wei group 2021).	14
Scheme 7	Proposed mechanism for [Cu]-catalysed oxidative cleavage of C(sp ³)–C(sp ³) bonds.	22
Scheme 8	Late stage functionalisation of linezolid.	27
Scheme 9	Putative intermediates detected by GC-MS.	28
Scheme 10	HDH of tetrabromobisphenol A (76a), a PBDE (77a), 1,2,4,5-tetrachlorobenzene (78a), and atrazine (79a).	38

LIST OF TABLES

Table 1	General Differences Between Homogeneous and Heterogeneous Catalysts	5
Table 2	Transition Metal Salts for C–C Bond Cleavage in Tri- <i>n</i> -Butylamine 1a^a .	18
Table 3	C–C Bond Cleavage in Amines Using Cu ^a	19
Table 4	Metal Catalysts for C–C Bond Cleavage in 25a^a	23
Table 5	Co and Mn Catalysts for C–C Bond Cleavage in 25a^a	24
Table 6	Influence of <i>N</i> -Ligands on the Standard Reaction ^a	25
Table 7	Bond Cleavage in Morpholines Using Co–Mn ^a	26
Table 8	Selective Cleavage of a C–C Bond in 25a Using Fe Precursors ^a	29
Table 9	Factors Investigated Using DoE for Piperazine Cleavage	29
Table 10	DoE Results for Cleavage of Piperazine 41a^a	30
Table 11	Primary DoE Screen: ANOVA	31
Table 12	Bond Cleavage Using Fe ^a	32
Table 13	DoE Results for HDH of Aryl Bromide 46a^a	34
Table 14	HDH in Aryl Bromides ^a	36
Table 15	HDH in Aryl Chlorides ^a	37
Table 16	Deuteration of 80a^a	39

TARGET AND MOTIVATION

The cleavage of C(sp³)–C(sp³) is arguably one of the most challenging transformations in chemistry, and doing so is highly difficult to achieve in a mild and selective manner that is compatible with organic synthetic strategies. C–C single bond cleavage reactions are of the utmost importance in the petrochemical industry where crude oil is *cracked* into an assortment of smaller hydrocarbon fractions for further processing and for maximising of value. Whilst these reactions are carried out routinely in the industrial sector using heterogeneous catalysts, the low selectivity and harsh reaction conditions necessitated (>300°C) renders this an unsuitable solution for the synthesis of a diverse range of functionalised organic compounds bearing sensitive chemical motifs.

Homogeneous catalysts generally offer the attractive properties of being both highly active and highly selective (cf. heterogeneous catalysts) whilst allowing more potential for catalyst *tuning* and greater mechanistic insight. In contrast to heterogeneous catalysts, where reactions take place on non-ideal surfaces, homogeneous catalysts typically exist in solution as single well-defined molecular species with only one available reaction site, resulting in fewer undesired byproducts.

Currently there are very few literature examples of selective cleavage of C(sp³)–C(sp³) bonds under mild reaction conditions. Success in this area may provide the potential for: (i) the synthesis of drug metabolites to enable more rapid selection of viable clinical candidates; (ii) improved energy efficiency and selectivity of fossil fuel cracking; (iii) providing renewable chemical feedstocks via the valorisation of biomass. In this thesis, different protocols for the activation of C(sp³)–C(sp³) bonds are presented. In each case, 3d metals are used as catalysts facilitating the oxidation processes, and molecular oxygen—air, in fact—is used as the sole oxidant.

Aside from that which is outlined above, other topics evolved which I contributed to. Also included in this thesis, therefore, is the development of a nickel-based heterogeneous catalyst for reductive dehalogenation of aryl halides.

INTRODUCTION

2.0.1 *Chemistry and Catalysis*

The natural science of chemistry owes a great deal its origin of *alchemy*—the ancient practice largely dedicated to the transmutation of matter (namely that of lead to gold), founded on the mystical beliefs in the Philosopher’s Stone or the Universal Elixir. Many alchemical methods—including also the knowledge acquired from the purification of metals extracted from mining; the preparation of herb-based medicinal remedies; as well as the creation of jewelery—have led to many of the practical techniques used in today’s chemistry labs. In fact, it was not until very recently, around the beginning of the seventeenth century, that chemistry began to emerge as a scientific discipline in the modern sense.^[1]

With growing concerns regarding anthropogenic climate change, environmental pollution and the rapid depletion of fossil resources we as chemists have persuasive incentives to ensure that chemistry is carried out efficiently, sustainably and in a way that minimises the output of undesirable by-products. To achieve these goals, catalysis remains a key technology by reducing the waste output and energy required for chemical reactions to occur, whilst enabling reactions which would not be possible in their absence, and increasing product selectivity and yield. Thus it is not surprising that catalysis is considered to be one of the twelve principles of green chemistry.^[2]

The power of (bio)catalysis has been recognised since ancient times and has in fact been utilised for the development and prosperity of mankind at least as far back as the Neolithic Revolution, ca. 12 500 years ago. This transitional period marked a worldwide shift in many human cultures away from lifestyles revolving around hunting and gathering towards agriculture and settlement, which is more akin to modern life. This cultural change led to the development of farming practices and the preservation of food supplies using microbes and their biological catalysts, known as enzymes.^[3]

The earliest evidence of enzyme-assisted brewing can be traced back to the Neolithic village of Jiahu in China around 7500 BC, where investigators found early evidence of alcoholic beverages.^[4] Furthermore, the Egyptians—who were well aware of early enzyme-assisted brewing techniques—also utilised microorganisms and malt to produce bread as far back as 2000–1200 BC.^[5]

Of course, mankind hasn’t limited its enzyme technologies to just bread and beer. Material applications are indispensable and enzymes have proven advantageous here also. Starting from pigeon and/or dog dung it is possible to use the microbacterial enzymes in the softening of leather. As early as 7000–3300 BC this was exploited for leather processing for all manner of tools including bags, boats, and shoes.^[6]

It was much later, in the beginning of the twentieth century, that catalysis as a scientific field was established. Nobel prizes have highlighted many of the most influential discoveries in this era. Friedrich Wilhelm Ostwald, who received a Nobel prize in 1907, was the first to identify the role of catalysts as accelerants of reactions without themselves being consumed in the process, as well as defining the principles of chemical equilibria. Paul Sabatier subsequently won the Nobel prize in 1912 for demonstrating the hydrogenation of organic compounds using fine powdered metals—a synthetic method which remains highly relevant in today's synthetic toolbox.^[7]

Undoubtedly, one of the greatest success stories in catalysis is the development of artificial nitrogen fixation, resulting from one of the world's most fruitful partnerships between the German chemists Fritz Haber and Carl Bosch. Once Haber demonstrated the catalytic generation of ammonia from nitrogen and hydrogen on benchtop scale, Bosch, who worked at *Badische Anilin- und Soda-Fabrik* (BASF), was instrumental in developing high pressure reaction vessels and scaling up the reaction to a viable industrial process. After rigorous, state-of-the-art experimentation, an iron catalyst developed by Mittasch,^[8] was successfully implemented for the generation of ammonia. The process, known now as the Haber–Bosch process, has facilitated the production of inorganic fertiliser and we no longer rely solely on *Rhizobium* bacteria for biofixation of the nitrogen our bodies need to synthesise vital proteins. As Figure 1 indicates,^[9] this advancement led to a population boom in the twentieth century from ca. 1.6 billion in the year 1900, to six billion in 1999.^[10] In fact, some estimations indicate that more than half of the world's agricultural yield relies on the Haber–Bosch process, which continues to feed the world's growing population. The scientific community recognised the advancement by bestowing two separate Nobel prizes in 1918 and 1931, to Haber and Bosch (along with F. Bergius), respectively.

In 1963, the Nobel prize in chemistry was awarded to Karl Ziegler and Giulio Natta for their chemical and technological discoveries which enable high polymers to be generated from 1-alkene monomers. A plethora of highly versatile Ziegler–Natta catalysts have been used since the inception of the so-called first-generation in the early 1950s.^[11] The industrial value of these findings has been tremendous and has led to the generation of some of the largest volume commodity chemicals on the planet.

The 1970s saw the development of palladium-mediated cross-coupling reactions and in 2010 the Nobel prize in chemistry was shared between Richard F. Heck, Ei-Ichi Negishi, and Akira Suzuki for *palladium-catalyzed cross couplings in organic synthesis*.^[12] Nowadays, the Suzuki–Miyaura reaction is the gold standard in biaryl coupling using homogeneous catalysis, and it has become ubiquitous in both academia and industry.

Over time the very definition of a catalyst has evolved as our understanding of them has grown, but nowadays a catalyst is considered: *a substance that increases the rate of a reaction without modifying the overall standard Gibbs energy change in the reaction*.^[13]

Catalysts by their very nature reduce the activation barrier (E_a) required for a reaction to occur and this is achieved by providing an alternative mechanism for the reactants to follow. Nowadays ca. 85% of all industrial chemical processes involve at least one catalytic step.

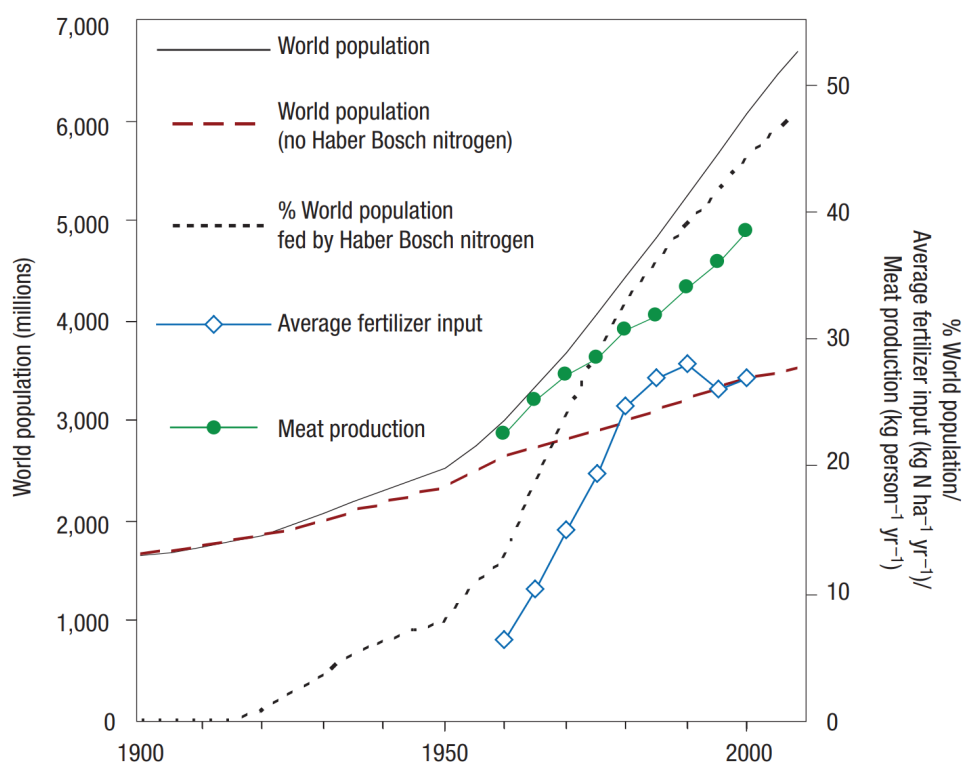


Figure 1: Trends in human population and nitrogen use throughout the twentieth century. Source: *Nat. Geosci.*^[9]

This is a reflection of their abilities in accelerating transformations, promoting selectivity, and reducing waste output and energy consumption. For many decades rare and precious second and third row transition metals have been at the forefront of catalysis, today's state-of-the-art catalysts are increasingly dependent on the talents of Earth-abundant 3d-metals.^[14]

2.0.2 Homogeneous vs. Heterogeneous Catalysis

Catalysts can be divided into two main categories: *homogeneous* catalysts and *heterogeneous* catalysts. The main distinction is the relative physical states of the catalyst and the reaction mixture; in homogeneous catalysis the catalyst is in the same phase as the rest of the reaction mixture, whereas in heterogeneous catalysis the catalyst is in a different phase from the rest of the reaction mixture.

Both classes of catalysts have their advantages and disadvantages (summarised in Table 1).

Heterogeneous catalysts are more widely utilised in the chemical industry than homogeneous catalysts. One of the main reasons for this is the ease of separation of the catalyst (normally a solid) from reaction mixtures.

Table 1: General Differences Between Homogeneous and Heterogeneous Catalysts

homogeneous	heterogeneous
well-defined active site	many possible active sites
high selectivity	low selectivity
difficult separation	facile separation
react at low temperature	react at high temperature

During the last decade, single atom-catalysis (SAC) has emerged as a new frontier in the field of catalysis by blending together the strengths of homogeneous and heterogeneous catalysts.^[15] Both categories of catalysts often feature metal centres at their active sites but in homogeneous molecular catalysis the metal utilisation can be as high as 100%. Heterogeneous catalysts, on the other hand, rely on only a fraction of the metal centres which reside on the surface of the catalyst, and thus, depending on the surface area of the solid support, the metal utilisation can be orders of magnitude lower than homogeneous catalysts. SAC attempts to bridge this gap between heterogeneous and homogeneous catalysis by atomically dispersing metals onto the surface of solid supports.^[16] In a nutshell, SAC attempts to attain the isolated mono-nuclear active sites and high metal utilisation of homogeneous catalysts on a robust solid support which is highly practical and can be readily separated from reaction mixtures.^[16-21]

The field of biocatalysis is often considered to lie outwith the categories of homogeneous and heterogeneous catalysis. Biocatalysis refers to the utilisation of enzymes and microbes to perform synthetic chemical reactions. With twenty-first century technologies, including directed evolution and protein engineering, it is now possible to tailor enzyme properties to synthesise non-natural products.^[22-24] Notably, in 2010, a collaboration between Merck and Codexis showcased the talents of enzymes by successfully synthesising sitagliptin (an anti-diabetic drug) in fewer synthetic steps and with higher yield and optical purity than a previously implemented chemocatalytic process.^[25]

In the following sections, selected catalyst metals and oxidation reactions are briefly discussed, which are highly relevant for this thesis.

2.1 COPPER

Copper, with the symbol Cu and atomic number 29 is positioned in the 3d-block of the periodic table between nickel and zinc. It is a naturally occurring trace element (i. e. it comprises $< 0.1 \text{ mg kg}^{-1}$ of the earth's crust) found in rocks and minerals and plays important biochemical roles as an essential micronutrient and for facilitating metabolic processes in both prokaryotes and eukaryotes.^[26]

Copper's capabilities in redox catalysis are well documented and widely utilised in nature in the metal centres of at least 25 biological enzymes. Myriad oxidation processes are facilitated by copper-containing enzymes, including: cytochrome c oxidase, superoxide dismutase, amine oxidase, lysyl oxidase, dopamine β -hydroxylase, peptidylglycine α -amidating monooxygenase, tyrosinase, galactose oxidase, hemocyanin, ceruloplasmin, laccase, and ascorbate oxidase. What's more, each of these enzymes relies on molecular oxygen as the oxidant.^[27]

Like iron, copper plays a crucial role in facilitating oxygen transport in animals in the form of haemocyanin. This is strikingly apparent in horseshoe crabs which have a distinctive blue colouration in their blood on account of the Cu^{2+} metal centre in haemocyanin's oxygenated form.

2.2 MANGANESE

Manganese, with the symbol Mn and atomic number 25, is positioned in the 3d-block of the periodic table between chromium and iron. It is the twelfth most abundant element in the Earth's crust,^[28] and it's known for its remarkable ability to exist in many oxidation states which range from -3 to $+7$, of which $+2$, $+3$, $+4$, $+6$, and $+7$ are most common.

Mn was not recognised as an element until 1774 when German-Swedish chemist, Carl Wilhelm Scheele, analysed pyrolusite (MnO_2) and realised that the ore and its extracts contained a previously undiscovered element! However, it wasn't until Scheele supplied Johan Gottlieb Gahn, a Swedish chemist and metallurgist, with pyrolusite that elemental manganese was first extracted later that year.^[29]

Despite appearing silver-grey in its pure metallic form, given its propensity towards oxidation, it's found in Nature in oxidised forms, such as the ores *pyrolusite*, *romanechite*, *manganite*, *hausmannite*, and *rhodochrosite*.

Mn is an element essential for all life on Earth and it takes an active role in the metabolism of amino acids, lipids, proteins, and carbohydrates. In fact it's encountered in myriad animal systems, including those responsible for immunity, reproduction, blood sugar regulation, and bone growth.^[30]

Plants also rely on Mn to facilitate photosynthesis—the process which generates the very oxygen we breathe—by forming the metalloenzyme core within the chloroplasts.^[30]

Despite its ubiquity in terrestrial life, some guidance regarding limits of consumption of Mn are given by the U. S. National Research Council (NRC). It has provided an *estimated safe and adequate dietary intake* (ESADDI), which recommends adults consume between 2–5 mg day^{-1} of Mn.^[30]

In fact, overexposure to Mn can be highly damaging towards human health. Manganism (Mn poisoning) was first observed in 1837 by James Couper, who documented the neurological damage of five Scottish men who were suffering after grinding manganese dioxide. Chronic exposure to Mn only proliferated thereafter as Mn became increasingly ubiquitous

in the steel alloy industry. Fortunately, exposure to the levels of Mn detailed by Couper is rare. Nevertheless, concerns regarding its impact on human health are valid.^[28]

For a comprehensive peer-reviewed toxicological overview, see the U.S. Agency for Toxic Substances and Disease Registry's 2012 report.^[31] Therein the authors quote *adequate intakes* of 2.3 mg day^{-1} and 1.8 mg day^{-1} for men and women, respectively, based on data sourced from the U.S. Institute of Medicine Food and Nutrition Board.^[32]

2.3 IRON

Iron, with the symbol Fe and atomic number 26 is positioned in the 3d-block of the periodic table between manganese and cobalt. Despite being the most abundant element on Earth (by mass), it constitutes just ca. 5% of the Earth's crust, making it the fourth most abundant element therein.^[33]

Metallic iron is rarely found in the earth's crust, occurring almost always in an oxidised form, and thus mankind has been extracting Fe from ores as far back as ca. 1200 BC. Oxides and carbonates, such as *magnetite* (Fe_3O_4), *hematite* (Fe_2O_3) and *siderite* (FeCO_3), constitute the most common ores of iron. Besides those, are sulfur- and silicate-based ores, including *pyrite* (FeS_2) and *silicate perovskite* (FeSiO).^[33]

Biologically speaking, iron is an essential element for much of the animal life on Earth, playing an important role in the blood of most vertebrates. It binds readily with porphyrin-derived ligands to form, most notably, the oxygen-transport metalloproteins haemoglobin and myoglobin.

Iron is ferromagnetic, and has a Curie point (the temperature at which certain magnetic materials undergo a sharp change in their magnetic properties) of 768°C , at which point it undergoes an endothermic transformation to its paramagnetic form.^[33] From the perspective of catalysis, iron has properties which make it a distinguished adversary in the field of catalysis as it has a wide breadth of formal oxidation states which range from -2 to $+6$.^[34]

Unsurprisingly, iron has been used extensively in organometallic chemistry and catalysis. Famously it was utilised by German chemist, Peter Pauson, and his student, Thomas J. Kealy, to create *ferrocene*—the first known sandwich complex. Regrettably, both failed to identify the correct structure of the complex, and it wasn't until 1952 that the *Journal of the American Chemical Society* and *Zeitschrift für Naturforschung B* published reports from G. Wilkinson, M. Rosenblum, M. C. Whiting, R. B. Woodward, and E. O. Fischer who collectively deduced the correct η^5 hapticity and recognised the aromatic properties of the iron metallocene.^[35-37]

2.4 COBALT

Cobalt, with the symbol Co and atomic number 27, is positioned in the 3d-block of the periodic table between iron and nickel. It derived its name in medieval times from the German word *Kobold*, meaning Goblin, due to its resemblance to the more sought-after silver-copper



Figure 2: The Mutanda Mine in the DRC. Source: *Bloomberg*.

ores mined in this era, but wasn't recognised as a discrete element until 1735 by Swedish chemist Georg Brand.

Cobalt has a d^7 electron configuration and readily achieves formal oxidation states ranging from -1 to $+3$. In catalytic transformations it has a clear tendency towards the $+1/+3$ oxidation states, much like its noble neighbours, rhodium and iridium.^[14]

The demand for cobalt is intense in today's technological society as consumers rely increasingly on devices integrating rechargeable batteries, including mobile phones, laptops, and increasingly, electric vehicles.^[38]

The copper–cobalt mines in the Central Africa Copperbelt in the Democratic Republic of the Congo (DRC) (such as the much-publicised Mutanda Mine, shown in figure 2) and Zambia account for more than two thirds of the world's cobalt production, much of which is obtained as a by-product of copper and nickel extraction. Cobalt is not found naturally in its elemental form due to the presence of oxygen in the Earth's atmosphere but instead occurs in several minerals. Cobalt arsenides (ca. 25%), laterites (ca. 25%) and sulfides are particularly common but it can also be extracted from *heterogenite* ($\text{CoO}(\text{OH})$) and *sphero-cobaltite* (CoCO_3).^[38, 39]

In biological systems, cobalt is an essential trace element, most notably as an integral component in all four forms of vitamin B_{12} . Despite playing far fewer roles of a biological nature, compared to an element like iron, cobaltoproteins are known to facilitate the metabolism of nitriles, the growth of blood cells, and even tissue repair.^[40]

Cobalt has played an important role in homogeneous catalysis as far back as the 1930s, when the German chemist, Otto Roelen, developed the world's first industrial hydroformylation process (the *oxo synthesis*) at Ruhrchemie.^[14]

Cobalt is also particularly well regarded for successful implementation in the famous Fischer–Tropsch process—which converts syngas or watergas into liquid hydrocarbons—relies almost universally on heterogeneous cobalt as the chief catalyst metal and has done

so since its inception in 1925. Besides this, presently there are endeavours to further capitalise on the catalytic talents of cobalt for water splitting and CO₂ reduction.^[41, 42]

2.5 OXIDATIONS

Molecular oxygen (O₂) is an attractive oxidant for many chemical reactions for several reasons.^[43] In fine chemical production settings, however, oxidations are often avoided since they are associated with intrinsic safety problems, use of toxic metals, halogenated solvents, undesired byproducts and specific infrastructure requirements. Therefore, process chemists are severely limited by their choice of possible reagents which must be obtained already in the necessary (or higher) oxidation level. From the perspective of atom economy, molecular oxygen is ideal, especially given its advantage towards waste minimisation. There are two chief drawbacks to the adoption of aerobic oxidations in large scale processes, most notably in the pharmaceutical industry: (i) using organic solvents in the presence of oxygen poses a risk to safety, and (ii) there is a lack of efficient catalysts with satisfactory activities and selectivities for such transformations.^[44]

Nitrous oxide (N₂O) gas is another attractive oxidant these days. Whereas oxidising with O₂ gas may be consumed in a reaction by incorporation into the substrate, N₂O gas has the advantage of being itself reduced, forming new—and very stable—N₂ gas molecules. Clearly a real benefit can be had over O₂ when it comes to achieving a favourable reaction entropy and providing a $-\Delta G$ (negative Gibbs free energy change) for any given oxidation.

In pharmaceutical synthesis, organic solvents are often necessary, particularly for ensuring complete solvation of reagents and catalysts, etc. Combining fuel/oxidiser mixtures under heating and increased pressure presents an obvious risk of ignition which is challenging to alleviate.^[45] Whilst there have been industry-sponsored studies on the flammability of organic solvent vapours,^[46, 47] there is a distinct lack of data on the safe operation of aerobic oxidations at temperatures and pressures conducive for pharmaceutical processes.^[44]

Nevertheless, the Amoco process (named after the now-defunct **American Oil Company**) represents a catalytic success story for aerobic oxidation chemistry and catalysis. The process is the predominant method of generating terephthalic acid, which is an industrially significant precursor for condensation polymers, such as polyethylene terephthalate. Interestingly, the autoxidation of *para*-xylene to terephthalic acid relies on a unique combination of two homogeneous catalysts and an additional bromide source, which acts as a promoter. The Co–Mn–Br catalyst system is the key to the success of the process, which introduces new catalyst pathways and increases the catalyst activity by 16 times, compared to a single cobalt catalyst.^[48, 49] Today this implementation continues to be used worldwide for terephthalic acid production.

2.6 C–C SINGLE BOND CLEAVAGE

Over the past several decades, the challenge of C–H bond activations has been tackled independently by many groups and has led to many novel publications. Notably, in 1993 Murai et al. reported a highly innovative means of C–H bond functionalisation using catalytic amounts of an organometallic ruthenium complex.^[50] This reaction—considered to be a milestone in contemporary chemistry—demonstrated that the site-selective functionalisation of non-polar σ -bonds could be both highly practical and atom-economic in the scope of organic synthesis, which has since become a well-established field of chemistry.^[51–53]

In addition to bond forming reactions, bond breaking can offer an alternative means of enhancing structural complexity into organic frameworks that are not easily generated in any other way. Despite their pervasiveness in organic compounds, C–C single bond activations remain a real synthetic challenge.

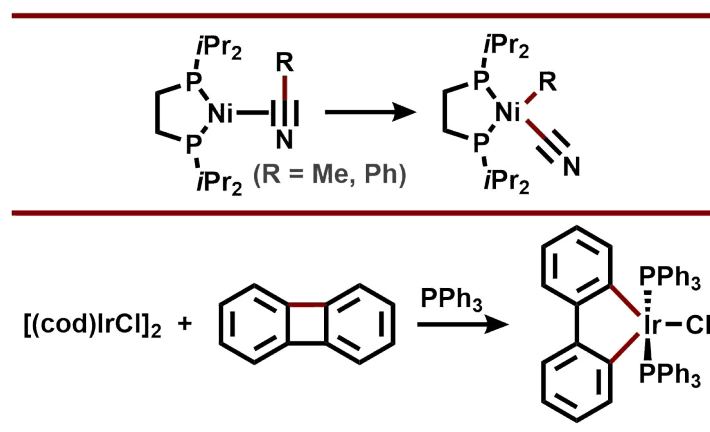
The bond dissociation energy (BDE) of C–C, C=C, and C \equiv C bonds are 347–377 kJ mol⁻¹, 710 kJ mol⁻¹, and 960 kJ mol⁻¹, respectively. One would expect, therefore, that C–C bonds are far more easily broken than C=C and C \equiv C bonds. However, oxidative addition of C–C bonds is difficult to achieve thermodynamically, as the strength of C–C bonds are far stronger than metal–carbon bonds.

Substrates may be typically more inclined towards C–C bond cleavage if they are high in cyclic strain, or if they can gain aromaticity and thus form products low in free energy.^[54, 55] Notably, however, C–C single bonds are particularly unreactive when both carbon atoms are sp³ hybridised. Such an electron configuration is kinetically highly stable due to a combination of steric hindrance of nearby atoms (e. g. C–H bonds) and the directional nature of the spⁿ hybridised orbitals used in covalent bonding. Furthermore, much of organic synthesis takes advantage of the reactivity of (i) π -bonds (e. g. C=C, C=O, etc.), (ii) polarised σ -bonds (e. g., C–Br, C–Li, etc.), and (iii) lone pairs of electrons.^[56] Carbon–hydrogen and carbon–carbon σ -bonds—which are ubiquitous in the scaffold of organic compounds—are distinctly lacking all three of these basic prerequisites for desirable reactivity.

2.6.1 Applications

The heart of many large chemical manufacturing plants is the steam cracker. This crucial piece of process technology provides the starting point for a value chains by taking crude oil fractions (typically naphtha) and "cracking" long chain saturated hydrocarbons into smaller unsaturated compounds, such as ethene and propene; these are the building blocks for myriad chemical commodities. The process for the cleavage of large hydrocarbons is facilitated by a heterogeneous catalyst—often zeolite-based—at temperatures of around 850°C. In contrast, in the organic synthetic laboratory, C–C bond cleavage is well-documented using (over)-stoichiometric oxidants, including O₃,^[57, 58] NaIO₄,^[59] H₅IO₆, Pb(OAc)₄,^[60] and KMnO₄.

Late-stage skeletal functionalisation via C(sp³)–C(sp³) bond cleavage offers great potential advantages in the preparation of small molecules, particularly of drugs, to pave the



Scheme 1: Rare examples of C–C oxidative additions.

way towards new areas of chemical space. The development of new methods for deconstructive functionalisation/ring-opening of heterocycles are regarded as desirable transformations, given their prevalence in pharmaceuticals and agrochemicals, and the current lack of existing strategies.^[53]

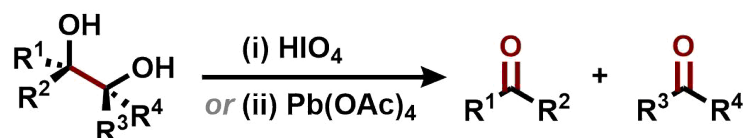
To shift from dependence on finite fossil resources, sustainable and renewable chemical feedstocks are becoming increasingly attractive to the chemical industry. In many ways, lignin is an ideal target for valorisation. Lignin is an inedible organic biopolymer present in vascular plants, providing structural support and water transport. Despite the large scale extraction of lignin from cellulose in the paper pulp industry, only around 1–2% of it is used to generate high-value products, with the rest being either discarded or burned for energy generation. Lignin, however, is a potentially rich source of valuable small molecules given its high density of methoxylated phenylpropane units. A great deal of effort is therefore being invested into the fragmentation and depolymerisation of lignin via pyrolysis, oxidation, hydrogenation, gasification, and microbial biotransformations. In addition to its prevalence of aromatics, lignin has many C(sp³)–C(sp³) linkages also. Thus, the cleavage of such bonds, if possible, provides an alternative pathway to accessing value-added small molecules. However, such techniques remain highly challenging in particular due to the incredible complexity of the 3D structure of lignin, coupled with its high thermodynamic stability.^[61] To this day, the only commercially viable valorisation of lignin is the production of vanillin on a 17 000 ton per annum scale.^[62]

2.6.2 Traditional Methods

In 1931 Rudolf Criegee and co-workers first reported the cleavage of C(sp³)–C(sp³) bonds in vicinal diols (glycols), utilising Pb(OAc)₄ as an oxidant to generate aldehyde C(sp²) centres on the resultant fragments.^[60] The Criegee oxidation works most effectively with diols and

glycols bearing hydroxy groups in close proximity. *cis*- and *trans*-substituted diols may both proceed by forming a 5-membered cyclic intermediate with the lead atom. In the case of *trans* substrates, a higher energy intermediate must be formed due to the relative orientation of the two oxygen atoms and high ring strain. The corresponding *cis* intermediates are generated much more easily and more rapidly, therefore the reaction exhibits much greater selectivity towards *cis* glycols. If the adoption of a highly strained 5-membered intermediate cannot be achieved, an alternative, slower, pathway is available.

In 1934 Léon Malaprade similarly reported a method for oxidative cleavage of C(sp³)–C(sp³) bonds in glycols but using hypervalent iodine reagent HIO₄ as an oxidant.^[63] Due to the strong oxidising nature of HIO₄, the reaction may be viewed as less widely applicable than the Criegee oxidation, however, to its credit the Malaprade oxidation additionally provides an effective means of cleaving β-aminoalcohols.



Scheme 2: (i) Criegee and (ii) Malaprade oxidations.

2.6.3 State-of-the-Art

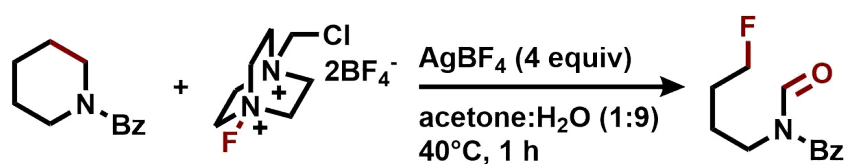
In recent years, C–C single bond activation reactions have come to the attention of chemists as a novel method for introducing valuable complexity within organic compounds. There are comparatively many reports of cleaving C–C bonds in their differently hybridised states,^[64–71] however the cleavage of C(sp³)–C(sp³) bonds is far less reported.

Jiao and co-workers presented in 2017 a novel approach for the oxidative cleavage of allylic C(sp³)–C(sp³) bonds, as well as more facile C(sp²)–C(sp³) bonds. Notably, this protocol requires no metal, relying instead on stoichiometric amounts of the oxidant 2,3-dichloro-5,6-dicyano-1,4-benzoquinone (DDQ) (1.2 equiv), alkyl azide nC₉H₁₉N₃ (1.2 equiv) and excess trifluoroacetic acid (10.0 equiv) (Scheme 3). Impressively, this transformation has proven effective for a wide variety of unfunctionalised olefins as a novel means of accessing cinnamyl aldehydes with great regio- and stereoselectivity.^[66]



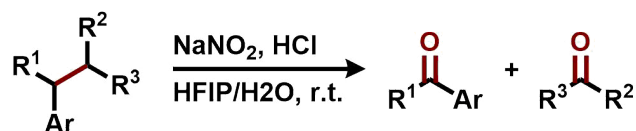
Scheme 3: Allylic C(sp³)–C(sp³) cleavage using azide/DDQ/TFA (Jiao group 2017).

In 2018, Sarpong and co-workers reported a compelling *deconstructive fluorination* methodology, which in a single step, cleaves a C(sp³)–C(sp³) bond and incorporates a new C–F bond in the process. Selectfluor (4 equiv) is used which acts as a fluorine donor to incorporate valuable complexity into an array of unstrained saturated *N*-heterocycles (Scheme ??).^[53] Fluorine is widely used in the pharmaceutical and agrochemical industries for its so-called *polar-hydrophobic* nature which can greatly impact lipophilicity, p*K*_a, and metabolic stability of small molecules.^[72] Whilst this protocol describes the generation of interesting deconstructed products, it does rely on the use of overstoichiometric Selectfluor and AgBF₄ (4 equiv of both), and is poorly atom efficient. Nevertheless, this innovative publication inspired many researchers to investigate the utility of activating C(sp³)–C(sp³) bonds for a fundamentally new approach to skeletal diversification.

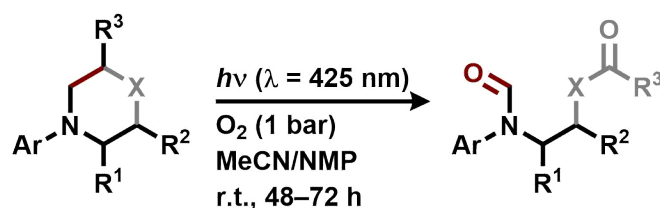


Scheme 4: Deconstructive fluorination using SelectFluor.

The utilisation of lignin in chemistry is highly sought after; it is the main component of lignocellulosic biomass and it is the most ubiquitous renewable source of aromatic units known. Thus it has real potential to be a lucrative feedstock, especially since lignin is a waste product from the paper pulp industry. Phenol, a simple hydroxylated benzene ring, is a valued industrial commodity with a total annual production greater than 11.5 megatons and is further processed to make dyes, polymers, pharmaceuticals and many other important products.^[73] The chemical industry produces phenol from benzene in multistep synthesis under harsh conditions, consuming vast quantities of energy in the process. Naturally, benzene is derived from fossil resources and overall the industrial synthesis of phenol has raised environmental concerns. Achieving selectivity is challenging via this route, given that the hydroxylation of aromatic rings tends towards overoxidation.^[74] Valorisation of lignin thus presents an interesting, albeit challenging, alternative route towards the synthesis of aromatics such as phenol. Recently, Han and co-workers demonstrated just that, by using a solid acid catalyst and water to facilitate the cleavage of C–C single bonds (C(sp²)–C(sp³) hybridised) and C–O bonds within the complex polymeric material. This procedure was demonstrably effective upon scale-up whereby 4.1 g of phenol was obtained from 50.0 g of lignin.^[75]



Scheme 5: C(sp³)–C(sp³) cleavage using NaNO₂/HCl (Liu group 2021).



Scheme 6: Photoinduced C(sp³)–C(sp³) cleavage (Wei group 2021).

In 2020, Liu and co-workers published their findings on the cleavage of C(sp³)–C(sp³) bonds. The reaction relies on catalytic amounts (1 mol %) of Ru(bpy)₃Cl₂ and initiation by visible-light, to facilitate bond activation at room temperature and an open system (i. e. exposure to O₂ in the air). Besides this remarkable reactivity, this methodology is also noteworthy due to the ability to cleave such bonds without the presence of an adjacent N or O atom, instead utilising an adjacent arene ring to achieve site-specific bond activation.^[76]

In the past months, the Liu group presented further developments in this area (Scheme 5). This time around, substantial improvements were made, including dispensing with the ruthenium metal altogether, instead relying on overstoichiometric amounts of NaNO₂ (as oxidant) and HCl (2.5 equiv and 3.0 equiv, respectively) to facilitate C(sp³)–C(sp³) bond activation adjacent to arenes. Notably, this method was also accomplished in a mixture of HFIP—a corrosive and possibly toxic miscible solvent which is environmentally persistent—mixed with water.^[77]

Wei and co-workers similarly reported a photoinduced C(sp³)–C(sp³) activation (Scheme 6). Using molecular oxygen as an oxidant (*p* = 1 bar), and light of a visible wavelength (λ = 425 nm), site selective cleavage within morpholines and piperazines was achievable without the inclusion of any metal catalyst.^[78] This work achieved similar outcomes as demonstrated by our group two years prior—all of which are included in this thesis.^[79, 80]

2.7 MULTIVARIATE OPTIMISATION

Experimental design is a central concern in academia and in industry, and influences the often challenging and time-consuming pursuit of reaction optimisation.

Univariate analyses of variables—which is undoubtedly the go-to method of optimisation for most chemists—is an investigation of one-factor-at-a-time (OFAT), whereby a single variable is altered and its effect on the reaction outcome (i. e. yield, selectivity, etc.) is measured. Despite its simplicity, this approach has many limitations; namely its small coverage of chemical space, poor accuracy, and its inability to detect any interactions between variables.

Fortunately, multivariate analyses of variables, whereby several variables are investigated simultaneously, can rectify many of these inadequacies of OFAT optimisations by facilitating investigations of large areas of chemical space in an efficient and expedient manner and realise optimum reaction conditions with greater accuracy.

Design of Experiments (DoE) is one such type of multivariate analysis that relies on statistics. In this way, not only can it be used to determine optimal reaction conditions, it also provides the advantage of quantifying the relative effect that each variable has on a reaction outcome. DoE is regularly employed in industry, however it is seldom used in academia despite its many advantages. Its increasingly favourable reputation and popularity amongst industrial chemists is a response to several key reasons:^[81, 82]

1. The development of high-throughput experimentation (HTE) using parallel reactors and flow reactor setups has become widely implemented.
2. Quality by testing has largely been superseded by quality by design (QbD) and led to more widespread understanding of design space.
3. Green Chemistry Principles^[83] have encouraged chemists to reduce the waste output from chemical reactions and increase efficiency by reducing the amounts of solvents and reagents used in chemical processes.

Figures 3 and 4 compare the different optimum values obtained from univariate and multivariate analyses and show how the order in which factors are investigated will often impact the set of favourable reaction conditions revealed, i. e. the combination of conditions which furnish the most desirable outcome.

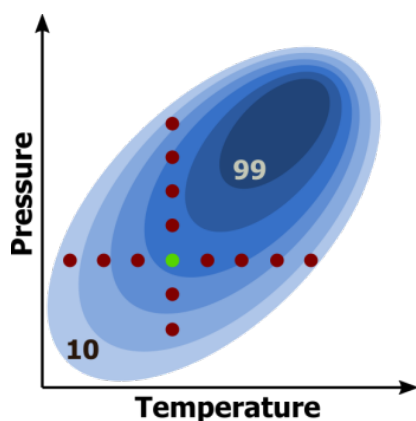


Figure 3: OFAT study:
two sequential studies, first exploring T, then p .

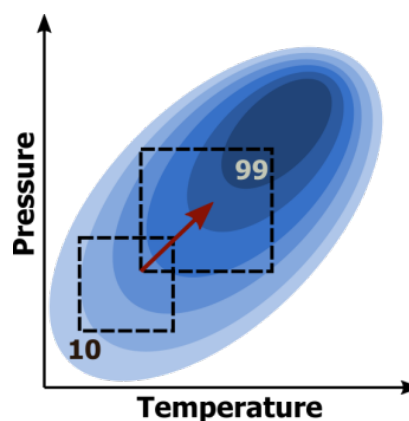
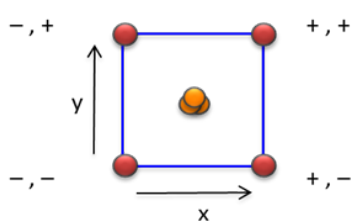
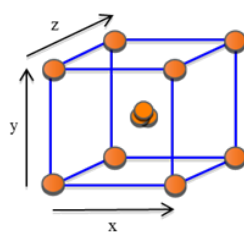
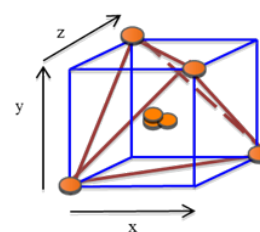


Figure 4: Full-factorial study:
one study exploring T and p at the same time.

DoE can be used to investigate the effects of variables at several different numerical values. For this reason, for an effective DoE, it is valuable to have some prior knowledge about the reaction under investigation to select a suitable range of conditions to explore; if all reactions reach zero conversion then it is difficult to ascertain which factors are impeding the progress of the reaction. In other words, one should have at least a vague idea of suitable chemical space to explore.

The most common type of DoE is a *factorial design*, which is represented as a *base* raised to a *power*. The *number of levels* is given by the base, and the *number of variables* is given by the power. Thus a 2^3 design signifies a two-level three-factorial design. A design of this kind would therefore consist of 8 experimental runs in addition to, perhaps, 4 *centre points*—additional experiments which are run at the very centre of the design space and allow for the reproducibility of a reaction to be assessed, and provide a further data point in the optimisation—for a total of 12 runs. In figure 6 such a design is shown.

As the number of investigation variables increases, the number of experimental runs grows exponentially. For large numbers of variables this can be exceptionally demanding not only in terms of the cost of materials and equipment, but also with respect to time. This is not unique to factorial designs, however, as it is also true that the number of experiments in univariate investigations increases rapidly as the number of variables increases.

Figure 5: 2^2 design.Figure 6: 2^3 design.Figure 7: 2^{3-1} design.

DoE has proven effective and gained popularity in industry as a practical tool for reaction optimisation and process improvements. This has been demonstrated by Pfizer with the simplified and cleaner synthesis of sertraline hydrochloride (Zoloft), a popular selective serotonin reuptake inhibitor, used to treat depression and anxiety-related disorders.^[84]

In 2002, Trevor Laird, at the time the editor of *Organic Process Research & Development* expressed his concerns regarding the reluctance of organic chemists to incorporate DoE techniques in their research, despite their efficacy in areas such as optimisation and for examining structure–activity relationships.^[85]

RESULTS AND DISCUSSION

The topic of C(sp³)-C(sp³) bond activations was initially developed within our group when attempts to realise C-H activation of tri-*n*-butylamine **1a** resulted in unexpected C-C cleavage products. Of the metal salts tested in this reaction, those of copper proved initially to facilitate such reactivity both cleanly and selectively.

3.1 COPPER-CATALYSED CLEAVAGE OF AMINES

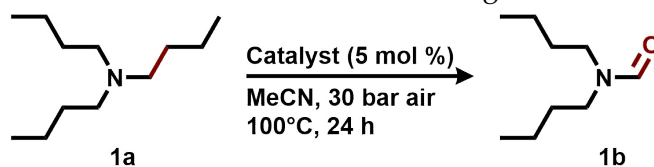
Following the discovery that copper salts could facilitate C(sp³)-C(sp³) bond activation in industrially relevant **1a**, further optimisation enabled tri-*n*-butylamine **1a** to be oxidatively cleaved to *N,N*-dibutylformamide **1b** in 90% yield (Table 2, entry 17). This was achieved using CuCl (5 mol %) and pyridine (2 equiv) under air (30 bar) at 100°C.

During a literature search we discovered that *N*-ligands have been demonstrated to positively influence oxidations.^[86, 87] This led us to perform an investigation of the impact of various *N*-ligands on the model reaction (the transformation of **1a** to **1b**), whereby pyridine was found to be similarly beneficial, furnishing a 16% increase in the yield of **1b**.

Spurred on by our initial findings, we tried attempted the reaction with other aliphatic amines and unsurprisingly received similar results (Table 12). Notably, tri-*n*-ethylamine **2a** was readily transformed to *N,N*-diethylformamide **2b**, which is regarded as a safer and considerably less toxic alternative to *N,N*-dimethylformamide (DMF), a widely used organic solvent. To examine the regioselectivity of this novel [Cu]/air system, we also applied the transformation to unsymmetrical amines. To our delight, we found excellent chemoselectivity and regioselectivity could be achieved in all cases (**4a-6a**, **8a-20a**) and the reaction did not proceed after the formation of the corresponding formamides. As shown in Table 12, we were able to synthesise and isolate 20 different formamides (**1b-20b**) in good to excellent yields.

Following the success with amines, we applied the protocol for C(sp³)-C(sp³) cleavage in *N*-heterocycles. Morpholines and piperazines are particularly highly valued structural motifs in industrial chemistry and are present in several of the top 50 best selling pharmaceuticals. For this reason, we believe the synthesis and derivatisation of such moieties is of considerable synthetic interest, not only for the purposes of late stage functionalisation, but also for synthesising and characterising potential drug metabolites.

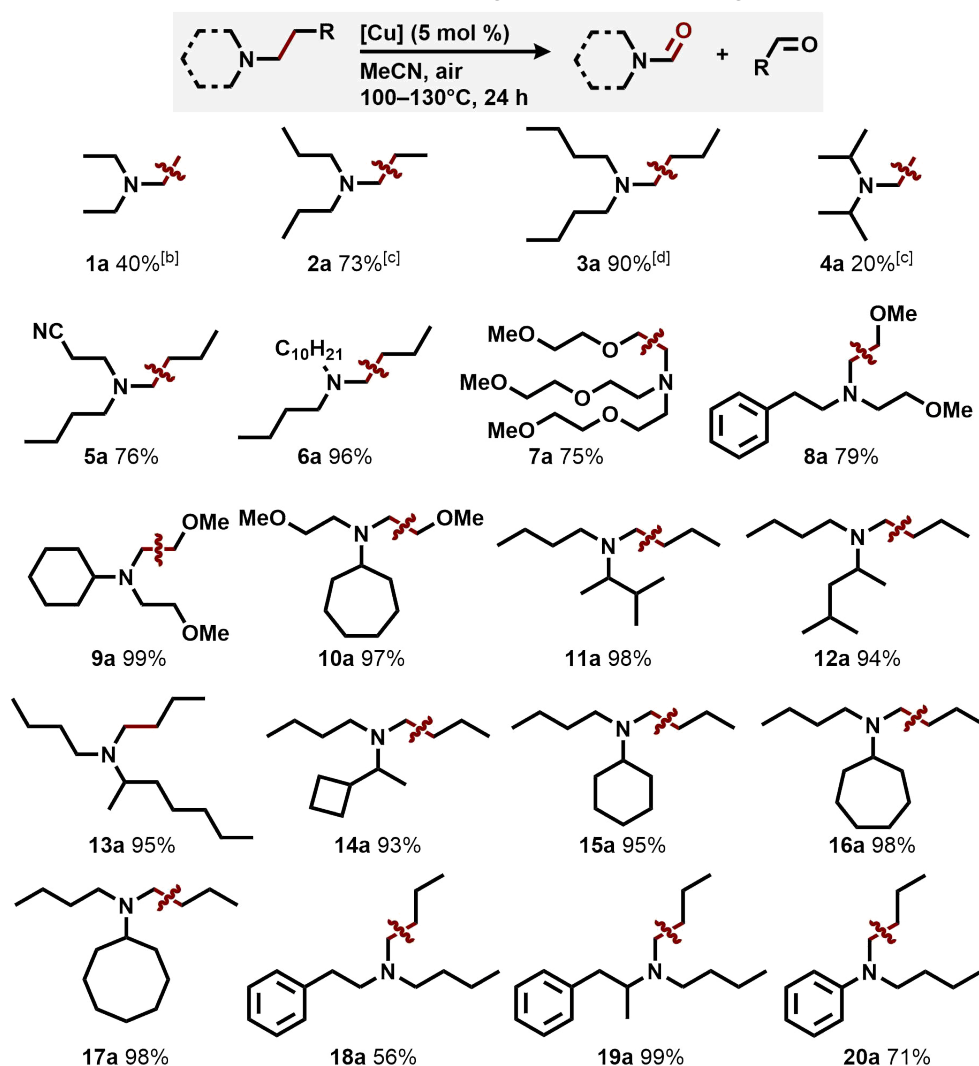
In view of this, a total of 26 morpholine and piperazine derivatives were converted to their C-C cleaved products using Cu(CF₃SO₃)₂ (3 mol %) *or* CuCl (5 mol %), pyridine (0.2-2.0 equiv), 20-30 bar air, at 100-130°C. Notably, we were able to demonstrate the utility of this protocol for the activation of C(sp³)-C(sp³) bonds in linezolid **21a** (an antibiotic used for the treatment of Gram-positive bacteria), emorfazone **22a** (an analgesic for treating dental pain),

Table 2: Transition Metal Salts for C–C Bond Cleavage in Tri-*n*-Butylamine **1a**^a

entry	catalyst	additive	yield (%) ^b
1	Pd(OAc) ₂	-	20
2	RuCl ₃	-	11
3	Ru(acac) ₃	-	trace
4	AgCF ₃ SO ₃	-	trace
5	Ag ₂ CO ₃	-	19
6	Co(OAc) ₂ · 4H ₂ O	-	20
7	Cu(OAc) ₂	-	60
8	CuCl	-	74
9	CuBr ₂	-	70
10	CuBr	-	70
11	CuI ₂	-	72
12	Cu(CF ₃ SO ₃) ₂	-	64
13	Cu(II) phthalocyanine	-	trace
14	CuCl	py (20 mol %)	74
15	CuCl	py (40 mol %)	80
16	CuCl	py (1 equiv)	84
17	CuCl	py (2 equiv)	90
18 ^c	CuCl	py (2 equiv)	72
19 ^d	CuCl	py (2 equiv)	74
20	-	py (2 equiv)	trace

^aReaction conditions: **1a** (0.5 mmol), catalyst (5 mol %), additive, in MeCN (2 mL), 30 bar air, 100°C, 24 h. ^bYield determined by GC-FID, using *n*-dodecane as an internal standard. ^c20 bar air, 80°C. ^dCuCl (3 mol %).

as well as several natural product derivatives (e. g. **23a** and **24a**) (Figure 8). Crucially, these (highly) functionalised organic molecules could be selectively transformed to the expected C–C bond cleavage products without any alteration to other chemical motifs.

Table 3: C–C Bond Cleavage in Amines Using Cu^a

^aReaction conditions: **a** (0.5 mmol), CuCl (5 mol %), pyridine (2.0 equiv), in MeCN (2 mL), 30 bar air, 100°C, isolated yield. ^b10 mmol triethylamine, Cu(CF₃SO₃)₂ (5 mol %), 40 bar air, 130°C. ^c40 bar air, 130°C. ^d10 mmol scale.

3.1.1 Mechanistic Investigations

To gain an understanding of this newly discovered catalytic system, a combination of electron paramagnetic resonance (EPR) and ultraviolet–visible (UV-Vis) spectroscopic methods, in conjunction with LC-MS and GC-MS, provided sufficient insightful data to pro-

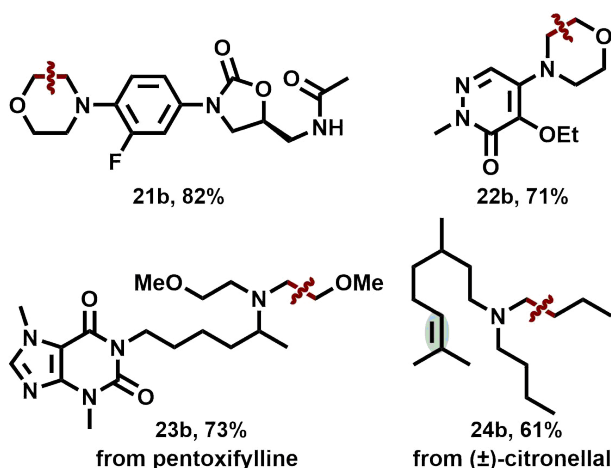


Figure 8: C–C bond cleavage in natural product derivatives and drugs.

pose a possible mechanism for the transformation of *N*-phenylmorpholine **25a** to 2-(*N*-phenylformamido)ethyl formate **25b** (Scheme 7).

In the absence of air (the proposed oxidant), and under an inert N₂ atmosphere, the reaction was unsuccessful. Furthermore, the addition of ¹⁸O-labelled water into the reaction mixture led to no incorporation of ¹⁸O in the product. With these observations, we are confident that O₂ from air is the oxygen donor in the reaction.

Possible reaction intermediates, 4-phenylmorpholine-2,3-dione and 4-phenylmorpholin-3-one, were each submitted to the standard reaction conditions (in the absence of **25a**) but both compounds remained stable and unaffected, and **25b** was not observed at the end of the reaction. We therefore rule out these compounds as potential intermediates.

The addition of overstoichiometric quantities (2.0 equiv) of radical trapping reagents, TEMPO or BHT, completely stopped the standard reaction of **25a**; this highly indicates the importance of free radicals in the reaction mechanism.

With this information in hand, we were able to propose the following sequence of events:

1. A single electron transfer occurs (SET) from **25a** to Cu²⁺, to form a radical cationic species **A** and Cu¹⁺.

This is corroborated by EPR, which revealed that the addition of **25a** to a solution of Cu²⁺ induces the temporary generation of an unresolved hyperfine signal at *g* = 2.004 which is characteristic of putative organic radical **A**, as well as the rapid loss of a signal indicative of Cu²⁺. The reduction of Cu²⁺ was further corroborated by UV-Vis measurements showing the decay of apparent ligand-to-metal charge transfer and d–d transition bands of Cu²⁺ below 300 nm and at ca. 700 nm. The formation of Cu¹⁺ is supported also by the observation of purported metal-to-ligand transfer bands at 320 nm and 466 nm.

2. A proton is lost from species **A** to generate intermediate **B**.

Species **C** was detected by GC-MS after running the standard reaction in the presence of TEMPO. This indirectly confirms **B** as an intermediate in the catalytic cycle.

3. Cu^{2+} is reduced, forming the intermediate **D** (now bearing a $\text{C}(\text{sp}^2)=\text{C}(\text{sp}^2)$ bond), and hydrogen peroxide, which then decomposes to water and oxygen.

Species **D** was observed directly in small quantities by GC-MS after performing the standard reaction in the presence of TEMPO.

From this point on, the intermediate **D** is oxidatively cleaved to yield the product **25b**, reminiscent of enamine oxidations.^[88]

4. In a manner similar to the first step (**A**→**B**), a SET reoccurs to form radical cation **E**, which is this time resonance stabilised by the adjacent C=C bond.
5. **E** is catalytically oxidised by Cu^{2+} -dioxygen (**I**) to afford intermediate **F**.
6. Intramolecular nucleophilic addition within **F** releases Cu^{2+} and unstable peroxide intermediate **G**.
7. Rapid decomposition of **G**—via C–C and O–O bond cleavages—yields the desired product **25b**.

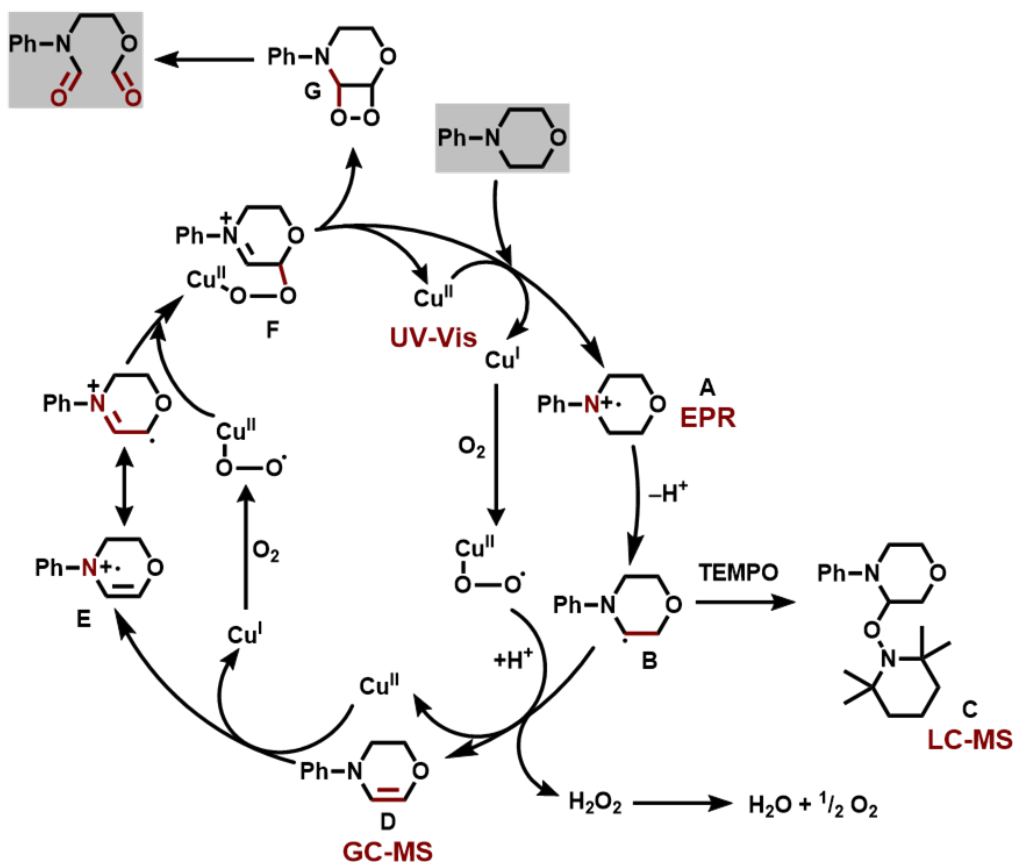
3.2 IMPROVED COBALT–MANGANESE CATALYSTS

The successful results of the copper catalyst system led us to explore the talents of other metals. Various metal salts were tested in catalytic amounts for $\text{C}(\text{sp}^3)\text{--C}(\text{sp}^3)$ bond cleavage, using *N*-phenylmorpholine **25a** as a model substrate. The results for this initial investigation, shown in Table 4, highlighted the competence of $\text{Mn}(\text{OAc})_2\cdot 4\text{H}_2\text{O}$ for oxidative cleavage of **25a** in the absence of any ligand and air as the sole oxidant. Notably, the more precious, noble metal salts that were investigated were either ineffective, or showed little activity for this reaction under the given conditions.

These initial discovery, in conjunction with our interest in non-noble metal catalysis, led to the decision to focus on 3d metals for this transformation. Very quickly it was discovered that cobalt(II) salts also showed activity in this reaction, albeit furnishing only low yields of **25b** (Table 5, entries 3 and 4).

The most important outcome occurred when cobalt *and* manganese salts were combined in the same reaction mixture; this simple change led to a profound and unexpected improvement to the reaction (Table 5). Specifically, yields of 13% and 26% of **25b** could be increased up to 96%! Naturally these excellent results were worthy of further investigation.

Different combinations of simple cobalt and manganese salts which were examined for the transformation of **25a** to **25b** under similar reaction conditions. Whilst $\text{Co}(\text{acac})_3$ proved

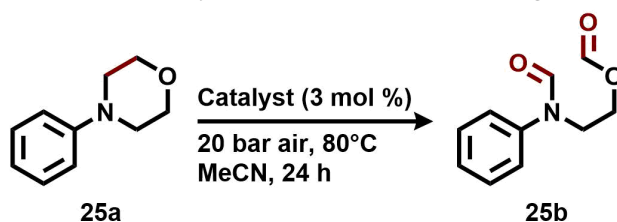


Scheme 7: Proposed mechanism for [Cu]-catalysed oxidative cleavage of C(sp³)–C(sp³) bonds.

to cooperate poorly with Mn(OAc)₂·4H₂O, all other cobalt and manganese salts interacted favourably for the desired C–C bond cleavage. Notably, the cleanliness of the GC-FID chromatograms indicated that the reaction proceeded selectively with no detectable side products.

Based on the previously published work using copper catalysts,^[79] as well as the often positive effect of *N*-ligands in oxidation reactions which has been described in the literature, an assortment of pyridines, amides, and amines were investigated to try to find the optimal ligand for the new cobalt–manganese catalyst system. The aim here was to identify the best ligand under mild conditions; the reactions were therefore conducted at considerably low temperature and pressure (60°C; 10 bar air).

The results in Table 6 once again show that the choice of ligand can make or break this type of reaction. The best ligand tested was 4-methoxypyridine **L8** which yielded 86% of **25b**. This is a massive improvement over the ligand-free reaction, which furnished only a 24% yield. It should be pointed out that 2,2'-bipyridine **L14**, and phenanthroline **L15** completely killed the catalysis; these ligands are commonly used in many catalytic applications, and this was

Table 4: Metal Catalysts for C–C Bond Cleavage in **25a**^a

entry	catalyst	yield (%) ^b
1	Pd(OAc) ₂	0
2	Ru(acac) ₃	22
3	RuCl ₃	44
4	Fe(OAc) ₂	0
5	Co(OAc) ₂ ·4H ₂ O	0
6	AgCF ₃ SO ₃	0
7	Ag ₂ CO ₃	0
8	Mn(OAc) ₂ ·4H ₂ O	30
9	Mn(acac) ₂	0

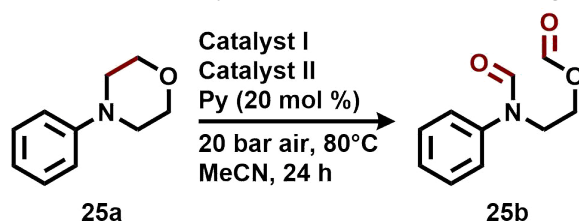
^aReaction conditions: **25a** (0.5 mmol), catalyst (3 mol %), in MeCN (2 mL), 20 bar air, 80°C, 24 h. ^bYield determined by GC-FID, using *n*-dodecane as an internal standard.

indeed unexpected. In fact, surprisingly, chelating compounds **L14**, **L15**, **L17**, and **L18** were all deleterious additives in this catalytic system. It is hard to see any trends regarding the effects of electron-withdrawing, electron-donating and sterically bulky groups on the activity of the cobalt–manganese catalysts but ultimately the decision was made to remain using pyridine as an ideal ligand for all future experiments, due to its high performance, ready availability, and low cost.

3.2.1 Reaction Scope

Using this new methodology for C(sp³)–C(sp³) bond cleavage a total of 17 substrates were cleaved under the same, or similar reaction conditions towards the desired oxidation products.

Table 7, shows the tolerance of the bimetallic system towards a variety of functional groups. Methyl-substituted morpholines **22a** and **23a** readily underwent the transformation, despite the added steric bulk present directly on the reaction centre. Substrates **25a**, **28a** and **33a**, all of which bear electron-withdrawing groups (NO₂, C≡C and COOEt) were similarly well-

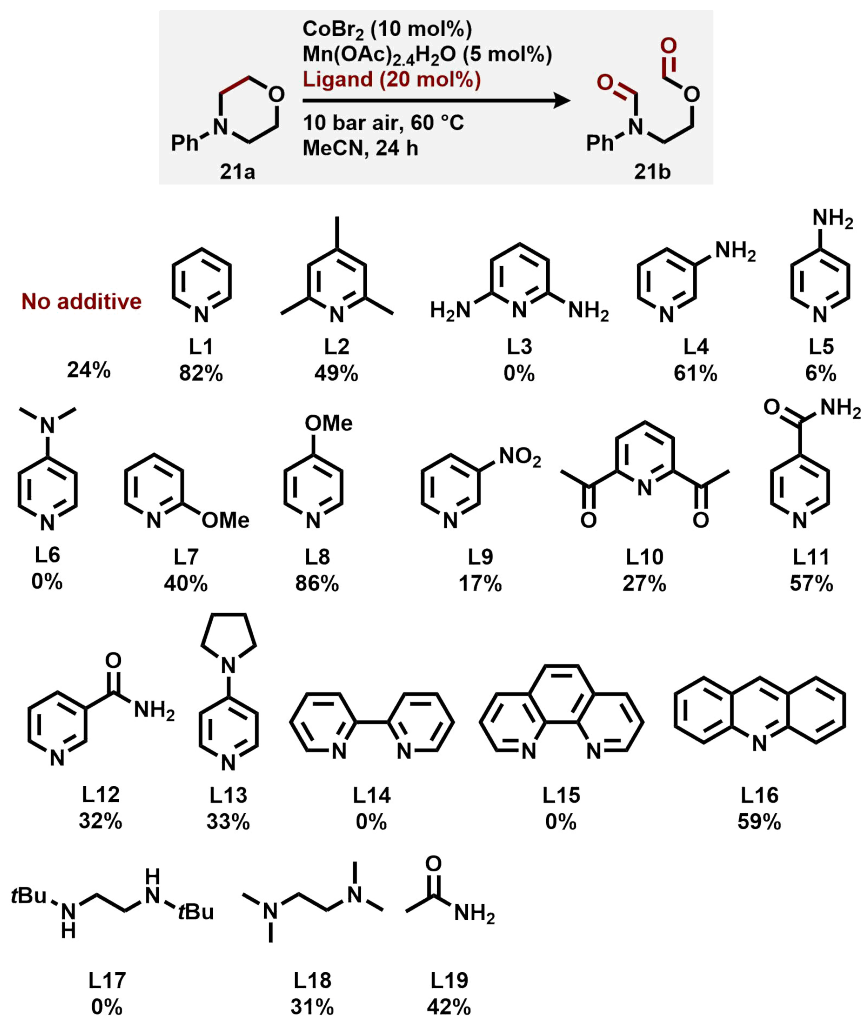
Table 5: Co and Mn Catalysts for C–C Bond Cleavage in **25a**^a

entry	catalyst I	catalyst II	yield (%) ^b
1	Mn(OAc) ₂ ·4H ₂ O		trace ^c
2	Mn(OAc) ₂ ·4H ₂ O		26
3		CoBr ₂	10 ^c
4		Co(OAc) ₂ ·4H ₂ O	13
5	Mn(OAc) ₂ ·4H ₂ O	Co(OAc) ₂ ·4H ₂ O	60 ^d
6	Mn(OAc) ₂ ·4H ₂ O	Co(OAc) ₂ ·4H ₂ O	96
7	Mn(OAc) ₂ ·4H ₂ O	CoBr ₂	94
8	Cu(OTf) ₂		55

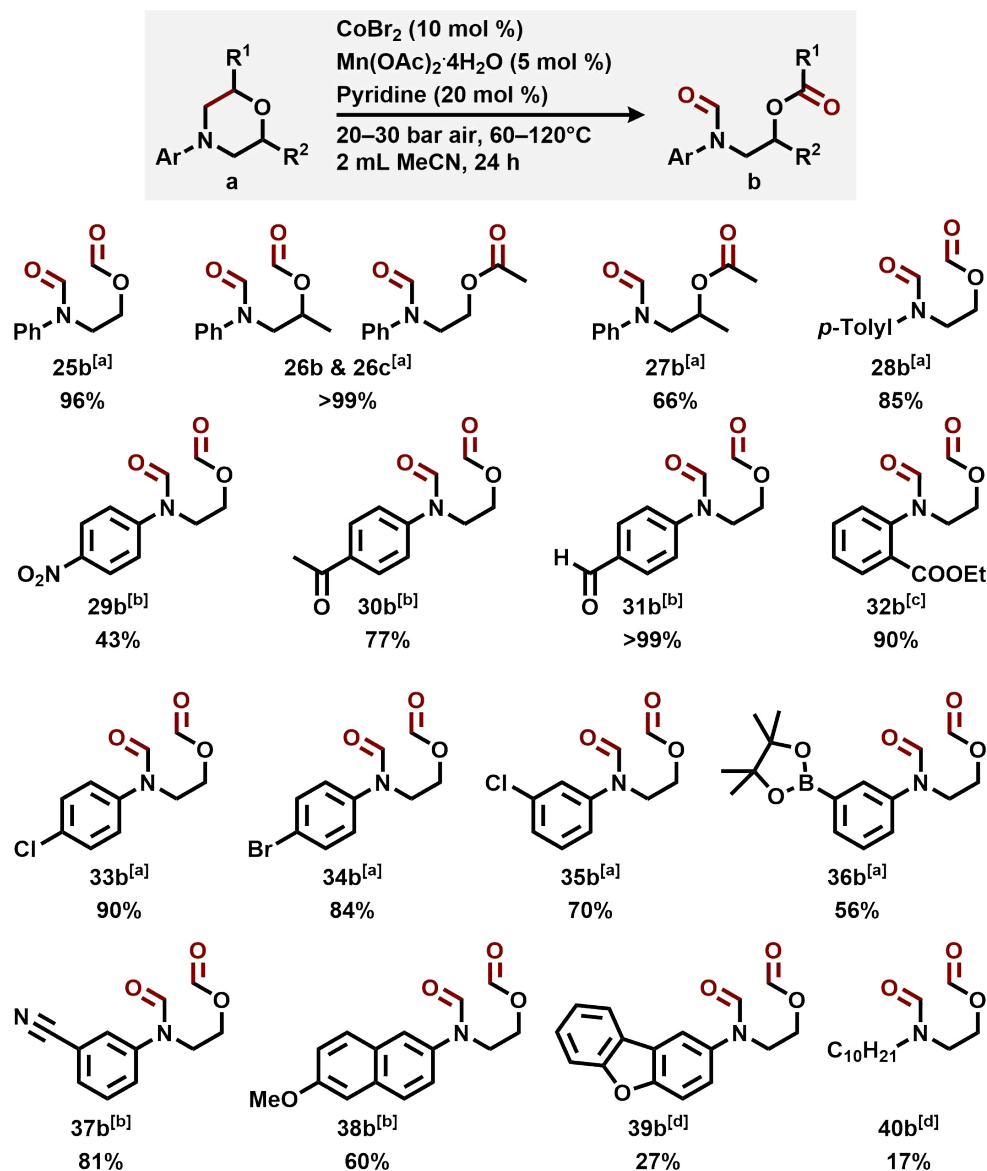
^aReaction conditions: **25a** (0.5 mmol), catalyst I (5 mol %), catalyst II (5 mol %), pyridine (20 mol %), in MeCN (2 mL), 20 bar air, 80°C, 24 h. ^bYield determined by GC-FID, using *n*-dodecane as an internal standard. ^cCatalyst I/II (10 mol %). ^dKBr (5 mol %) added.

tolerated leading to high yields of the desired cleavage products. Gratifyingly, aryl halide substrates **29a** and **30a**, which represent valuable coupling substrates, were readily transformed to the desired products cleanly with the C–X bonds untouched. Boronate ester **32a**—which models the class of suitable Suzuki–Miyaura cross-coupling partners—was likewise selectively oxidised to the corresponding product with good yield at only 60°C! Further success was achieved with carbonyl substrates **26a** and **27a**, and remarkably, even under the oxidative reaction conditions, the aldehyde moiety in **27a** was unaffected, yielding none of the corresponding carboxylic acid! The improved reactivity of the bimetallic system is exemplified by its ability to perform C–C bond cleavages of substrates **21a**, **24a**, **29a** and **30a** which were able to be oxidatively cleaved to the corresponding products in high yields at 60°C and 20 bar air pressure. This distinctly highlights the substantial improvements of this Co–Mn system over the previously reported copper-based system!

The cleavage of linezolid—a synthetic prescription antibiotic—proceeded smoothly towards the expected and desired product and successfully isolated with 82% yield (Scheme 8). Not only did this result prove that this procedure is selective and tolerant towards functionalised

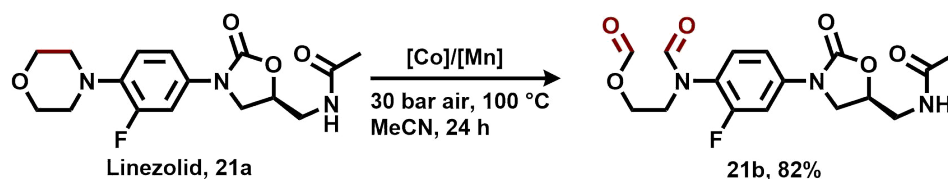
Table 6: Influence of *N*-Ligands on the Standard Reaction^a

^aReaction conditions: **25a** (0.5 mmol), CoBr₂ (10 mol %), Mn(OAc)₂ · 4H₂O (5 mol %), ligand (20 mol %), in MeCN (2 mL), 10 bar air, 60°C, 24 h. Yield determined by GC-FID, using *n*-dodecane as an internal standard.

Table 7: Bond Cleavage in Morpholines Using Co–Mn^a

^aReaction conditions: **a** (0.5 mmol), CoBr₂ (10 mol %), Mn(OAc)₂·4H₂O (5 mol %), pyridine (20 mol %), in MeCN (2 mL), 20 bar air, 60°C, isolated yield. ^b30 bar air, 100°C. ^c20 bar air, 120°C. ^d30 bar air, 120°C, pyridine (1 equiv).

organic compounds, but it also highlighted the potential for late-stage functionalisation of pharmaceuticals.



Scheme 8: Late stage functionalisation of linezolid.

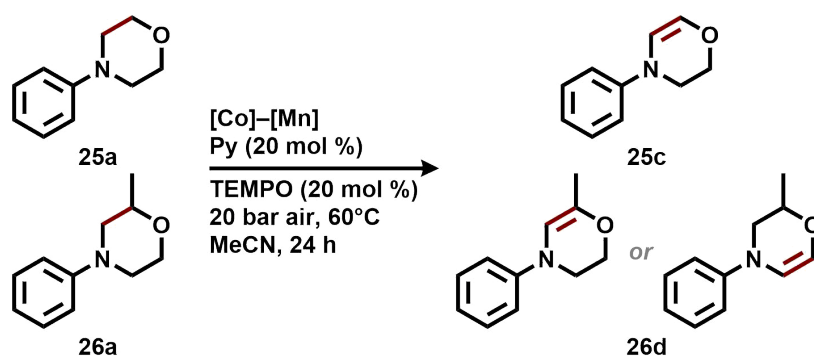
Whilst the cobalt–manganese catalysts showed a definitive improvement for the cleavage of morpholine derivatives, unlike the previous copper system we were unable to achieve bond cleavages in aliphatic amines and in piperazines. These were indeed the chief drawbacks of this new bimetallic system.

3.2.2 Mechanistic Investigations

Despite the high performance of this reaction, the mechanistic understanding of the catalysis was unclear at this point. We initially hypothesised that there would be similarities between the cobalt–manganese system and the previously reported copper-catalysed system.^[79] To probe the existence of radicals—either in the form of catalyst-centred intermediates, or substrate-centred intermediates—the cleavage of **25a** was attempted under the optimised reaction conditions with the addition of (2,2,6,6-tetramethylpiperidin-1-yl)oxyl (TEMPO). As expected, the catalysis was stopped almost completely and **25b** was not detectable by GC-FID. Interestingly, it was possible to detect traces of **25c**, resulting from partial oxidation of the C(sp³)–C(sp³) bond to a more labile C(sp²)–C(sp²) (shown in Scheme 9). Confirmation that this reaction proceeds via a radical mechanism led to experimentation using electron paramagnetic resonance (EPR) (with help from Dr Jabor Rabeah) to detect further reaction intermediates. Unfortunately, despite best efforts, no insightful data could be obtained other than the detection of a manganese(II) species.

Based on these limited mechanistic data, it is assumed that the cobalt and manganese catalysts cooperate in the following manner: (i) Substrate **25b** undergoes partial oxidation, leading to the formation of **25c**, catalysed (predominantly) by either a cobalt *or* manganese species, and (ii) the more reactive intermediate **25c** is further oxidised, via the incorporation of an O₂ molecule, catalysed (predominantly) by whichever metal was not used in the first step, to form **25b**. To confirm this, we proposed the following experiments:

1. Perform the reaction of **25c** using the standard reaction conditions without the substrate **25a**.
2. Perform the reaction of **25c** using the standard reaction conditions without the substrate **25a** and without CoBr₂.



Scheme 9: Putative intermediates detected by GC-MS.

3. Perform the reaction of **25c** using the standard reaction conditions without the substrate **25a** and without $\text{Mn(OAc)}_2 \cdot 4\text{H}_2\text{O}$.

Unfortunately, these reactions were never performed as no practical means of synthesising the intermediate **25c** was identified.

3.3 A SIMPLE IRON CATALYST

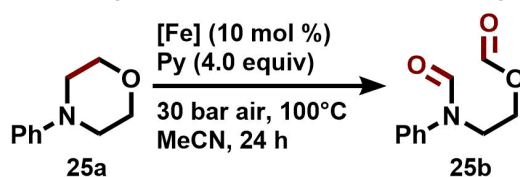
During the further investigation of non-noble metals for $\text{C(sp}^3\text{)}\text{-C(sp}^3\text{)}$ bond activation, several iron catalysts showed promising activity for such transformations under aerobic conditions. Best of all was FeCl_3 , a simple and low cost iron salt.

Unlike the previously discussed bimetallic Co–Mn catalyst system, this system had the advantage of showing activity for cleavage within *N,N*-diphenylpiperazine in addition to morpholines. The iron's effectiveness with piperazines was particularly remarkable to us, as the previous copper catalysts showed only moderate compatibility with piperazines and the cobalt–manganese catalysts were completely inactive towards these substrates.

Notably, the catalytic activity could be significantly enhanced in the presence of substoichiometric amounts of TEMPO—a compound which had previously eliminated catalytic activity. Unsurprisingly, pyridine once again proved beneficial to catalyst activity; both electron-withdrawing and electron-donating substituents furnished only poorer yields of **25b**.

For the purposes of reaction optimisation, we postulated that DoE would be a valuable tool to establish a more realistic process. We expected that catalyst loading, temperature, air pressure, pyridine loading, and TEMPO would all significantly affect the yield of **41b** from the reaction.

Using our intuition and existing knowledge of the reaction, a half-fractional two-level five-factorial design with four centre points was used for optimising the oxidative cleavage of **41a**. A total of 20 experiments later (Table 10), the results could be analysed (with the aid of Minitab[®]) to determine the most significant factors influencing the yield of **41b**.

Table 8: Selective Cleavage of a C–C Bond in **25a** Using Fe Precursors^a

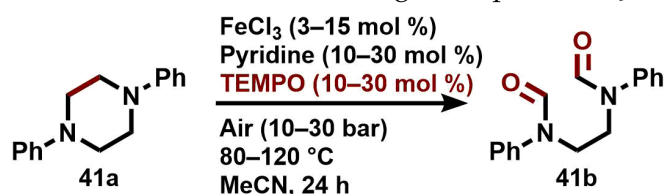
entry	Fe salt	yield (%) ^b
1	Fe(III) citrate	0
2	Fe(OAc) ₂	0
3	Fe(acac) ₃	0
4	FeNO ₃ · 3H ₂ O	21
5	Fe(II) phthalocyanine	23
6	FeCl₃	76
7 ^c	FeCl ₃	65
8 ^d	FeCl ₃	43
9 ^e	FeCl ₃	63
10 ^f	FeCl ₃	71

^aReaction conditions: **25a** (0.5 mmol), [Fe] salt (5 mol %), pyridine (4.0 equiv), in MeCN (2 mL), 30 bar air, 100°C, 24 h. ^bYield determined by GC–FID, using *n*-dodecane as an internal standard. ^cPyridine (2.0 equiv). ^dPyridine (20 mol %). ^eFeCl₃ (5 mol %). ^fFeCl₃ (15 mol %).

Table 9: Factors Investigated Using DoE for Piperazine Cleavage

factor	low level (–)	high level (+)
FeCl ₃ (mol %)	3	15
temperature (°C)	80	120
pressure (bar)	10	30
pyridine (mol %)	10	30
TEMPO (mol %)	10	30

The results of Table 10 show that the greatest yields of **41b** were achieved at the upper limits of temperature and pressure (entries 10, 11, 16). Unsurprisingly, the lower limits of temperature and pressure furnished significantly lower yields of **41b** (entries 3, 5, 9). These data appear to validate the necessity of providing enough heat to the reaction to overcome

Table 10: DoE Results for Cleavage of Piperazine **41a**^a

entry	FeCl ₃ (mol %)	TEMPO (mol %)	pyridine (mol %)	<i>p</i> (bar)	T (°C)	yield (%) ^b	1b
1	3	10	10	10	120	25	
2	15	10	10	10	80	38	
3	3	30	10	10	80	5	
4	15	30	10	10	120	45	
5	3	10	30	10	80	7	
6	15	10	30	10	120	52	
7	3	30	30	10	120	30	
8	15	30	30	10	80	33	
9	3	10	10	30	80	12	
10	15	10	10	30	120	59	
11	3	30	10	30	120	56	
12	15	30	10	30	80	52	
13	3	10	30	30	120	41	
14	15	10	30	30	80	36	
15	3	30	30	30	80	16	
16	15	30	30	30	120	60	
17 ^c	9	20	20	20	100	51	
18 ^c	9	20	20	20	100	44	
19 ^c	9	20	20	20	100	40	
20 ^c	9	20	20	20	100	45	

^aReaction conditions: **41a** (0.5 mmol), FeCl₃ (3–15 mol %), TEMPO (10–30 mol %), pyridine (10–30 mol %), in MeCN (2 mL), 10–30 bar air, 80–120 °C, 24 h. ^bYield determined by GC-FID, using *n*-hexadecane as an internal standard. ^cCentre point conditions.

the high thermodynamic stability of C(sp³)–C(sp³) bonds. It is worth noting entries 4 and

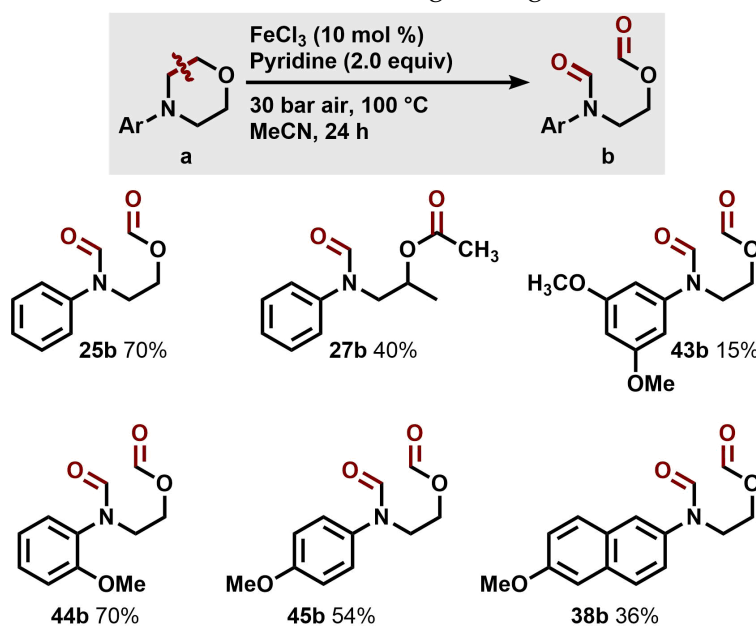
6, as these results highlight the catalyst's ability to achieve good yields of **41b** under lower pressures of air (10 bar), thus benefitting operational convenience and safety.

Table 11: Primary DoE Screen: ANOVA

source	<i>p</i> -value	significant (y/n)
<i>1-way interactions</i>		
FeCl₃	0.002	yes
TEMPO	0.234	no
pyridine	0.419	no
air	0.013	yes
temp	0.003	yes
<i>2-way interactions</i>		
FeCl ₃ × TEMPO	0.419	no
FeCl ₃ × pyridine	0.655	no
FeCl ₃ × air	0.373	no
FeCl ₃ × temp	0.057	no
TEMPO × pyridine	0.332	no
TEMPO × air	0.090	no
TEMPO × temp	0.960	no
pyridine × air	0.150	no
pyridine × temp	0.526	no
air × temp	0.187	no

An analysis of variance (ANOVA) of the five factors (and their interactions) provided additional useful insight into their influence on the yield of **41b**. ANOVA concurred with our observations that the temperature and pressure were both very significant towards the reaction yield. In fact, a total of three factors (catalyst loading, temperature, and air pressure) were found to be statistically significant (Table 11) in the reaction (i. e. *p*-values < 0.05 under the null hypothesis), and the high-level conditions for each of these three factors furnished the greatest yields of **41b**. Interestingly, the TEMPO and pyridine loadings (from 10–30 mol %) were found not to be statistically significant, however, their presence in the reaction mixture proved to be beneficial. From these data, we explored higher temperatures and pressures, but to our surprise these harsher conditions were detrimental towards the yield, and we could not accomplish yields greater than 60% (Table 10, entry 16).

Using these information *vide supra*, we successfully applied the optimised conditions to derivatised *N*-heterocycles to yield the corresponding C–C bond cleavage products in up to

Table 12: Bond Cleavage Using Fe^a

^aReaction conditions: **a** (0.5 mmol), FeCl₃ (10 mol %), pyridine (2.0 equiv), in MeCN (2 mL), 30 bar air, 100°C, isolated yield.

70% yield. Notably, such activity towards C–C bonds within a piperazine ring had not been possible using either the copper, or cobalt–manganese catalysts previously established by our group.

Whilst the reaction proceeded cleanly—with no visible side products or intermediates observed using GC-FID, or GC-MS—and appeared to have any noticeable induction period, however a brown precipitate was formed during the reaction on the walls of the vials. When isolated, this solid material proved to be catalytically active, yielding up to 9% of **2b** under the standard reaction conditions.

Scanning transmission electron microscopy (STEM) was used in conjunction with electron energy loss spectroscopy (EELS) to unearth the nature of the brown catalytically-active precipitate. The analyses identified iron oxide particles on the surface of a bulk carbon layer with nitrogen and traces of iron present also.

3.4 NICKEL-CATALYSED HYDRODEHALOGENATION

Catalytic hydrodehalogenation (HDH) using heterogeneous materials is a topic which has been an area of investigation within our group for several years.^[89] To identify a suitable catalyst for such reactivity, the project was initiated by preparing a library of heterogeneous nickel-

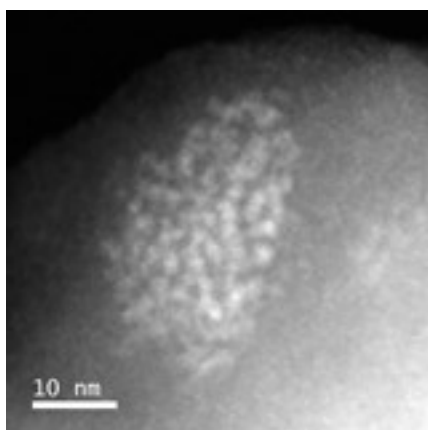


Figure 9: STEM HAADF image of the precipitate formed during the reaction. Iron oxide particles are visible (see the bright spots).

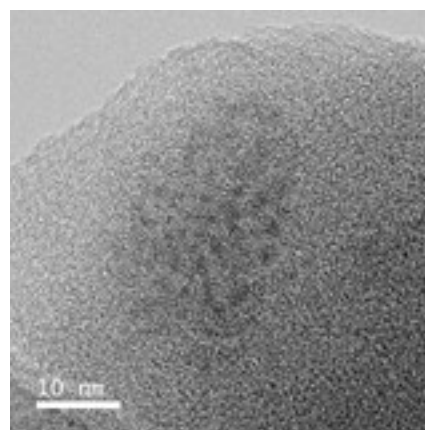


Figure 10: STEM ADF image of the precipitate formed during the reaction. Iron oxide particles are visible (see the dark spots).

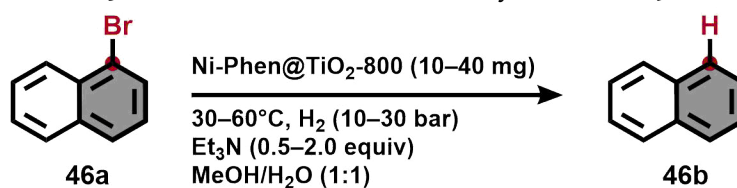
based materials. The simple procedure for preparation involved (i) heating nickel precursor $\text{Ni}(\text{OAc})_2 \cdot 4\text{H}_2\text{O}$ in the presence of ligand 1,10-phenanthroline monohydrate in ethanol, (ii) mixing in the solid support (e. g. SiO_2 , TiO_2 , C, etc.), (iii) drying the mixtures *in vacuo*, and lastly, (iv) pyrolysis of the dried material at high temperature (600–1000 °C) under argon.

With the various heterogeneous nickel-based materials in hand, we investigated their activities for the reductive dehalogenation of 1-bromonaphthalene **46a** using molecular hydrogen and (excess) triethylamine as an HBr scavenger. We found that Ni-Phen@ TiO_2 -800 was the most effective in this transformation and could achieve a 99% yield of the dehalogenated congener **46b** at ambient temperature!

With the target of minimizing reagent and catalyst use, and given that there are several variables which would likely influence the product yields from our newly developed catalytic system, we once again decided to use DoE as a robust and expedient multivariate analysis of the reaction parameters.

A two-level full-fractional investigation (2^4 design) of temperature, pressure, catalyst loading, and amount of base necessitated 20 reaction runs, including the runs performed in the center of the design space (which were performed in quadruplicate). Using an analysis of variance (ANOVA), we identified the following statistically significant parameters: (i) amount of base, (ii) catalyst loading, and (iii) temperature. Statistically significant interactions were also detected between (iv) catalyst loading and temperature, as well as (v) catalyst loading and amount of base. The contour plots (Figure 11) provide an illustration of these interactions, and give an indication of the most favourable areas of chemical space unearthed during the DoE.

Using this information we were able to achieve full conversion of **46a** and 92% yield of **46b** after 18 hours at 45 °C, using just 20 bar H_2 and 1.25 equiv triethylamine. The influence of

Table 13: DoE Results for HDH of Aryl Bromide **46a**^a

entry	[Ni] (mg)	Et ₃ N (equiv)	<i>p</i> (bar)	T (°C)	yield (%) ^b
1	10	0.50	10	30	25
2	10	0.50	10	60	38
3	10	0.50	30	30	5
4	10	0.50	30	60	45
5	40	0.50	10	30	7
6	40	0.50	10	60	52
7	40	0.50	30	30	30
8	40	0.50	30	60	33
9	10	2.00	10	30	12
10	10	2.00	10	60	59
11	10	2.00	30	30	56
12	10	2.00	30	60	52
13	40	2.00	10	30	41
14	40	2.00	10	60	36
15	40	2.00	30	30	16
16	40	2.00	30	60	60
17 ^c	25	1.25	20	45	51
18 ^c	25	1.25	20	45	44
19 ^c	25	1.25	20	45	40
20 ^c	25	1.25	20	45	45

^aReaction conditions: **46a** (0.5 mmol), Ni-Phen@TiO₂-800 (10–40 mg), Et₃N (0.50–2.00 equiv), 10–30 bar H₂, 30–60°C, 2 ml MeOH:H₂O (1:1), 20 h. ^bYield determined by GC-FID, using *n*-hexadecane as an internal standard. ^cCentre point conditions.

the base was not at all surprising for two reasons: firstly, as the reaction progresses, a bromine atom is displaced from the substrate to form increasing amounts of acidic HBr, and secondly,

we our group had previously observed that NEt_3 can promote an additional pathway for the heterolytic cleavage of molecular hydrogen.^[90]

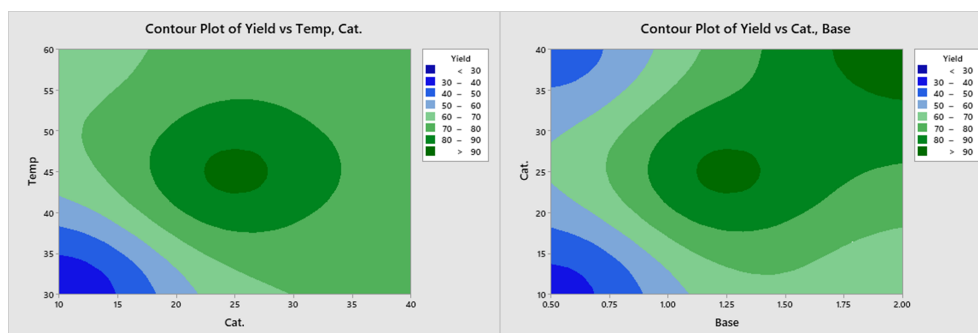


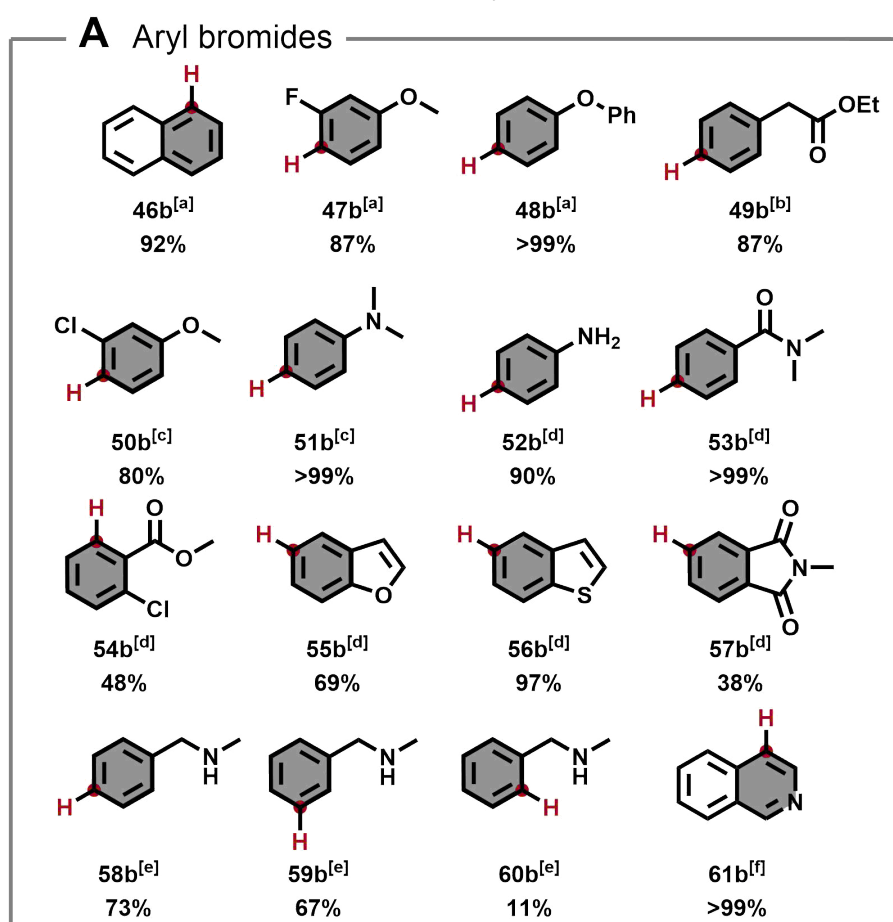
Figure 11: Contour plots illustrating the interactions between temperature and catalyst loading, and base and catalyst loading.

More than 30 aryl bromides and aryl chlorides were subjected to our newly optimised catalyst system, the results of which are summarised in Tables ???. In general, we observed that electron rich and weakly electron deficient substrates **46a–52a** are favoured in this reaction and can undergo dehalogenation possible under mild conditions and provide good to excellent yields (80 to >99%). On the other hand, comparatively harsher conditions were required for electron deficient aryl bromides **53a–61a**, as well as all aryl chlorides **62a–75a** which were tested.

Notably, by moderating the reaction temperature, we were able to promote chemoselective dehalogenation of anisoles **47a** and **50a** which both bear more than one halide atom (and thus more than one possible reaction site). Under equivalent reaction conditions were observed declines in HDH yield in phenylmethanamines **58a–60a** upon moving from *para*- to *meta*- to *ortho*- substitution. This could be either caused by a decrease in proximity between the inductively-withdrawing methylmethanimine and bromine atom or due to increased steric bulk at the reaction centre. HDH of representative heterocycles 4-bromo-1-benzofuran **55a** and 4-bromobenzo-1-furanthiophene **56a** furnished the corresponding congeners in 69% and 97% yield, respectively, at 80°C and 20 bar H_2 pressure. 5-Bromo-2-methylisoindoline-1,3-dione **57a** proved more challenging under these conditions, providing only a modest 38% yield of the expected product. Similarly, 4-bromoisquinoline **61a** was found to be a particularly challenging substrate, however, an increased temperature of 120°C led to product formation in quantitative yield.

Due to transesterification with our chosen solvent system, ethyl ester **49a** was reacted in aqueous ethanol (40%) with no issues resulting in an 87% yield of **49b**.

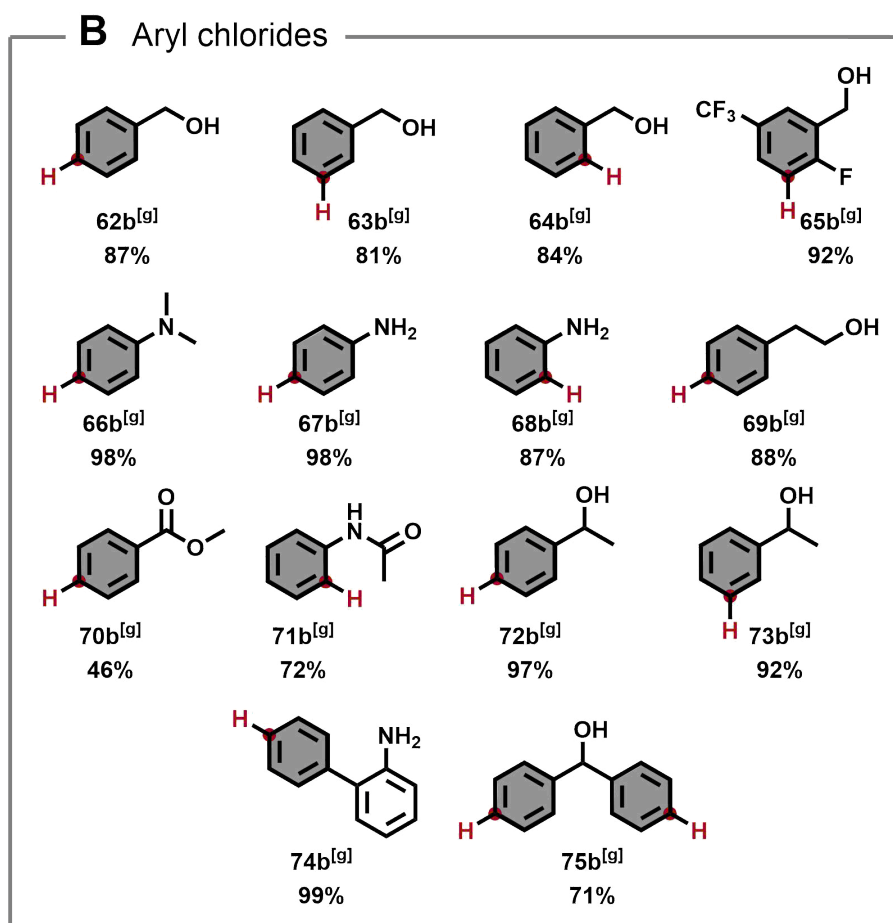
Besides obtaining a comparatively low dehalogenation yield for substrate **70b** (46%), which contains an electron withdrawing methyl ester substituent, all of the aryl chlorides tested were obtained in good to excellent yields (71–99%) at 130°C under 30 bar pressure of H_2 .

Table 14: HDH in Aryl Bromides^a

^aReaction conditions: **a** (0.5 mmol), Ni-Phen@TiO₂-800 (25 mg, ca. 3 mol % Ni), Et₃N (1.25 equiv), 20 bar H₂, 45°C, 2 ml MeOH:H₂O (1:1), 20 h. ^b50°C, 2 ml EtOH:H₂O (1:1). ^c60°C. ^d80°C. ^e30 bar H₂, 90°C. ^f30 bar H₂, 120°C.

The efficacy of our reaction was highlighted by the successful degradation of thermally inert substances. Tetrabromobisphenol A **76a**—a widely applied fire retardant and precursor for fire-resistant polymers—underwent complete HDH of all four bromine atoms to the expected product **76b** in 71% yield at 100°C. This transformation attests to the nickel catalyst's ability to convert highly stable compounds which are resistant to degradation into compounds which can readily be treated and disposed of.

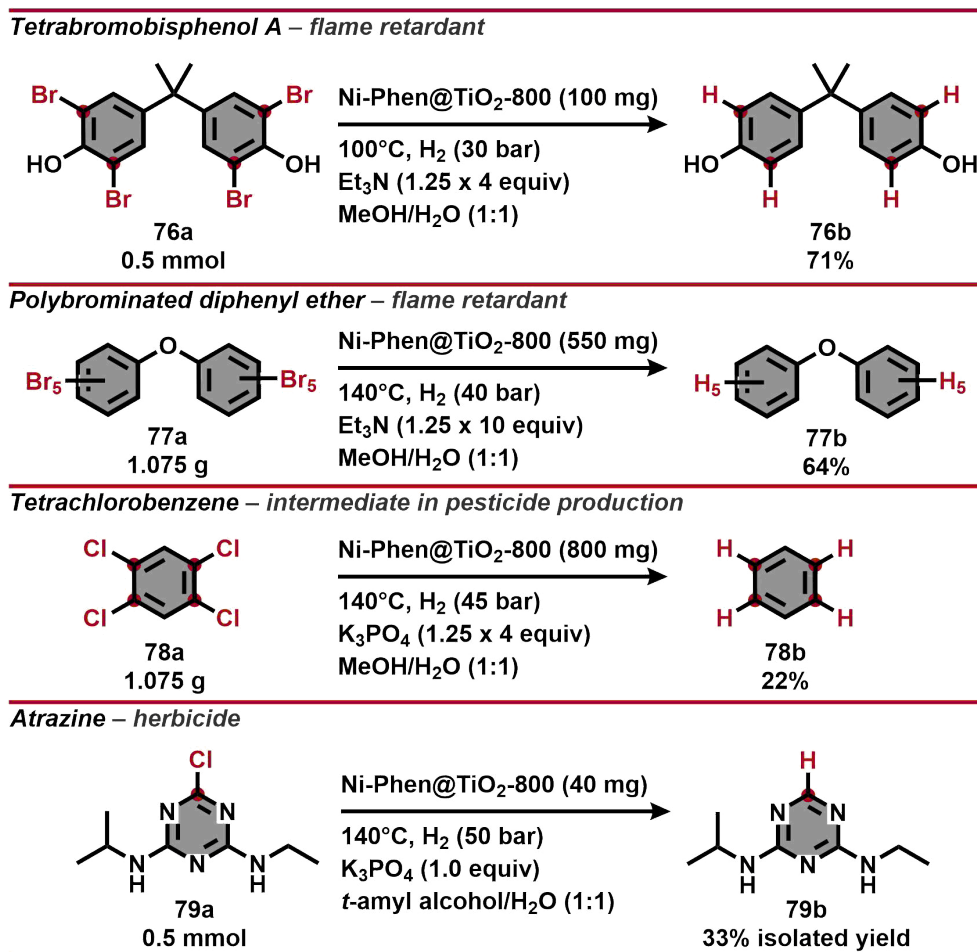
Upscaling was successfully demonstrated with gram-scale (5 mmol) HDHs of industrially relevant substrates. **77a** represents the class of polybrominated diphenylethers (PBDEs) which are recognised as persistent organic pollutants which tend to bioaccumulate in different or-

Table 15: HDH in Aryl Chlorides^a

^aReaction conditions: **a** (0.5 mmol), Ni-Phen@TiO₂-800 (25 mg, ca. 3 mol % Ni), Et₃N (1.25 equiv), 30 bar H₂, 130°C, 2 ml MeOH:H₂O (1:1), 20 h.

ganisms. Besides this, PBDEs are regarded as being highly resistant towards degradation. 1,2,4,5-tetrachlorobenzene **78a** is a precursor which is widely used in the production of herbicides and poses a unique demonstration of the catalyst's high capability of activating multiple C–Cl bonds in a clean and efficient manner. In both cases, full conversions and yields of 64% and 22% of the corresponding HDH products were achieved for **77b** and **78b**, respectively, using our catalytic protocol. We attribute the low yield of **78b** to the volatility of benzene.

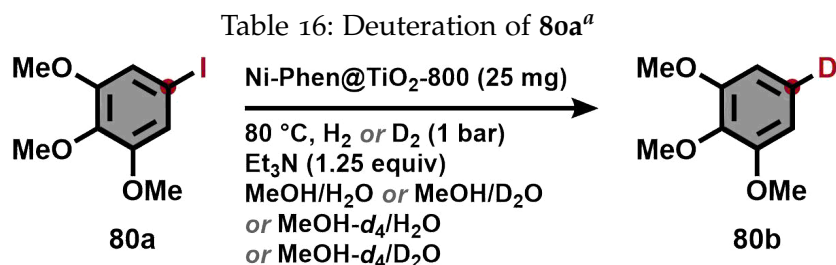
Syngenta's atrazine **79a** is a pre-emergent herbicide widely used in the United States and Australia for broad spectrum weed control. Despite its continued operation today, since 2004 it has been banned in the European Union due to its concentrations in groundwater which exceeded regulatory limits. When subjected to our nickel catalyst, this environmentally persis-



Scheme 10: HDH of tetrabromobisphenol A (**76a**), a PBDE (**77a**), 1,2,4,5-tetrachlorobenzene (**78a**), and atrazine (**79a**).

tent chlorinated triazole compound experienced HDH of its C–Cl bond to yield the corresponding product **79b** with 33% isolated yield.

There has been a recent surge in interest in developing new deuteration methods, which can greatly benefit the properties of drugs by significantly reducing rates of metabolism leading to less frequent dosing to achieve therapeutic effects. Accordingly, we explored the potential of using HDH for achieving deuterium incorporation. 5-Iodo-1,2,3-trimethoxybenzene **80a**—which undergoes full dehalogenation with Ni-Phen@TiO₂-800 using just 1 bar H₂ at 80°C—was exposed to deuterium sources for selective D-labelling at the 5-position on the benzene ring. Remarkably, very high D incorporation (86%) could be realised using a combination of MeOH-*d*₄ and D₂O under H₂ (see Table 16). Surprisingly, switching from hydrogen to deuterium gas quenched all reactivity and only starting material could be recovered from the reaction vessel. This observation is in agreement with increased bond strength of D–D



entry	solvent A	solvent B	reductant	d (%) ^b
1	D ₂ O	MeOH	H ₂ (1 bar)	49
2	H ₂ O	MeOH-d ₄	H ₂ (1 bar)	9
3	D ₂ O	MeOH-d ₄	H ₂ (1 bar)	86
4	H ₂ O	MeOH	D ₂ (1 bar)	<i>no reactivity</i>
5	D ₂ O	MeOH	D ₂ (1 bar)	<i>no reactivity</i>
6	H ₂ O	MeOH-d ₄	D ₂ (1 bar)	<i>no reactivity</i>
7	D ₂ O	MeOH-d ₄	D ₂ (1 bar)	<i>no reactivity</i>
8	H ₂ O	MeOH	D ₂ (6 bar)	<i>no reactivity</i>
9	D ₂ O	MeOH	D ₂ (6 bar)	<i>no reactivity</i>
10	H ₂ O	MeOH-d ₄	D ₂ (6 bar)	<i>no reactivity</i>
11	D ₂ O	MeOH-d ₄	D ₂ (6 bar)	<i>no reactivity</i>

^aReaction conditions: **80a** (0.5 mmol), Ni-Phen@TiO₂-800 (25 mg, ca. 3 mol %), Et₃N (1.25 equiv), in MeOH *or* MeOH-d₄ (1 mL) and H₂O *or* D₂O (1 mL), 1 bar H₂ *or* 1–6 bar D₂, 80°C, 18 h. ^bd-incorporation determined by ¹H-NMR.

compared to H–H and would explain an impedance in bond cleavage. From these data, we infer that the D₂O is the most effective deuterium source for deuteration of **80a**. From a practical point of view, it is important to note that D₂O is relatively inexpensive (as D-sources go) and it is the parent compound of other D-sources, including D₂.

SUMMARY AND OUTLOOK

The aim of this work was to develop new catalysts for the scission of highly inert C(sp³)-C(sp³) bonds. In particular we were interested in applying non-noble metals to facilitate the catalysis and to utilise air as a sustainable, non-toxic and highly abundant oxidant.

In detail, two copper catalysts—Cu(OTf)₂ and CuCl—were used for the oxidative cleavage of a wide range of aliphatic and aromatic tertiary amines, in addition to pharmaceutically relevant piperazines and morpholines. The applied catalysts were shown to work more efficiently in the presence of *N*-ligands, particularly pyridine. Notably, a series of spectroscopic methods, in addition to radical trapping experiments, has provided considerable mechanistic insight for the reaction. Herein, we have tentatively proposed a sound reaction mechanism.

An alternative system using a combination of cobalt and manganese metal salts was tested for the oxidative cleavage of C(sp³)-C(sp³) bonds and demonstrated enhanced reactivity towards derivatised morpholines. The performance of the catalysis was shown to benefit greatly by the presence of both metals in this bimetallic system. Once again, *N*-ligands proved to be highly influential towards the effectiveness of the catalysis, with *para*-methoxypyridine providing the greatest enhancement of the product yields. Radical trapping agents were demonstrated to quench the catalysis and allowed putative intermediates to be identified by GC-FID. Disappointingly, the reactivity could not be translated to accommodate piperazines or amines.

A third methodology for achieving our aims was realised using low cost, highly abundant and "biocompatible" iron. Unlike the previously described systems, *N,N*-diphenylpiperazine could be oxidatively cleaved in good yields. The reactivity also extended to morpholine substrates to provide good isolated yields of these coveted pharmaceutically-relevant cyclic motifs. Design of experiments was used to identify optimal regions of chemical space for the transformation and showed that high temperatures and pressures were vital to achieve good yields of the desired oxidised products.

In future it would be worthwhile to attempt C-C bond activation methodologies towards the valorisation of lignin. Such a compound, which is rich in heteroatoms and aromaticity might provide a source of highly desirable small molecules and improve lignin's status from a waste product (from the paper pulp industry) to a valued carbon feedstock.

Our work in C(sp³)-C(sp³) bond activation may be improved upon in the years that follow by continuing to explore the mutualistic effects of combining two (or more) different metals to enhance their individual reactivities; after all such an idea is not without its success in industry (see the AMOCO process).

As a final thought, whilst air proved to be a competent source of oxygen in our reactions, other oxidants can be envisioned, such as N₂O—an abundant and highly potent alternative oxidant. Needless to say, we didn't have success with it in our work.

SELECTED PUBLICATIONS

The following chapter contains the original publications wherein the previously presented research was reported. My contribution to each chapter is outlined in the subchapters.

5.1 PRACTICAL CATALYTIC CLEAVAGE OF C(SP³)-C(SP³) BONDS IN AMINES

Wu Li, Weiping Liu, David K. Leonard, Jabor Rabeah, Angelika Brückner, Kathrin Junge, and Matthias Beller.

Angew. Chem., Int. Ed. **2019**, *58*, 10693–10697.

International Edition: DOI: [10.1002/anie.201903019](https://doi.org/10.1002/anie.201903019)

German Edition: DOI: [10.1002/ange.201903019](https://doi.org/10.1002/ange.201903019)

© 2019 Wiley-VCH Verlag GmbH & Co. KGaA, Weinheim.

Electronic supporting information for this article is available free of charge at <https://doi.org/10.1002/anie.201903019>.

This manuscript was prepared in cooperation with Dr Wu Li and Dr Weiping Liu. I helped optimising the reaction conditions. Moreover, I took part in the substrate scope and in the writing process of the manuscript. I mainly assessed the analytical data and wrote the supporting information. My contribution accounts 30%.



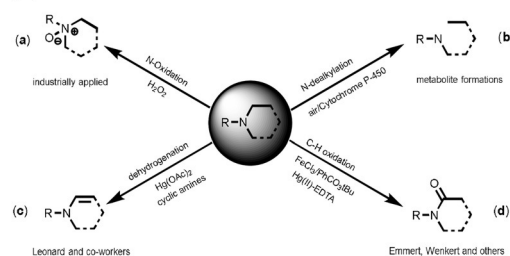
Practical Catalytic Cleavage of C(sp³)–C(sp³) Bonds in Amines

Wu Li, Weiping Liu, David K. Leonard, Jabor Rabeah, Kathrin Junge, Angelika Brückner, and Matthias Beller*

Abstract: The selective cleavage of thermodynamically stable C(sp³)–C(sp³) single bonds is rare compared to their ubiquitous formation. Herein, we describe a general methodology for such transformations using homogeneous copper-based catalysts in the presence of air. The utility of this novel methodology is demonstrated for C_α–C_β bond scission in > 70 amines with excellent functional group tolerance. This transformation establishes tertiary amines as a general synthon for amides and provides valuable possibilities for their scalable functionalization in, for example, natural products and bioactive molecules.

Carbon–carbon single bonds are arguably one of the least reactive “functional” groups in chemistry and biology.^[1] While in the past decades, the site-selective activation of C–H bonds attracted widespread interest,^[2] related transformations of C–C bonds are rare in the context of synthetic chemistry.^[3] Obviously, nonpolar C–C σ-bonds are both thermodynamically stable and lesser accessible,^[4] which makes their selective cleavage one of the most challenging transformations in chemistry.^[5] In contrast, several types of such transformations catalyzed by metalloenzymes are known in biology.^[6] Interestingly, in the active site of most of these enzymes (dioxxygenases) iron or copper metal ions are found,^[7] which productively use both dioxygen atoms in the metabolism of steroids (cholesterol)^[8] and amino acids (tryptophan)^[9] as well as xenobiotics.^[10] Notably, in synthetic chemistry the oxidative cleavage of C–C σ-bonds is only achieved using (over)stoichiometric amounts of hazardous oxidants such as O₃,^[11] NaIO₄, H₅IO₆, Pb(OAc)₄, and KMnO₄, which result often in poor functional group tolerance. Very recently, it has been demonstrated that these latter limitations can be overcome by so-called deconstructive functionalizations using AgNO₃ and ammonium persulfate as final oxidants.^[12] From a green and practical perspective there is still substantial need for selective methodologies, which make

(1) State-of-the-art oxidative transformations of tertiary amines.



(2) This work:

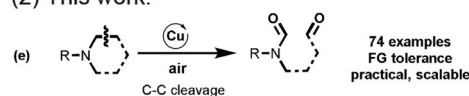


Figure 1. Oxidative transformation of tertiary amines. (a) N-Oxidation to amine oxides. (b) N-dealkylation (c) Oxidative dehydrogenation. (d) C–H oxidation. (e) Selective cleavage of C(sp³)–C(sp³) bonds in tertiary amines.

use of more benign oxidants. In this respect, air is the ideal reagent in terms of price and waste generation.^[13]

The oxidation of amines plays a vital role in nature from both transformative and mechanistic aspects.^[14] The main transformations currently known are summarized in Figure 1. Most prominent is the preparation of amine oxides using different oxidants such as hydrogen peroxide (Figure 1 a). In addition, N-dealkylation processes are known to be catalyzed by oxidases to yield the corresponding secondary amines (Figure 1 b).^[15] Much less explored is the synthesis of enamines from amines in the presence of stoichiometric amounts of mercuric(II) acetate as shown in Figure 1 c.^[16] Finally, the preparation of amides by α–C–H oxidation has been reported to some extent (Figure 1 d).^[17] Complementary to all of these known transformations, we herein communicate a general copper-catalyzed selective cleavage of C(sp³)–C(sp³) single bonds within amines using simply air (Figure 1 e).

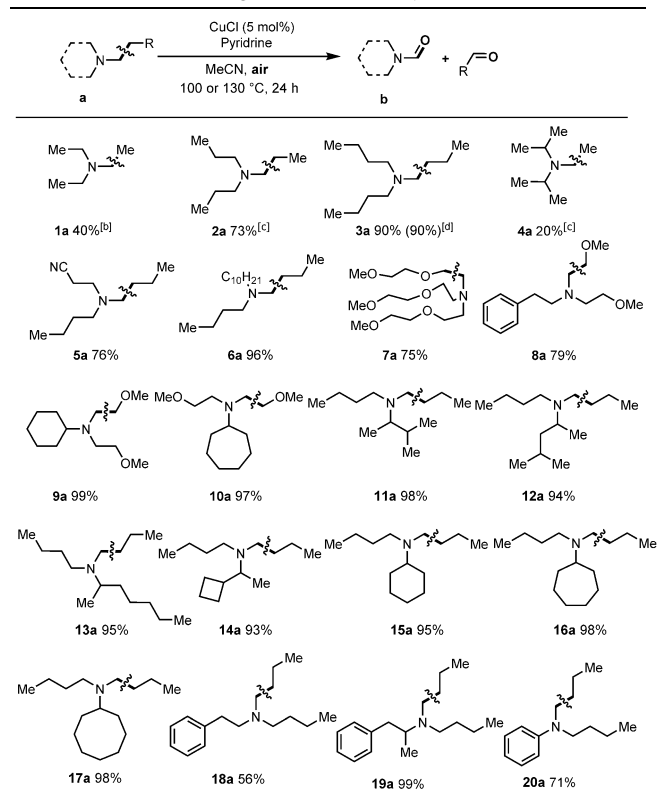
We commenced this work studying the C–H oxidation of industrially relevant tri-*n*-butylamine as a benchmark system using a broad range of metal salts, ligands, oxidants, and solvents. Surprisingly, employing copper salts under pressure of air resulted in the cleavage of C–C bonds leading to dibutylformamide **3b**.^[18] After optimization we obtained product **3b** in 90 % yield with very high selectivity by using 5 mol % CuCl and 2 equiv pyridine at 30 bar air and 100 °C in acetonitrile (Tables S1 and S2). It is worth noting that this reaction can be easily performed on a gram scale even in the presence of water.

Next, we were interested in evaluating the reactivity of other aliphatic amines. As shown in Table 1, 20 different amines underwent smooth and selective C–C bond cleavage

[*] Dr. W. Li, Dr. W. Liu, D. K. Leonard, Dr. J. Rabeah, Dr. K. Junge, Prof. Dr. A. Brückner, Prof. Dr. M. Beller
Leibniz-Institut für Katalyse e.V. an der Universität Rostock
Albert-Einstein Straße 29a, 18059 Rostock (Germany)
E-mail: matthias.beller@katalysis.de

Supporting information and the ORCID identification number(s) for the author(s) of this article can be found under:
<https://doi.org/10.1002/anie.201903019>.

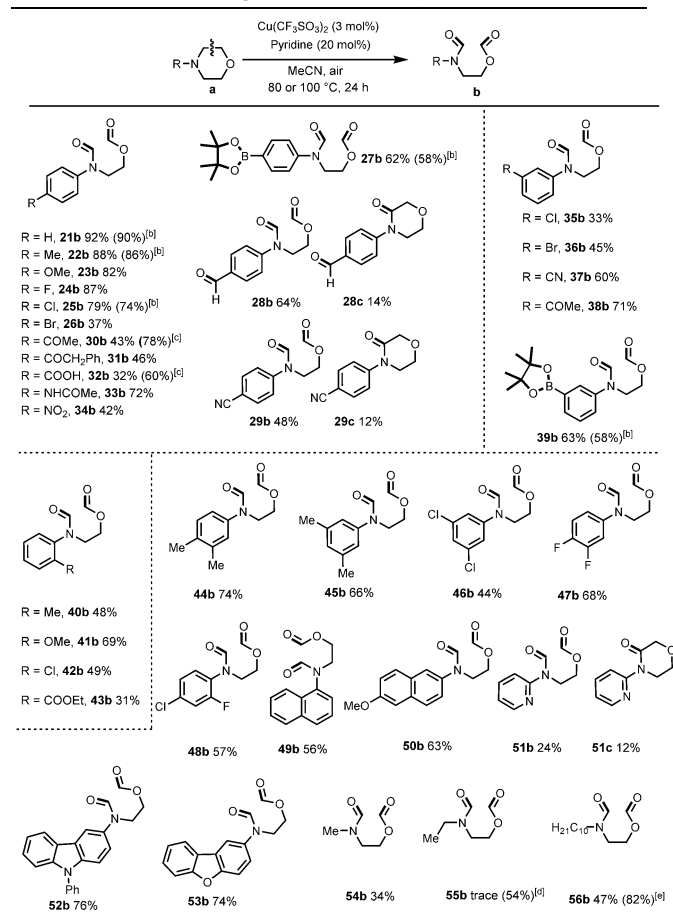
© 2019 The Authors. Published by Wiley-VCH Verlag GmbH & Co. KGaA. This is an open access article under the terms of the Creative Commons Attribution Non-Commercial NoDerivs License, which permits use and distribution in any medium, provided the original work is properly cited, the use is non-commercial, and no modifications or adaptations are made.

Table 1: C–C Bond cleavage reactions: tertiary amines.^[a]

[a] Reaction conditions: Substrates **a** (0.5 mmol), CuCl (5 mol%), and pyridine (2.0 eq.), 30 bar air, MeCN, 100 °C, isolated yield. [b] 10 mmol triethylamine, Cu(CF₃SO₃)₂ (5 mol%), 40 bar air, 130 °C. [c] 40 bar air, 130 °C. [d] 10 mmol scale.

to give the corresponding formamides **1b–20b** in general in high yields. Using inexpensive triethylamine shows the general possibility to synthesize *N,N*-diethylformamide, which is a less toxic alternative to the frequently used solvent *N,N*-dimethylformamide. However, for practical applications the procedure still has to be improved. Given the importance of nonsymmetrical amines, we explored the regioselective cleavage of carbon–carbon bonds in substrates containing different alkyl substituents or more than one potential site for functionalization. Gratifyingly, this protocol exhibits both excellent chemoselectivity and regioselectivity (**4a–10a**). For example, several substituted butylamines containing C2–C6 branched alkyl groups and C4–C8 cyclic alkyl groups were converted into the desired products with $\geq 93\%$ yields (**11b–17b**). Notably, *N,N*-dibutyl 2-phenylethan-1-amine afforded the butyl-cleaved product in 56% yield along with trace amounts of benzaldehyde and *N,N*-bis(2-methoxyethyl)formamide, which is observed by GC–MS (**18b**) (Scheme S2). The more sterically encumbered *N,N*-dibutyl (1-phenylpropan-2-yl) amine gave the desired product quantitatively (**19b**). Finally, *N,N*-dibutylaniline afforded the oxidized product (**20b**) in 71% yield.

Nitrogen heterocycles such as morpholines and piperazines constitute privileged scaffolds in modern drugs.^[19] In fact, several out of the top 50 pharmaceuticals belong to this class of compounds. Thus, their preparation and derivatization continues to attract considerable attention. As shown in

Table 2: C–C Bond cleavage reactions of morpholines.^[a]

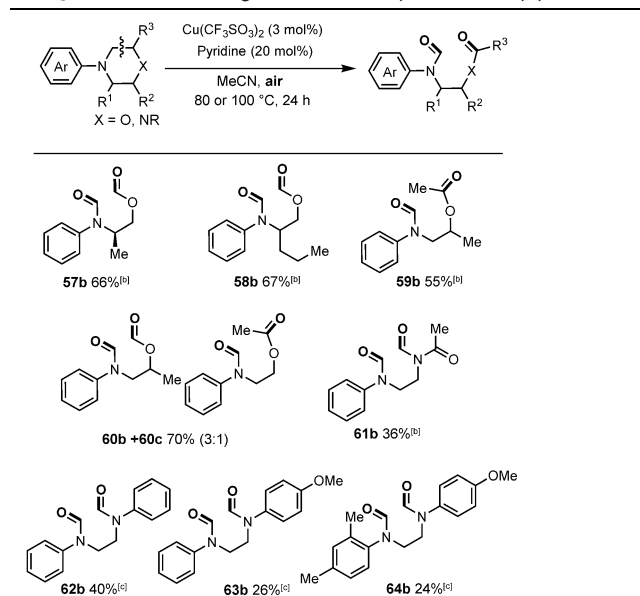
[a] Reaction conditions: Substrates **a** (0.5 mmol), Cu(CF₃SO₃)₂ (3 mol%) and pyridine (20 mol%), 30 bar air, MeCN, 100 °C, isolated yield. [b] 20 bar air, 80 °C. [c] 30 bar air, 120 °C. [d] CuCl (5 mol%) and pyridine (2.0 eq.), 30 bar air, 100 °C. [e] 0.5 mmol pyridine, 40 bar air and 130 °C.

Table 2, 33 different *N*-(hetero)aryl morpholines provided the desired products under a set of standard conditions (3 mol % Cu(CF₃SO₃)₂, 20 mol % pyridine, MeCN, 100 °C, 24 hours) with often excellent selectivity (Tables S3 and S4; see the Supporting Information for further experimental details.) The transformations can be easily run on a gram scale as shown by conversion of *N*-phenylmorpholine (**21a**), which gave 68% isolated yield of **21b** [Eq. (S2)]. More sensitive benzylic C–H bonds in **22b**, **40b**, **44b** and **45b**, as well as a methoxy substituent in **23b** are well tolerated giving the desired products in 48–87% isolated yields. *N*-Aryl morpholines bearing -F, -Cl, -Br, -CN, and -COOMe groups are shown to be compatible with this procedure, too (**24b**, **25b**, **26b**, **29b**, **35b**, **36b**, **37b**, **42b**, **43b**, **46b**, **47b**, and **48b**). Although homogeneous aerobic copper catalysis is known to cleave α -C–C bonds of ketones,^[20] the ketone groups were untouched with our [Cu]/air system (**30b**, **31b**, and **38b**). Most surprisingly, even the formyl-substituted starting material gave mainly the C–C bond-cleavage product **28b** in 64% yield and no expected acid was formed. To the best of our knowledge this is a rare example of oxidative C–C cleavage in the presence of an aldehyde. Interestingly, along with C–C cleavage also formation of the amide **28c** resulted. Similar

side products were observed in the case of **29c** and **51c**. Substrates bearing one or more electron-withdrawing functional groups such as ketones, nitro, carboxylic acid, and ester were also active (**30b**, **31b**, **32b**, **34b**, **38b**, and **43b**). Boron-containing compounds represent important building blocks for all kinds of life science molecules and allow for numerous further valorizations. Gratifyingly, **27a** and **39a** gave the preferred products in 62% and 63% yield. Moreover, a 72% yield of the amide-containing product **33b** was isolated under the standard conditions. In addition, 4-(naphthalen-1-yl)morpholine (**49a**) and 4-(6-methoxynaphthalen-2-yl)morpholine (**50a**) provided **49b** and **50b** in 56% and 63% yield, respectively. Even nitrogen- and oxygen-heteroaryl-substituted morpholines such as 4-(pyridin-2-yl)morpholine (**51a**), 4-(9-phenyl-9*H*-carbazol-3-yl)morpholine (**52a**), and 4-(dibenzo[*b,d*]furan-2-yl)morpholine (**53a**) underwent smooth oxidative cleavage in the presence of the catalytic system. We were pleased to find that the alkyl-substituted derivatives undergo a similar transformation. Indeed, *N*-methylmorpholine, *N*-ethylmorpholine, and *N*-decylmorpholine yielded the cleavage products **54b–56b** in 34–82% yield. For comparison,^[18a] we used commercially available CuO and Cu₂O as the catalysts for the cleavage of morpholines such as 4-(*p*-tolyl)morpholine (**22a**), 4-morpholinobenzaldehyde (**28a**), and 1-(4-morpholinophenyl)ethan-1-one (**30a**) (Table S5). All these results (yields < 32%) show that the heterogeneous systems CuO and Cu₂O are not comparable to the Cu(CF₃SO₃)₂/pyridine system and are less efficient, especially for functionalized substrates (Tables S2, S4, and S5).

As shown in Table 3, ring-substituted morpholines reacted in a similar manner and provided the corresponding products (**57b–60b**). Notably, a methyl group in C2 position of the

Table 3: C–C Bond cleavage reactions: morpholines and piperazines.^[a]

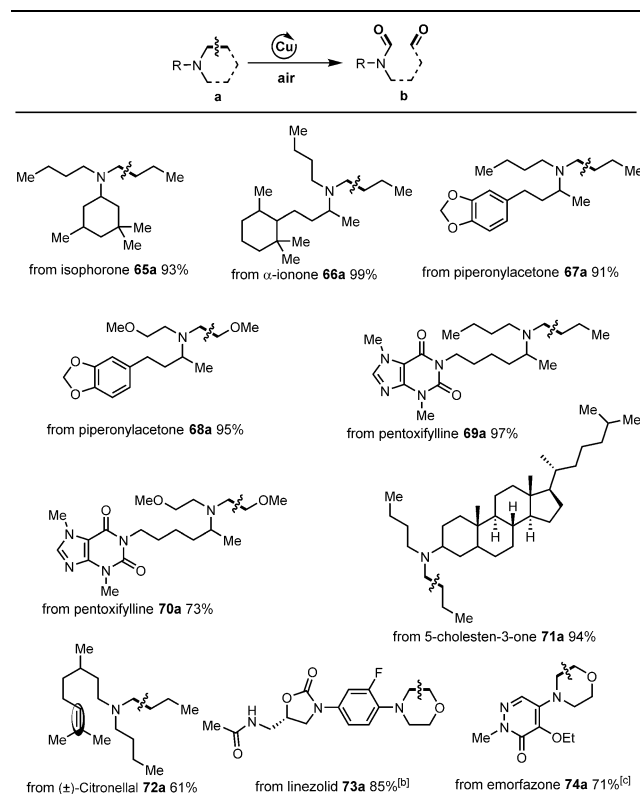


[a] Reaction conditions: Substrates **a** (0.5 mmol), Cu(CF₃SO₃)₂ (3 mol%) and pyridine (20 mol%), 20 bar air, MeCN, 80 °C, isolated yield. [b] 30 bar air, 100 °C. [c] 2.0 mmol instead of 20 mol% pyridine, 30 bar air, 100 °C.

morpholine ring allowed for selective cleavage of the C5–C6 vs. the C2–C3 bond (75:25), while alkyl substituents in the 3-position led exclusively to activation of the nonsubstituted bond. Apart from morpholines, also the oxidative cleavage of piperazines was investigated. Although somewhat lower yields of the corresponding products (**61b–64b**) were observed, the products can be easily isolated due to their different physical properties. In addition, we have also tried *N*-phenylpyrrolidine and *N*-phenylpiperidine under the standard conditions, but no C–C cleavage products were observed.

To demonstrate the utility of this copper-catalyzed oxidation reaction, we evaluated late-stage C–C bond cleavage reactions of functionalized natural products and bioactive molecules including derivatives of isophorone, terpenoids such as ionone, citronellal, piperonylacetone, and 5-cholesten-3-one. As shown in Table 4, the corresponding

Table 4: Late-stage C–C bond cleavage of modified natural products and bioactive molecules.^[a]



[a] Yields refer to isolated yields of products after chromatography. Standard conditions: tertiary amines (0.5 mmol), CuCl (5 mol%) and pyridine (2.0 eq.), 30 bar air, MeCN, 100 °C. [b] Linezolid (0.5 mmol), Cu(CF₃SO₃)₂ (3 mol%) and pyridine (20 mol%), 20 bar air, MeCN, 80 °C, isolated yield. [c] Emorfazone (0.5 mmol), Cu(CF₃SO₃)₂ (3 mol%) and pyridine (2.0 equiv.), 40 bar air, 130 °C.

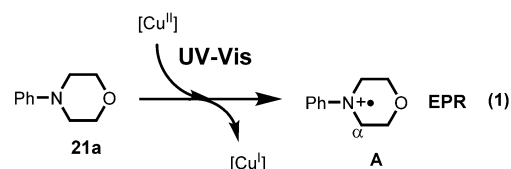
amides were obtained in high yield and selectivity (**65b**, **66b**, **67b**, **68b**, **71b**, and **72b**). Notably, in the case of **72b** the cleavage of the C _{α} (sp³)–C _{β} (sp³) single bond proceeded selectively in the presence of a C=C double bond! Furthermore, the amination product of pentoxifylline, a xanthine derivative used to treat muscle pain, was evaluated and the corresponding products were smoothly isolated (**69b** and

70b). Finally, to showcase late-stage drug modifications as well as to prepare putative drug metabolites, we performed the reactions of linezolid (**73a**), which is a morpholine-containing antimicrobial used for the treatment of infections caused by Gram-positive bacteria, and the nitrogen-containing heterocycle emorfazone (**74a**), a nonsteroidal anti-inflammatory drug used to treat dental pain and inflammation. Under aerobic conditions in the presence of homogeneous copper, **73b** and **74b** were formed in good yield with excellent selectivity.

To understand the mechanism of this general oxidative cleavage reaction, several experiments and in situ spectroscopic investigations were performed using *N*-phenylmorpholine (**21a**). Firstly, to prove the stability of the cocatalyst/ligand, which significantly improves the conversion, deuterated [D₅]pyridine was employed instead of pyridine. However, a standard catalytic experiment revealed only [D₅]pyridine was detected by GC-MS after 24 h [Eq. (S3)]. To understand the formation of the oxidative cleavage products, possible intermediates 4-phenylmorpholin-3-one (**75a**) and 4-phenylmorpholine-2,3-dione (**76a**) were submitted to the regular reaction conditions [Eqs. (S4) and (S5)]. Both compounds proved to be stable and no formation of **21b** was observed. Thus, these compounds can be excluded as putative intermediates. On the other hand, trapping experiments demonstrate the importance of radical intermediates in this transformation. When 2 equivalents of TEMPO (2,2,6,6-tetramethyl-1-piperidinyloxy) or BHT (2,6-di-*tert*-butyl-4-methylphenol) were added, the reaction completely stopped [Eq. (S6)], along with the dehydrogenated product 4-phenyl-3,4-dihydro-2*H*-1,4-oxazine detected by GC-MS analysis [Eq. (S7), Scheme S3]. A related intermediate was observed by GC-MS in the oxidation of tri-*n*-butylamine, too (Figure S1 and Scheme S1).

Notably, in the absence of air *N*-phenylmorpholine (**21a**) gave no desired product, even in the presence stoichiometric amounts of copper(II) pre-catalyst [Eq. (S8)]. In order to gain more details on this copper/air catalysis, we performed kinetic studies utilizing **21a** under the standard conditions. As shown in Figure S2, no induction period is required for the in situ generation of the active catalytic species and 32% yield of the product **21b** is formed in the first hour. However, no intermediates were detected by gas chromatography during the whole process. Finally, we added ¹⁸O-labeled water to the model reaction under standard conditions; however, no ¹⁸O-incorporated product was observed. This clearly demonstrates that only O₂ from the air acts as the oxygen donor in this transformation [Eq. (S9)]. Finally, EPR and UV/Vis investigations were performed to further explore the reaction steps. The Cu^{II} precursor reacts with **21a** via single-electron transfer (SET) to generate the free-radical cation **A** and Cu^I [Eq. (1)]. This assumption is confirmed by EPR investigations, which showed that addition of *N*-phenylmorpholine to a Cu^{II} solution under inert atmosphere resulted in a fast disappearance of the Cu^{II} EPR signal and the formation of a temporary signal at *g* = 2.004 with unresolved hyperfine structure typical for an organic radical **A** (Figure S3).

The reduction of Cu^{II} to Cu^I by **21a** is also evident from UV/Vis measurements, which showed the decay of the ligand-



to-metal charge transfer (LMCT) and the weak d-d transition bands of Cu^{II} below 300 nm and around 750 nm, while new metal-to-ligand charge transfer bands (MLCT) of Cu^I at 320 and 466 nm appeared (Figure S4). In addition, transient UV/Vis bands at 913 and 1034 nm were detected, which we assign tentatively to the formation of radical intermediate **A** [Eq. (1)]. No further detailed knowledge has been obtained from in situ EPR investigations, since the next, very complex step in the catalytic reaction might involve H or proton abstraction from amino radical as well as activation of O₂ by Cu^I or intermediate **A** to form superoxide species.

In conclusion, we have developed a general protocol for the aerobic cleavage of C_α(sp³)-C_β(sp³) single bonds in amines (> 70 examples) using a practical and inexpensive copper catalyst. This system is effective for the conversion of industrial bulk amines as well as for the late-stage functionalization of modified natural products and bioactive molecules. Complementary to other oxidation reactions of amines, excellent site-selectivity and functional-group tolerance are observed, for example, aldehyde and olefins remained untouched.

Acknowledgements

We gratefully acknowledge the support from the Federal Ministry of Education and Research (BMBF) and the State of Mecklenburg-Vorpommern. We thank Dr. Wolfgang Baumann, Susann Buchholz, and Dr. Christine Fischer for their excellent analytical support, and Dr. Haijun Jiao, Zhihong Wei, Bianca Wendt, and Dr. Basudev Sahoo (all at LIKAT) for valuable discussions.

Conflict of interest

The authors declare no conflict of interest.

Keywords: air · amines · C–C cleavage · copper · morpholines

How to cite: *Angew. Chem. Int. Ed.* **2019**, *58*, 10693–10697
Angew. Chem. **2019**, *131*, 10803–10807

- [1] a) M. Murakami, N. Ishida, *J. Am. Chem. Soc.* **2016**, *138*, 13759–13769; b) F. Chen, T. Wang, N. Jiao, *Chem. Rev.* **2014**, *114*, 8613–8661; c) M. Murakami, N. Ishida, *Nat. Chem.* **2017**, *9*, 298–299.
- [2] a) T. W. Lyons, M. S. Sanford, *Chem. Rev.* **2010**, *110*, 1147–1169; b) J. He, M. Wasa, K. S. L. Chan, Q. Shao, J. Q. Yu, *Chem. Rev.* **2017**, *117*, 8754–8786.
- [3] a) J. B. Roque, Y. Kuroda, L. T. Gottemann, R. Sarpong, *Science* **2018**, *361*, 171–174; b) Y. Xia, G. Lu, P. Liu, G. Dong, *Nature* **2016**, *539*, 546–550; c) J. Liu, X. Qiu, X. Huang, X. Luo, C.

- Zhang, J. Wei, J. Pan, Y. Liang, Y. Zhu, Q. Qin, S. Song, N. Jiao, *Nat. Chem.* **2019**, *11*, 71–77; d) E. Ota, H. Wang, N. L. Frye, R. R. Knowles, *J. Am. Chem. Soc.* **2019**, *141*, 1457–1462.
- [4] a) A. Masarwa, D. Didier, T. Zabrodski, M. Schinkel, L. Ackermann, I. Marek, *Nature* **2014**, *505*, 199–203; b) M. Gozin, A. Weisman, Y. Ben-David, D. Milstein, *Nature* **1993**, *364*, 699–701.
- [5] C. J. Allpress, L. M. Berreau, *Coord. Chem. Rev.* **2013**, *257*, 3005–3029.
- [6] a) S. S. Stahl, *Angew. Chem. Int. Ed.* **2004**, *43*, 3400–3420; *Angew. Chem.* **2004**, *116*, 3480–3501; b) C. E. Elwell, N. L. Gagnon, B. D. Neisen, D. Dhar, A. D. Spaeth, G. M. Yee, W. B. Tolman, *Chem. Rev.* **2017**, *117*, 2059–2107; c) K. V. N. Esguerra, J. P. Lumb, *Angew. Chem. Int. Ed.* **2018**, *57*, 1514–1518; *Angew. Chem.* **2018**, *130*, 1530–1534.
- [7] a) T. J. Osberger, D. C. Rogness, J. T. Kohrt, A. F. Stepan, M. C. White, *Nature* **2016**, *537*, 214–219; b) A. E. Wendlandt, A. M. Suess, S. S. Stahl, *Angew. Chem. Int. Ed.* **2011**, *50*, 11062–11087; *Angew. Chem.* **2011**, *123*, 11256–11283.
- [8] H. al Kandari, N. Katsumata, S. Alexander, M. A. Rasoul, *J. Clin. Endocrinol. Metab.* **2006**, *91*, 2821–2826.
- [9] J. Basran, I. Efimov, N. Chauhan, S. J. Thackray, J. L. Krupa, G. Eaton, G. A. Griffith, C. G. Mowat, S. Handa, E. L. Raven, *J. Am. Chem. Soc.* **2011**, *133*, 16251–16257.
- [10] F. Varfaj, S. N. Zulkifli, H. G. Park, V. L. Challinor, J. J. De Voss, P. R. Ortiz de Montellano, *Drug Metab. Dispos.* **2014**, *42*, 828–838.
- [11] a) F. Saliu, M. Orlandi, M. Bruschi, *ISRN Org. Chem.* **2012**, 281642; b) R. Suarez-Bertoa, F. Saliu, M. Bruschi, B. Rindone, *Tetrahedron* **2012**, *68*, 8267–8275.
- [12] J. B. Roque, Y. Kuroda, L. T. Gottemann, R. Sarpong, *Nature* **2018**, *564*, 244–248.
- [13] a) D. Hruszkewycz, S. McCann, S. Stahl, *Liquid Phase Aerobic Oxidation Catalysis*, Wiley-VCH, Weinheim, **2016**, pp. 67–83; b) L. Que, Jr., W. B. Tolman, *Nature* **2008**, *455*, 333–340; c) M. J. Schultz, M. S. Sigman, *Tetrahedron* **2006**, *62*, 8227–8241; d) Q. Wu, Y. Luo, A. Lei, J. You, *J. Am. Chem. Soc.* **2016**, *138*, 2885–2888; e) K. Wu, Z. Huang, Y. Ma, A. Lei, *RSC Adv.* **2016**, *6*, 24349–24352.
- [14] M. T. Schümperli, C. Hammond, I. Hermans, *ACS Catal.* **2012**, *2*, 1108–1117.
- [15] J. Rose, N. Castagnoli, *Med. Res. Rev.* **1983**, *3*, 73–88.
- [16] N. J. Leonard, A. S. Hay, R. W. Fulmer, V. W. Gash, *J. Am. Chem. Soc.* **1955**, *77*, 439–444.
- [17] C. J. Legacy, A. Wang, B. J. O'Day, M. H. Emmert, *Angew. Chem. Int. Ed.* **2015**, *54*, 14907–14910; *Angew. Chem.* **2015**, *127*, 15120–15123.
- [18] For a similar copper oxide catalyzed reaction of tri-*n*-butyl amine see: a) M. Wang, X.-K. Gu, H.-Y. Su, J.-M. Lu, J.-P. Ma, M. Yu, Z. Zhang, F. Wang, *J. Catal.* **2015**, *330*, 458–464; for photocatalytic cleavage reactions see: b) Y. Zhao, S. Cai, J. Li, D. Z. Wang, *Tetrahedron* **2013**, *69*, 8129–8131; c) W. Ji, P. Li, S. Yang, L. Wang, *Chem. Commun.* **2017**, *53*, 8482–8485; for metabolite studies using a Cu catalyst see: d) J. Genovino, S. Lutz, D. Sames, B. B. Toure, *J. Am. Chem. Soc.* **2013**, *135*, 12346–12352.
- [19] M. Al-Ghorbani, B. A. Begum, Zabiulla, S. V. Mamatha, S. A. Khanum, *J. Chem. Pharm. Res.* **2015**, *7*, 281–301.
- [20] A. S. Tsang, A. Kapat, F. Schoenebeck, *J. Am. Chem. Soc.* **2016**, *138*, 518–526.

Manuscript received: March 11, 2019

Revised manuscript received: May 16, 2019

Accepted manuscript online: May 24, 2019

Version of record online: July 1, 2019

5.2 IMPROVED BIMETALLIC COBALT–MANGANESE CATALYSTS FOR SELECTIVE OXIDATIVE CLEAVAGE OF MORPHOLINE DERIVATIVES

David K. Leonard, Wu Li, Kathrin Junge, and Matthias Beller.

ACS Catal. **2019**, *9*, 11125–11129.

DOI: [10.1021/acscatal.9b03476](https://doi.org/10.1021/acscatal.9b03476)

© 2019 American Chemical Society.

Electronic supporting information for this article is available free of charge at <https://doi.org/10.1002/acscatal.9b03476>.

This manuscript was prepared in cooperation with Dr Wu Li. Most experimental work was performed by myself, including the optimisation of the reaction conditions, exploration of the substrate scope and writing the manuscript. I also assessed the analytical data and wrote the supporting information. My contribution accounts 70%.

Improved Bimetallic Cobalt–Manganese Catalysts for Selective Oxidative Cleavage of Morpholine Derivatives

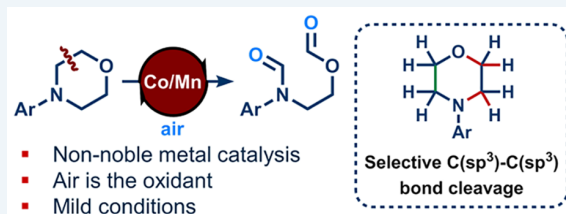
David K. Leonard, Wu Li, Kathrin Junge, and Matthias Beller*^{1b}

Leibniz Institute for Catalysis at the University of Rostock, Albert-Einstein-Straße 29a, 18059 Rostock, Germany

Supporting Information

ABSTRACT: Catalytic methods for the site-selective scission of C(sp³)–C(sp³) bonds remain scarcely explored in contrast to the vast literature on C–C coupling. In view of this, we report a means of oxidative C–C single-bond cleavage in morpholines, made possible by a synergy between cobalt and manganese catalysts using air as a benign oxidant. We demonstrate the synthetic utility of this system with the late-stage oxidative cleavage of Linezolid.

KEYWORDS: manganese, cobalt, oxidation, C–C bond activation, heterocycles



Despite being so highly prevalent in the scaffold of organic compounds, cleavage of C(sp³)–C(sp³) bonds remains a

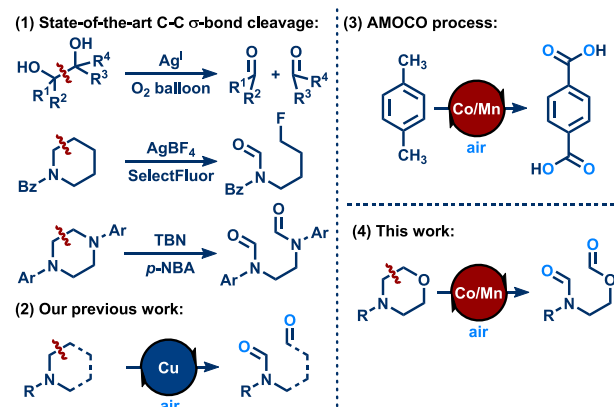


Figure 1. Selected examples of C–C bond cleavage reactions and Co/Mn-catalyzed oxidations.^{9–12}

real synthetic challenge, particularly in the presence of more reactive functional groups. C–C single bonds are kinetically stable because of steric hindrance and the directional nature of spⁿ-hybridized orbitals used in covalent bonding. Additionally, oxidative addition of C–C bonds is difficult to achieve thermodynamically, as the strength of M–H bonds exceeds that of M–C bonds.¹

In traditional synthetic methods (e.g., the Criegee and Malaprade reactions), chemists employed oxidants, such as O₃,² NaIO₄,³ HIO₄,⁴ Pb(OAc)₄,⁵ and KMnO₄, to enable C–C bond scission. Regrettably, these harsh oxidizing reagents are unsuitable for most substrates containing more reactive functional groups. Thus, mild catalytic protocols for C–C bond activations are in demand as novel deconstructive strategies and functionalizations of organic compounds.

Table 1. Co and Mn Catalysts for C–C Bond Cleavage in *N*-Phenylmorpholine^a

entry	catalyst I	catalyst II	yield 1b (%) ^d
1	Mn(OAc) ₂ ·4H ₂ O ^b		trace
2	Mn(OAc) ₂ ·4H ₂ O		26
3		CoBr ₂ ^b	10
4		Co(OAc) ₂ ·4H ₂ O	13
5	Mn(OAc) ₂ ·4H ₂ O	Co(OAc) ₂ ·4H ₂ O	60 ^c
6	Mn(OAc) ₂ ·4H ₂ O	Co(OAc) ₂ ·4H ₂ O	96
7	Mn(OAc) ₂ ·4H ₂ O	CoBr ₂	94
8		Cu(OTf) ₂	55

^aReaction conditions: 1a (0.5 mmol), catalyst I (5 mol %), catalyst II (5 mol %), pyridine (20 mol %), in MeCN (2 mL), 20 bar air, 80 °C.

^bCatalyst I/II (10 mol %). ^cKBr (5 mol %) added. ^dYields determined by gas chromatograph-flame ionization detector (GC-FID) using *n*-dodecane as an internal standard.

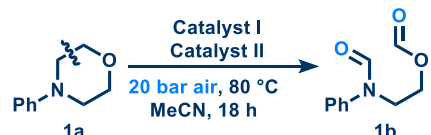
Furthermore, this field may even lead to innovative methods for breaking biomass into high-value chemicals/fuels, or to “crack” fossil fuel feedstocks with greater efficiency and improved selectivity.

In nature, several metalloenzymes are capable of aerobic C–C single-bond cleavages under mild conditions and play a key role in animal metabolism. Examples of such reactivity is shown by the diketone-cleaving enzyme (Dke 1), capable of oxidatively cleaving acetylacetone into less toxic metabolites,⁶

Received: August 16, 2019

Revised: October 22, 2019

Published: October 24, 2019

Table 2. Variation of Catalysts and Optimization^a


entry	catalyst I	catalyst II	ligand	yield 1b ^b (%)
1	Mn(OAc) ₂ ·4H ₂ O	Co(acac) ₃	Py	19
2	Mn(OAc) ₂ ·4H ₂ O	Co(OAc) ₂ ·4H ₂ O		54
3	MnBr ₂	Co(OAc) ₂ ·4H ₂ O	Py	63
4	Mn(acac) ₂	Co(OAc) ₂ ·4H ₂ O	Py	72
5	MnCl ₂	Co(OAc) ₂ ·4H ₂ O	Py	92
6	Mn(OAc) ₂ ·4H ₂ O	CoBr ₂	Py	94
7	Mn(OAc) ₂ ·4H ₂ O	Co(OAc) ₂ ·4H ₂ O	Py	96

^aReaction conditions: **1a** (0.5 mmol), catalyst I (5 mol %), catalyst II (5 mol %), ligand (20 mol %) in MeCN (2 mL), 20 bar air, 80 °C.
^bYields determined by GC-FID using *n*-dodecane as an internal standard.

2-hydroxyethylphosphonate dioxygenase (HEPD)⁷ and 2,4-dihydroxyacetophenone dioxygenase (DAD).⁸ Remarkably, one of the key features of these enzymes is that they all contain iron metal ions, thus demonstrating the ability of non-noble metals to cleave C–C σ -bonds under mild conditions.


Drug compounds are also sensitive to metabolic pathways which alter their physicochemical properties and toxicity. Thus, the ability to synthesize and characterize drug metabolites may greatly benefit the pharmaceutical industry by guiding the selection of safe and viable drug candidates.

Modern developments have enabled C(sp³)–C(sp³) bonds to be utilized as synthons for various structural diversification strategies. The state-of-the-art publications in this field include the following (Figure 1): the deconstructive fluorination of *N*-heterocycles using AgBF₄ and SelectFluor;⁹ the AgOTf-catalyzed cleavage of 1,2-diols;¹⁰ the Cu(I)-mediated cleavage of amines;¹¹ and *tert*-butyl nitrite (TBN)-enabled bond

activations in diarylpiperazines.¹² In summary, these works highlight that the cleavage of C–C σ -bonds is feasible under mild conditions and need not be restricted to simple substrates.

In a similar fashion to C–C bond activations, the structural diversification of C–H bonds is hindered by their inertness and pervasiveness within the framework of organic compounds. These initial restraints have been tackled over several decades of intense focus, which has led to a number of successful industrial developments, including the AMOCO process.¹³ This process has been adopted worldwide for the autoxidation of *para*-xylene to terephthalic acid,¹⁴ a valuable precursor for condensation polymerizations. Interestingly, this reaction uses a combination of two homogeneous catalysts, in addition to a source of bromide, which acts as a promoter. The key to the success of this reaction is a unique Co/Mn/Br combination, which introduces new catalytic pathways to increase the catalyst activity by 16 times, compared to a single cobalt catalyst.¹³ Reminiscently, we herein report a method for the selective cleavage of C(sp³)–C(sp³) bonds within functionalized morpholines using a combination of cobalt and manganese catalysts under aerobic conditions (Figure 1).

From the outset we were investigating the ability of non-noble metals for the cleavage of C–C single bonds under air. Inspired by our recent work using Cu catalysts,¹¹ we tested various metal species for the site-selective cleavage of *N*-phenylmorpholine **1a**, applying 20 bar of air at 80 °C. While Pd(OAc)₂, Ru(acac)₃, RuCl₃, Fe(OAc)₂, Co(OAc)₂·4H₂O, CoBr₂, AgCF₃SO₃, Ag₂CO₃, Mn(OAc)₂·4H₂O, Mn(acac)₂, MnCl₂, and MnO₂ displayed only low activity for the desired transformation (Table S1), to our delight, we discovered that by using Mn(II) and Co(II) salts in tandem, we could realize a dramatic increase in catalytic activity. As a result, we observed an increase in the yield of 2-(*N*-phenylformamido)ethyl formate (**1b**) from 10% to 94% (Table 1). In contrast to the aforementioned AMOCO process, the addition of a bromide source (KBr) was disadvantageous here (Table 1, entry 5).

Table 3. Influence of *N*-Containing Ligands on the Benchmark Reaction^a


Ligand	Yield (%)
No additive	24%
L1	82%
L2	49%
L3	0%
L4	61%
L5	6%
L6	0%
L7	40%
L8	86%
L9	17%
L10	27%
L11	57%
L12	32%
L13	33%
L14	0%
L15	0%
L16	59%
L17	0%
L18	31%
L19	42%

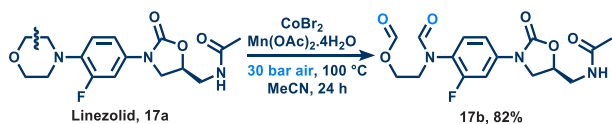
^aReaction conditions: **1a** (0.5 mmol), CoBr₂ (10 mol %), Mn(OAc)₂·4H₂O (5 mol %), ligand (20 mol %) in MeCN (2 mL), 10 bar air, 60 °C. Yields determined by GC-FID using *n*-dodecane as an internal standard.

Table 4. C–C Bond Cleavage Reactions of Morpholines^a

entry	product(s)	T (°C)	P (bar)	yield (%) ^b	entry	product(s)	T (°C)	P (bar)	yield (%) ^b
1		60	20	96	9		60	20	90
2		60	20	>99	10		60	20	84
3		60	20	66	11		100	30	70
4		60	20	85	12		60	20	56
5		100	30	43	13		100	30	81
6		100	30	77	14		100	30	60
7		100	30	>99	15		100	30	27 ^c
8		120	20	90	16		120	20	17 ^c

^aReaction conditions: **1a** (0.5 mmol), CoBr₂ (5 mol %), Mn(OAc)₂·4H₂O (10 mol %), pyridine (20 mol %) in MeCN (2 mL). ^bIsolated yields by column chromatography. ^cPyridine (1 equiv).

Scheme 1. Late-Stage C–C Bond Cleavage of Bioactive Linezolid^a

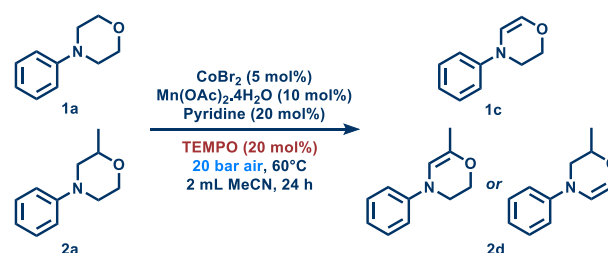


^aReaction conditions: **17a** (0.5 mmol), CoBr₂ (5 mol %), Mn(OAc)₂·4H₂O (10 mol %), pyridine (20 mol %) in MeCN (2 mL), 30 bar air, 100 °C.

Notably, significantly lower yield is observed in the presence of our previously developed Cu catalyst (Table 1, entry 8), clearly demonstrating the improved reactivity of the bimetallic system.

Spurred on by these initial findings, we investigated the activity of various Co(II) and Mn(II) salts. As shown in Table 2, the combinations Mn(OAc)₂·4H₂O/Co(OAc)₂·4H₂O, Mn(OAc)₂·4H₂O/CoBr₂, and MnCl₂/Co(OAc)₂·4H₂O all exhibited comparably excellent yields of **1b** (Table 2). It is noteworthy to highlight that, in the absence of pyridine, the

Scheme 2. Putative Intermediates Detected by GC-MS^a



^aReaction conditions: **1a** or **2a** (0.5 mmol), CoBr₂ (5 mol %), Mn(OAc)₂·4H₂O (10 mol %), pyridine (20 mol %), TEMPO (20 mol %) in MeCN (2 mL), 20 bar air, 60 °C.

reaction yield is decreased from 96% to 54%, supporting the documented positive influence of N-containing ligands in oxidations.^{11,15}

To investigate this effect further, we tested a range of pyridines, amides, urea, and amines as alternative ligands in

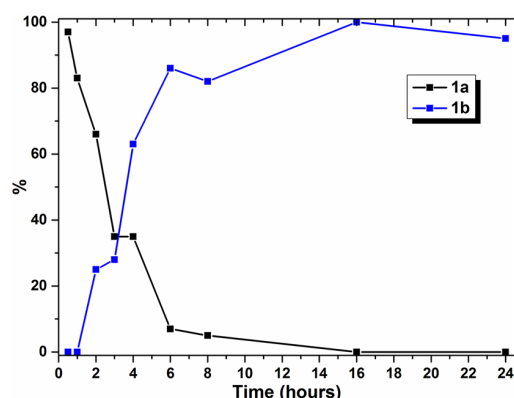


Figure 2. Reaction monitoring of C–C bond cleavage.

this reaction under mild conditions (60 °C, 10 bar air). As shown in Table 3, most substituted pyridines proved to be beneficial here. Notably, pyridine (L1) and 4-methoxypyridine (L8) were most effective in this regard, improving the yield of 1b to 82% and 86%, respectively.

Unpredictably, chelating agents proved either disadvantageous (L14, L15, L17) or provided only weak activation (L18) for this transformation. 2,2'-bipy and phenanthroline—which are widely adopted ligands in catalysis—stopped the catalysis entirely! Ultimately, owing to its high performance, ready availability, and low cost, pyridine was chosen as an ideal ligand in this reaction.

Before proceeding, nitrous oxide (N₂O) was also considered as an alternative oxidant in this reaction,¹⁶ as when reduced, this strong oxidant can be reduced to dinitrogen, and thus provide a beneficial entropic gain and driving force in the reaction. To our disappointment, this approach was unsuccessful and no reaction was observed (see Supporting Information for experimental details). Nevertheless, air had proven to be an effective oxidizer in our system, and thus it was utilized for all subsequent reactions.

With an effective catalyst, ligand, and oxidant in hand, we were able to obtain full conversion of 1a, with no detectable side reactions taking place using 20 bar air at 60 °C. After isolation, 1b was afforded with 96% yield. It is important to note that this reaction was not successful at low pressure when using a balloon filled with air, indicating the involvement of oxygen in the rate-limiting reaction step. To explore the applicability of this new system, a variety of functionalized morpholines were applied as substrates in this reaction under the optimized catalytic conditions (Table 4).

Methyl-substituted derivatives (2a and 3a) were well-tolerated, despite introducing extra steric bulk directly at the reaction center. Likewise, with the inclusion of electron-withdrawing groups on the phenyl ring (e.g., NO₂, C≡N, COOEt), high yields of the desired products (5b, 8b, 13b) could be obtained. Gratifyingly, aryl halides, which are invaluable building blocks for the pharmaceutical and agrochemical industries, were able to afford high yields with the C–X bond intact. Similarly, boronate ester (12b), which represents a privileged substrate for Suzuki–Miyaura cross-coupling reactions, was able to be cleaved at low temperature (60 °C) with a yield of 56%.

In addition to the ester moiety, ketone (6a) posed no issues. Astonishingly, even under our oxidation conditions, the analogous aldehyde *para*-formylphenylmorpholine (7a) did

not undergo oxidation to the corresponding carboxylic acid. The desired product 7b was obtained selectively in quantitative yield! Furthermore, compounds 1b, 4b, 9b, and 10b were synthesized with high yields at only 60 °C and 20 bar air. Notably, this is a substantial improvement from our recently reported [Cu]/air protocol, which utilizes harsher conditions (80–100 °C, 20–30 bar air).¹¹

To further probe the general applicability of the Co/Mn system toward functionalized molecules, we attempted the cleavage of the prescription antibiotic Linezolid. Successfully, we managed to obtain an 82% isolated yield of the expected product 17b (Scheme 1). Therefore, we argue that this highlights the potential of this protocol for late-stage functionalization and for the introduction of valuable structural complexity to nonstrained heterocycles.

To initially probe the existence of radical intermediates, we performed cleavage of 1a under optimized conditions in the presence of (2,2,6,6-tetramethylpiperidin-1-yl)oxyl (TEMPO). With addition of substoichiometric amounts of TEMPO (10 mol %) to the mixture, the reaction was stopped completely and none of the desired product was detected by GC-FID. We infer, therefore, that radical intermediates are crucial in this process. While no radical intermediates could generally be observed over the entire course of the reaction, we were able to detect trace amounts of 1c and 2d (Scheme 2) by GC-MS by quenching the reaction with TEMPO (20 mol %). From these data, we infer that dehydrogenation of the C(sp³)–C(sp³) bond to a more labile C(sp²)–C(sp²) bond occurs prior to oxidative cleavage.

On the basis of a recent report from He et al.,¹² further experiments were performed to capture some intermediates by the addition of NaNO₂ to the reaction mixture but without success. Similarly, using C₁₀F₂₁I, which easily reacts with carbon-centered radicals, was also ineffective for this purpose (see Supporting Information).

A kinetic profile was recorded to monitor the reaction. As seen on Figure 2, there is no apparent induction period needed for the catalysis. After just 30 min, the starting material is consumed and after 6 h the yield is greater than 80%. Unfortunately, we were unable to detect any intermediates by GC-FID over the entire course of the reaction.

In conclusion, we have developed a mild protocol for the cleavage of C(sp³)–C(sp³) bonds in functionalized morpholines using a combination of cobalt and manganese salts and air as an oxidant. In addition, the system has exhibited good tolerance toward a variety of chemical moieties, including halides, nitriles, and carbonyl substrates. Importantly, this protocol has proven effective for the late-stage functionalization of the drug Linezolid, with other functional groups remaining untouched.

■ ASSOCIATED CONTENT

Supporting Information

The Supporting Information is available free of charge on the ACS Publications website at DOI: 10.1021/acscatal.9b03476.

Experimental procedures; characterization data for compounds prepared (PDF)

■ AUTHOR INFORMATION

Corresponding Author

*E-mail: matthias.beller@catalysis.de (M.B.).

ORCID 

Matthias Beller: 0000-0001-5709-0965

Notes

The authors declare no competing financial interest.

ACKNOWLEDGMENTS

We gratefully acknowledge the support from the Federal Ministry of Education and Research (BMBF) and the State of Mecklenburg-Vorpommern. Financial support by Fonds der Chemischen Industrie (Kekulé-Stipendium n. 103231) for D.K.L. is also acknowledged. We thank the analytical staff of the Leibniz-Institute for Catalysis, Rostock, for their excellent service.

REFERENCES

- (1) (a) Sattler, A.; Parkin, G. Cleaving Carbon–Carbon Bonds by Inserting Tungsten into Unstrained Aromatic Rings. *Nature* **2010**, *463*, 523. (b) Masarwa, A.; Didier, D.; Zabrodski, T.; Schinkel, M.; Ackermann, L.; Marek, I. Merging Allylic Carbon-Hydrogen and Selective Carbon-Carbon Bond Activation. *Nature* **2014**, *505*, 199–203.
- (2) (a) Saliu, F.; Orlandi, M.; Bruschi, M. *N*-Aryl Lactams by Regioselective Ozonation of *N*-Aryl Cyclic Amines. *ISRN Org. Chem.* **2012**, *2012*, 1–5. (b) Suarez-Bertoa, R.; Saliu, F.; Bruschi, M.; Rindone, B. Reaction Products and Mechanism of the Regioselective Oxidation of *N*-Phenylmorpholine by Ozone. *Tetrahedron* **2012**, *68*, 8267–8275.
- (3) Binder, C. M.; Dixon, D. D.; Almaraz, E.; Tius, M. A.; Singaram, B. A Simple Procedure for C–C Bond Cleavage of Aromatic and Aliphatic Epoxides with Aqueous Sodium Periodate Under Ambient Conditions. *Tetrahedron Lett.* **2008**, *49*, 2764–2767.
- (4) Malaprade, L. *Bull. Soc. Chim. Fr.* **1934**, *3*, 833.
- (5) Criegee, R. Eine Oxydative Spaltung von Glykolen. *Ber. Dtsch. Chem. Ges. B* **1931**, *64*, 260–266.
- (6) Straganz, G. D.; Glieder, A.; Brecker, L.; Ribbons, D. W.; Steiner, W. Acetylacetonate-Cleaving Enzyme Dke1: A Novel C–C-Bond-Cleaving Enzyme from *Acinetobacter johnsonii*. *Biochem. J.* **2003**, *369*, 573–581.
- (7) Peck, S. C.; Cooke, H. A.; Cicchillo, R. M.; Malova, P.; Hammerschmidt, F.; Nair, S. K.; van der Donk, W. A. Mechanism and Substrate Recognition of 2-Hydroxyethylphosphonate Dioxygenase. *Biochemistry* **2011**, *50*, 6598–6605.
- (8) Keegan, R.; Lebedev, A.; Erskine, P.; Guo, J.; Wood, S. P.; Hopper, D. J.; Rigby, S. E. J.; Cooper, J. B. Structure of the 2,4'-Dihydroxyacetophenone Dioxygenase from *Alcaligenes sp.* 4HAP. *Acta Crystallogr., Sect. D: Biol. Crystallogr.* **2014**, *70*, 2444–2454.
- (9) Roque, J. B.; Kuroda, Y.; Göttemann, L. T.; Sarpong, R. Deconstructive Fluorination of Cyclic Amines by Carbon-Carbon Cleavage. *Science* **2018**, *361*, 171–174.
- (10) Zhou, Z. Z.; Liu, M.; Lv, L.; Li, C. J. Silver(I)-Catalyzed Widely Applicable Aerobic 1,2-Diol Oxidative Cleavage. *Angew. Chem., Int. Ed.* **2018**, *57*, 2616–2620.
- (11) Li, W.; Liu, W.; Leonard, D. K.; Rabeah, J.; Junge, K.; Brückner, J.; Beller, M. Practical Catalytic Cleavage of C(sp³)–C(sp³) Bonds in Amines. *Angew. Chem.* **2019**, *131*, 10803–10807.
- (12) He, K.; Zhang, T.; Zhang, S.; Sun, Z.; Zhang, Y.; Yuan, Y.; Jia, X. Tunable Functionalization of Saturated C–C and C–H Bonds of *N,N'*-Diarylpiperazines Enabled by *tert*-Butyl Nitrite (TBN) and NaNO₂ Systems. *Org. Lett.* **2019**, *21*, 5030–5034.
- (13) Tomas, R. A.; Bordado, J. C.; Gomes, J. F. *p*-Xylene Oxidation to Terephthalic Acid: A Literature Review Oriented Toward Process Optimization and Development. *Chem. Rev.* **2013**, *113*, 7421–69.
- (14) (a) Brill, W. Terephthalic Acid by Single-Stage Oxidation. *Ind. Eng. Chem.* **1960**, *52*, 837–840. (b) Zuo, X.; Niu, F.; Snavely, K.; Subramaniam, B.; Busch, D. H. Liquid Phase Oxidation of *p*-Xylene to Terephthalic Acid at Medium-High Temperatures: Multiple Benefits of CO₂-Expanded Liquids. *Green Chem.* **2010**, *12*, 260. (c) Raghaven-

drachar, P.; Ramachandran, S. Liquid-phase catalytic oxidation of *p*-xylene. *Ind. Eng. Chem. Res.* **1992**, *31*, 453–462.

(15) (a) Stahl, S. S. Palladium-Catalyzed Oxidation of Organic Chemicals with O₂. *Science* **2005**, *309*, 1824. (b) Wang, D.; Weinstein, A. B.; White, P. B.; Stahl, S. S. Ligand-Promoted Palladium-Catalyzed Aerobic Oxidation Reactions. *Chem. Rev.* **2018**, *118*, 2636–2679.

(16) Ettetdgui, J.; Neumann, R. *J. Am. Chem. Soc.* **2009**, *131*, 4–5.

5.3 AEROBIC IRON-CATALYZED SITE-SELECTIVE C(SP³)-C(SP³) BOND CLEAVAGE IN *n*-HETEROCYCLES

David K. Leonard, Wu Li, Nils Rockstroh, Kathrin Junge, and Matthias Beller.

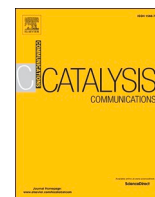
Catal. Commun. **2021**, *157*, 106333.

DOI: [10.1016/j.catcom.2021.106333](https://doi.org/10.1016/j.catcom.2021.106333)

© 2021 The Authors. Published by Elsevier B.V. This is an open access article under the CC BY license (<https://creativecommons.org/licenses/by/4.0/>).

Electronic supporting information for this article is available free of charge at <https://doi.org/10.1016/j.catcom.2021.106333>.

This manuscript was prepared in cooperation with Dr Wu Li. Most experimental work was performed by myself, including the optimisation of the reaction conditions, exploration of the substrate scope and writing the manuscript. I also assessed the analytical data and wrote the supporting information. Dr Nils Rockstroh conducted STEM measurements and co-wrote a section in the manuscript and supporting information. My contribution accounts 70%.



Short communication

Aerobic iron-catalyzed site-selective C(sp³)-C(sp³) bond cleavage in N-heterocycles

David K. Leonard, Wu Li, Nils Rockstroh, Kathrin Junge, Matthias Beller*

Leibniz-Institut für Katalyse e.V., Albert-Einstein-Straße 29a, 18059 Rostock, Germany



ARTICLE INFO

Keywords:

Iron
Oxidation
C-C bond activation
Design of experiments

ABSTRACT

The kinetic and thermodynamic stability of C(sp³)-C(sp³) bonds makes the site-selective activation of these motifs a real synthetic challenge. In view of this, herein a site-selective method of C(sp³)-C(sp³) bond scission of amines, specifically morpholine and piperazine derivatives, using a cheap iron catalyst and air as a sustainable oxidant is reported. Furthermore, a statistical design of experiments (DoE) is used to evaluate multiple reaction parameters thereby allowing for the rapid development of a catalytic process.

1. Introduction

Iron is the most abundant metal in the universe, and due to its propensity towards oxidation it is found in the earth's crust as one of its several ores, namely hematite (Fe₂O₃), magnetite (Fe₃O₄), and siderite (FeCO₃). In the field of catalysis, no base metal has impacted the world quite like iron; in fact, heterogeneous iron catalysis has triumphed in some of the world's most important industrial processes [1]. For instance, the Fischer-Tropsch process has established itself as an indispensable technology for the synthesis of liquid hydrocarbons and has been implemented by leading petrochemical companies. Undoubtedly, the Haber-Bosch process has had the most significant impact since its introduction in 1913 at BASF. At present this remains the leading industrial method for artificial nitrogen fixation, producing ammonia from N₂ and H₂, and is a vital technology for securing global food production. Notably, both revolutionary processes utilize iron-based catalysts [2-4].

The contemporary literature has often highlighted the talents of iron for enabling an extensive range of organic transformations [5-7]. Thanks to its position in the center of the 3d block of the periodic table, iron may be considered by chemists as either an *early* or *late* transition metal, and due to its formal oxidation states, which range from -2 to +6, it has a vast potential for all kinds of redox transformations [1,8-11]. New applications for iron are eagerly sought after, especially in the field of catalysis, thanks to its ready availability, low cost, and typically low toxicity.

1.1. C(sp³)-C(sp³) bond activation

There is an ongoing surge in new methodologies for the activation of C(sp³)-C(sp³) bonds which are ubiquitous within the framework of organic compounds [12-17]. Due to their kinetic and thermodynamic stability, traditional methods—such as the Criegee [18] and Malaprade [19] reactions—are ill-suited transformations for organic compounds bearing sensitive functional motifs. For this reason there has been an aim towards realizing mild reaction conditions and greater functional group tolerance. With this goal in mind, our group was able to establish a copper-mediated system for the cleavage of C(sp³)-C(sp³) bonds in amines [20]. Following this initial report, we developed an improved bimetallic cobalt-manganese system with activity and selectivity towards the cleavage of morpholine derivatives [21]. Although we were able to shift to more earth-abundant metals, we were intrigued to utilize cheap and non-toxic iron for such transformations (Fig. 1).

1.2. Experimental design

Compared to classic optimization strategies, statistical design of experiments (DoE) has gained increasing reputation among industrial chemists in recent years as an effective methodology for reaction optimization and identification of critical reaction parameters [22,23]. More specifically, this paradigm shift is a result of:

1. the development of parallel reactors, high-throughput experimentation (HTE) and flow reactor setups having been implemented widely,

* Corresponding author.

E-mail address: matthias.beller@katalyse.de (M. Beller).<https://doi.org/10.1016/j.catcom.2021.106333>

Received 17 March 2021; Received in revised form 8 June 2021; Accepted 16 June 2021

Available online 18 June 2021

1566-7367/© 2021 Published by Elsevier B.V. This is an open access article under the CC BY-NC-ND license (<http://creativecommons.org/licenses/by-nc-nd/4.0/>).

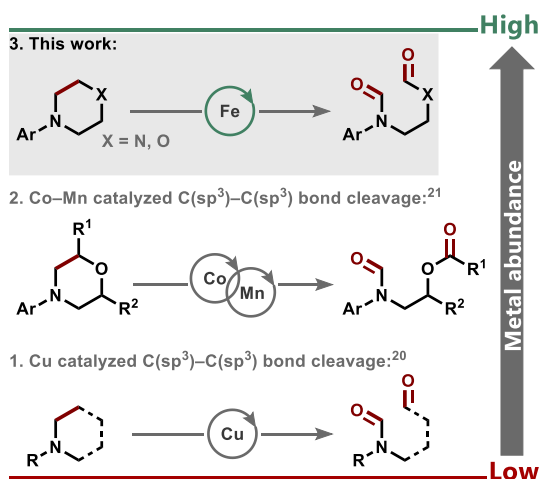


Fig. 1. Selected recent methods of metal catalyzed oxidative C–C bond cleavage reactions [20,21], and this work: iron-catalyzed C–C bond cleavage.

- the shift away from quality by testing towards the adoption of quality by design (QbD), with the concept of design space becoming more widely known,
- the Green Chemistry Principles [24] having encouraged chemists to reduce waste output from chemical reactions and increase efficiency by reducing the amounts of solvents and reagents used in chemical processes.

Interestingly, DoE tools are not widely adopted in academia despite their advantages. In contrast to univariate—i.e. linear, or one-factor-at-a-time (OFAT)—analyses, multivariate approaches to experimental design allow expansive areas of chemical space to be explored in an efficient and expedient manner [25].

Since many factors can influence the outcome of a chemical reaction (e.g. conversion, yield, selectivity, byproduct formation), DoE can be an invaluable addition to the synthetic chemist's toolbox. Not only can DoE cut down on the number of experimental runs used in optimization, but it also allows significant factors—and interactions between factors—to be identified; this is simply not feasible using a one-factor-at-a-time approach. What's more, DoE can streamline the process of locating the global maximum response for a reaction (i.e. the conditions furnishing the most desirable outcome) by investigating multiple dimensions simultaneously (as illustrated in Fig. 2).

In an effort to expand upon our previous methodologies, and building more sustainable practices, we herein report a new catalytic system for the site-selective cleavage of C(sp³)–C(sp³) bonds in (cyclic) amines.

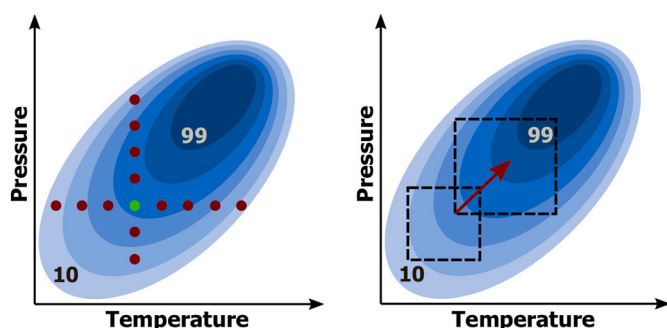


Fig. 2. Comparison between a univariate OFAT study (two sequential studies, first exploring T, then *p*) (left) and a multivariate full-factorial study (one study exploring T and *p* at the same time) for a hypothetical reaction. Dark blue regions indicate more desirable responses. (For interpretation of the references to colour in this figure legend, the reader is referred to the web version of this article.)

DoE was used for efficient optimization of the reaction by mapping of chemical space, analyzing multiple variables simultaneously. Advantageously, not only were we able to employ a very cheap, readily available, and “biocompatible” iron catalyst but also utilize air as the most green and sustainable oxidant. Notably, oxidation reactions in aerated solvents inherently possess significant safety concerns, which must be addressed appropriately. Indeed, organic chemists in academia but also the pharmaceutical industry in particular try to avoid such synthetic steps [28]. Starting materials tend therefore to be acquired in at least the correct (or higher) oxidation levels. This can certainly generate an additional hurdle in route design, and thus new practical methodologies are readily sought to address this [29]. On the other hand it's true that aerobic oxidations are applied in several large and medium scale industrial processes, which demonstrates the possibilities to perform such transformations in a selective, safe, and environmentally benign manner [26,27]. In our case, safety concerns were in large part circumvented by using (synthetic) air which uses diluted oxygen in inert nitrogen, as well as oxidation resistant solvents.

2. Experimental

2.1. General experimental details

Most substrates were obtained from commercial sources and used as supplied; others were prepared as detailed below.

All metal catalysts were obtained from commercial sources and used as supplied.

Unless otherwise mentioned, all catalytic oxidation reactions were carried out in 2 mL glass vials, which were set in an alloy plate and placed inside a 300 mL autoclave (Parr® Instrument Company).

All oxidation reactions were performed in a Parr® Instrument Company autoclave.

Deuterated solvents were ordered from Deutero GmbH. NMR spectra were recorded using Bruker 300 Fourier, Bruker AV 300 and Bruker AV 400 spectrometers. Chemical shifts are reported in ppm, relative to the deuterated solvent. Coupling constants are expressed in Hertz (Hz). The following abbreviations are used: s = singlet, d = doublet, t = triplet, and m = multiplet. The residual solvent signals were used as references for ¹H and ¹³C NMR spectra (CDCl₃: δH = 7.26 ppm, δC = 77.12 ppm; DMSO-*d*₆: δH = 2.50 ppm, δC = 39.52 ppm). All measurements were carried out at room temperature unless otherwise stated.

GC-FID analyses were carried out using an Agilent 7890B gas chromatograph fitted with an Agilent HP5 column (30 m × 0.25 mm I.D. × 0.25 μm).

Solvents were used directly without further purification. HPLC grade MeCN was supplied by Fisher Chemical.

Scanning transmission electron microscopy (STEM) was performed with a probe aberration-corrected JEM-ARM200F (Jeol Ltd., CEOS Corrector) at 200 kV. The microscope is further equipped with an Enfinium ER (Gatan) electron energy loss spectrometer. For STEM imaging a High-Angle Annular Dark Field (HAADF) and an Annular Bright Field (ABF) detector were applied, while EELS acquisition was done with the Annular Dark Field (ADF) detector. The solid sample was dried in advance of the electron microscopy measurements and then placed without any further pretreatment on a holey carbon supported Cu-grid (mesh 300), which was then transferred to the microscope. EEL spectra were background subtracted and deconvolved.

2.2. General procedure for the synthesis of substrates

2.2.1. General procedure A (GP-A)

A mixture of aryl bromide (10 mmol), morpholines (20 mmol), K₂CO₃ (20 mmol), CuI (1.0 mmol) and L-proline (2.0 mmol) in 10 mL of DMSO was heated at 90 °C and for 24 h. The cooled mixture was partitioned between water and ethyl acetate. The organic layer was separated, and the aqueous layer was extracted with ethyl acetate. The

combined organic layers were dried over Na_2SO_4 , and concentrated in vacuo. The desired products were isolated by silica gel column chromatography (*n*-heptane/ethyl acetate mixtures) [34].

2.3. General procedure for catalytic oxidations

2.3.1. General procedure B (GP-B)

A 4 mL glass vial equipped with a magnetic stir bar was charged with aryl morpholine (0.5 mmol) and FeCl_3 (8.1 mg; 10 mol%). The vial was capped, and the septum was pierced with a small needle. HPLC grade acetonitrile (2 mL) was added via a 2 mL syringe. Pyridine (80 μL ; 2.0 equiv) was added via a glass microsyringe. The vial was then placed into an aluminium heating block and then sealed inside an autoclave (Parr® Instrument Company). The autoclave was then pressurized with air (30 bar). The reaction mixture was stirred for 24 h at 100 °C. Next, the reaction was cooled to room temperature. A sample of the reaction mixture was analyzed by GC-FID and TLC. The product was purified via flash column chromatography (RediSep® Rf + automatic column) using heptane/ethyl acetate. Solvent was removed in vacuo to yield the desired product.

2.3.2. General procedure C (GP-C)

A 4 mL glass vial equipped with a magnetic stir bar was charged with 1,4-diphenylpiperazine (59.6 mg; 0.25 mmol), TEMPO (3.9–11.7 mg; 10–30 mol%) and FeCl_3 (2.0–6.1 mg; 3–15 mol%) in that order. The vial was capped, and the septum was pierced with a small needle. HPLC grade acetonitrile (1 mL) was added via a 2 mL syringe. Pyridine (2.0–6.0 μL ; 10–30 mol%) was added via a glass microsyringe. The vial was then placed into an aluminium heating block and then sealed inside an autoclave (Parr® Instrument Company). The autoclave was then pressurized with air (10–30 bar). The reaction mixture was stirred for 24 h at 80–120 °C. Next, the reaction was cooled to room temperature. A sample of the reaction mixture was analyzed by GC-FID and yield was determined using *n*-hexadecane as an internal standard (see appendix for GC-FID calibration graphs). Product isolation was achieved via flash column chromatography (RediSep® Rf + automatic column) using a suitable mixture of heptane/ethyl acetate determined by TLC. Solvent was removed in vacuo to yield the desired product.

3. Results and discussion

To develop our expertise in the area of base metal-catalyzed $\text{C}(\text{sp}^3)\text{--C}(\text{sp}^3)$ bond cleavage reactions, we investigated various metal salts for the cleavage of *N*-phenylmorpholine **1a** under aerobic conditions [20,21]. In addition to our recently published [Cu]/air and [Co–Mn]/air systems, several iron catalysts showed promising activity for this transformation (Table S3).

The most favorable results were obtained using iron(III) chloride (entry 7), although lower yields could also be obtained using iron(III) nitrate nonahydrate (entry 5) and iron(II) phthalocyanine (entry 6). Encouraged by these initial findings we opted to compare the performance of the catalyst in various solvents (see Table S4) and found that acetonitrile proved to be the most effective solvent, which is consistent with our previously disclosed catalytic systems [20,21]. At this point it is important to note that the use of organic solvents in oxidation reactions is always potentially hazardous; especially performing reactions under aerobic conditions without appropriate safety measures. Hence, we completed all experiments in standard autoclave equipment with synthetic air as the oxidant—which contains just $20.5 \pm 0.5\%$ O_2 diluted in N_2 gas—as an operationally safer system to pure O_2 . In addition, we used solvents with high resistance to autooxidation. Notably, the chosen solvent, acetonitrile, has an autoignition temperature of 524 °C, as well as lower and upper explosive limits of 4.4 and 16%, respectively (see safety data sheets) [30], which allows for safe and reproducible work under our reaction conditions. It should be also mentioned that in all experiments we never observed any evidence of solvent oxidation.

Unlike our recently reported [Co–Mn]/air system, iron(III) chloride was able to perform oxidative cleavage outwith the class of morpholines (Table 1). The catalyst's activity towards 1,4-diphenylpiperazine (**2a**) under the pre-optimized conditions using (2,2,6,6-tetramethyl-piperidin-1-yl)oxyl (TEMPO)—a stable free radical reagent—was particularly encouraging. It is noteworthy to point out that the presence of pyridine ligands highly influenced the yield of **2b** (Table 1); a documented effect of *N*-ligands in oxidations [20,21,31,32]. However, a reproducible positive effect was only observed in the presence of the parent ligand. Pyridines both substituted with electron-donating as well as electron-withdrawing substituents gave inferior results.

In contrast to our previously reported systems for C–C single bond cleavage, which showed high activity towards a variety of amines (in the case of [Cu]) and functionalized morpholines (in the case of [Co–Mn]), with this new FeCl_3 catalyst system, better performance was obtained with piperazine substrates. Notably, the [Co–Mn] system was found to be completely ineffective with such substrates.

With a suitable catalyst, solvent and additives in hand for site-selective $\text{C}(\text{sp}^3)\text{--C}(\text{sp}^3)$ bond cleavage in **2a** to **2b**, we postulated that a DoE methodology is a suitable tool for establishing a more realistic process. It is expected that the reaction parameters: catalyst loading, temperature, air pressure, pyridine loading, and TEMPO loading could all significantly influence the reaction yield of **2b** (Table 2).

The rationale behind the ranges of the low-level (–) and high-level conditions (+) of the selected variables is that they must be large enough to ensure any effects on reaction yield should be easily detectable. Additionally, using a wide range between these two values is one of the best ways to improve the signal/noise ratio. A two-level half-fractional (2^{5-1}) factorial design was selected to enable a large area of chemical space to be covered whilst keeping the number of experimental runs to a minimum and avoid compounding effects.

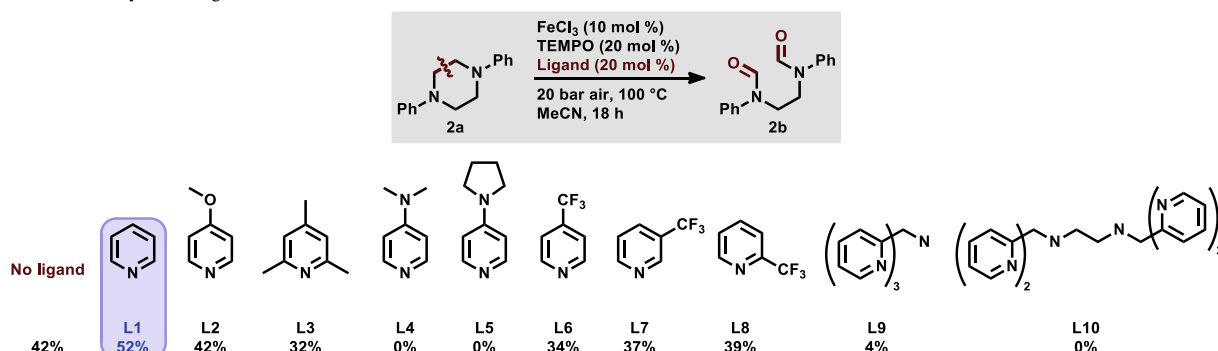
Using a software statistics package (Minitab) [33], we generated a list of all necessary experimental runs to cover the chosen design space. Included in the design are four runs in the center of the design space (9 mol% catalyst loading, 100 °C, 20 bar air, 20 mol% pyridine, 20 mol% TEMPO), leading to a total of twenty experimental runs. The yield of **2b** in each run was determined by gas chromatograph-flame ionization detector (GC-FID) using *n*-hexadecane as an internal standard.

From first inspection of the data in Table 3, the most desirable results are obtained using high temperature and high air pressure (entries 10, 11, 16). It was therefore unsurprising that mostly low yields were achieved at milder temperature and pressure (entries 3, 5, 9). This may be explained by the high thermodynamic stability of $\text{C}(\text{sp}^3)\text{--C}(\text{sp}^3)$ bonds thus making the reaction inaccessible without significant heating. Notably, entries 4 and 6 reveal the possibility to achieve good product yields under just 10 bar air pressure, thereby benefitting both convenience and safety. The analysis of variance (ANOVA) table (Table S11) was consistent with the observation that temperature and pressure were favorable towards the yield of **2b**. In fact, the ANOVA identified three factors as being statistically significant in the reaction (i.e. *p*-values < 0.05 under the null hypothesis), these being: catalyst loading, temperature, and pressure. In other words, the high-level conditions for these three factors generated the best results. Whilst the presence of TEMPO and pyridine had proven to be beneficial in the reaction, variation from 10 to 30 mol% had no statistically significant impact on the yield of **2b**.

Based on the results *vide supra*, the decision was made to try to explore higher temperatures and pressures, as well as greater amounts of TEMPO and pyridine in solution. In all cases, catalyst loading was maintained at 10 mol% (see Tables S12 & S13). Notably, the harsher conditions employed were in fact disadvantageous and could not reach the yield of 60% of **2b** obtained in the first DoE screen.

Using the optimization process outlined above allowed us to isolate derivatized morpholines and derivatized diphenylpiperazine in good yields (up to 70%), as shown in Table 4. It is noteworthy to highlight that such reactivity could not be realized with our previously reported

Table 1
Influence of Pyridine Ligands on the Benchmark Reaction.



^aReaction conditions: **2a** (0.25 mmol), FeCl_3 (10 mol%), TEMPO (20 mol%), ligand (20 mol%) in MeCN (2 mL), 20 bar air, 100 °C. Yields determined by GC-FID using *n*-hexadecane as an internal standard.

Table 2
Reaction Conditions Selected for DoE Analysis of Oxidative Cleavage of **2a** Using FeCl_3 .

factor	low level (–)	high level (+)
catalyst loading (mol%)	3	15
temperature (°C)	80	120
air pressure (bar)	10	30
pyridine loading (mol%)	10	30
TEMPO loading (mol%)	10	30

Table 3
Results of the Initial DoE Screen for Oxidative Cleavage of **2a**^a.

entry	catalyst loading (mol%)	TEMPO (mol%)	pyridine (mol%)	air pressure (bar)	temperature (°C)	yield ^b (%)
1	3	10	10	10	120	25
2	15	10	10	10	80	38
3	3	30	10	10	80	5
4	15	30	10	10	120	45
5	3	10	30	10	80	7
6	15	10	30	10	120	52
7	3	30	30	10	120	30
8	15	30	30	10	80	33
9	3	10	10	30	80	12
10	15	10	10	30	120	59
11	3	30	10	30	120	56
12	15	30	10	30	80	52
13	3	10	30	30	120	41
14	15	10	30	30	80	36
15	3	30	30	30	80	16
16	15	30	30	30	120	60
17	9	20	20	20	100	51 ^c
18	9	20	20	20	100	44 ^c
19	9	20	20	20	100	40 ^c
20	9	20	20	20	100	45 ^c

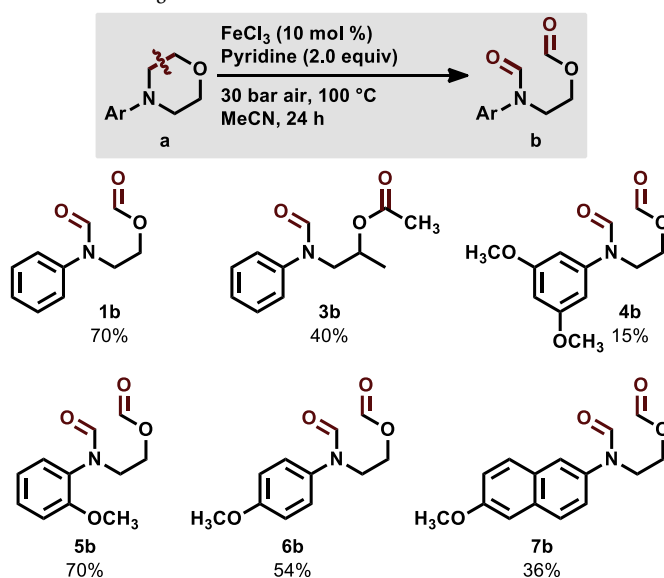
^a Reaction conditions: **2a** (0.25 mmol), FeCl_3 (3–15 mol%), TEMPO (10–30 mol%), pyridine (10–30 mol%) in MeCN (2 mL), 10–30 bar air, 80–120 °C. ^b Yields determined by GC-FID using *n*-hexadecane as an internal standard. ^c Center point conditions.

catalytic systems.

The high activity of this benign system is further illustrated by the lack of any noticeable induction period, leading to rapid conversion of starting material and a 13% yield of **2b** after just 30 min of reaction time. Furthermore, after 8 h full conversion is observed for the model reaction and the desired product is obtained in up to 60% yield, with no detectable co-product formation.

During the benchmark reaction, the formation of a brown solid was observed which proved to be somewhat catalytically active, capable of

Table 4
C–C Bond Cleavage Reactions



^aReaction conditions: **a** (0.5 mmol), FeCl_3 (10 mol%), pyridine (2.0 equiv) in MeCN (2 mL), 30 bar air, 100 °C, isolated yield.

furnishing a 9% yield of **2b** after reaction overnight (see Supporting Information).

Scanning transmission electron microscopy (STEM) together with electron energy loss spectroscopy (EELS) was performed to reveal the nature of this precipitate (Figs. 3 & S1). The iron oxide particles are found on a bulk phase which was proved to consist mainly of carbon, but also contains some nitrogen and tiny amounts of iron.

4. Conclusions

In conclusion, a convenient iron-based catalyst is shown to be effective for the site-selective cleavage of $\text{C}(\text{sp}^3)\text{--C}(\text{sp}^3)$ bonds in diphenylpiperazine and derivatized morpholines. The activation of unstrained and highly inert sp^3 -hybridized centers to sp^2 -hybridized aldehyde motifs unlocks the potential for new functionalization of such molecules. The use of air in this reaction is ideal as an oxidant. To the best of our knowledge, this is the first example of a competent iron-based catalytic system for the cleavage of $\text{C}(\text{sp}^3)\text{--C}(\text{sp}^3)$ bonds in unstrained *N*-compounds. DoE provided a rapid and effective analysis of a complex $\text{C}(\text{sp}^3)\text{--C}(\text{sp}^3)$ bond cleaving reaction involving five variables. Three

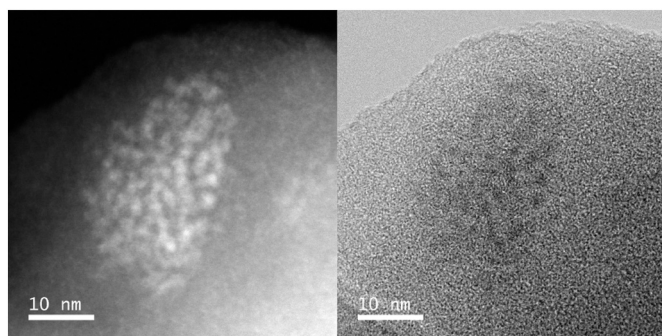


Fig. 3. STEM HAADF (left) and STEM ABF (right) images of the precipitate formed during the reaction. A group of iron oxide particles (see the brighter parts in the left image) can be seen on the bulky phase, which contains mainly carbon.

variables—temperature, air pressure and catalyst loading—were found to be significant in this reaction (i.e. p -values < 0.05 under the null hypothesis). Whilst the catalyst proved more active in the presence of TEMPO and pyridine, the amount of these additives was not found to be statistically significant (p -values > 0.05) in the region of chemical space explored in the factorial design.

Credit author statement

David K. Leonard: Conceptualization, data curation, investigation, writing - original draft, writing - review & editing. **Wu Li:** Conceptualization, data curation, investigation, writing - review & editing. **Nils Rockstroh:** Data curation, investigation, writing - original draft, writing - review & editing. **Kathrin Junge:** Supervision, conceptualization, writing - review & editing. **Matthias Beller:** Supervision, conceptualization, writing - review & editing.

Declaration of Competing Interest

Authors declare that they have no competing interests.

Acknowledgments

We gratefully acknowledge the support from the Federal Ministry of Education and Research (BMBF) and the State of Mecklenburg-Vorpommern. Financial support by Fonds der Chemischen Industrie (Kekulé-Stipendium n. 103231) for D.K.L. is also acknowledged. We are grateful to Dr. Pavel Ryabchuk (Galapagos NV) for his valuable contribution of ideas to the project. We thank the analytical staff of the Leibniz Institute for Catalysis, Rostock, for their excellent service.

Appendix A. Supplementary data

Supplementary data to this article can be found online at <https://doi.org/10.1016/j.catcom.2021.106333>.

References

- [1] A. Fürstner, Iron catalysis in organic synthesis: a critical assessment of what it takes to make this base metal a multitasking champion, *ACS Cent. Sci.* 2 (2016) 778–789.
- [2] E. de Smit, B.M. Weckhuysen, The renaissance of iron-based Fischer–Tropsch synthesis: on the multifaceted catalyst deactivation behaviour, *Chem. Soc. Rev.* 37 (2008) 2758–2781.
- [3] M.M. Rodriguez, E. Bill, W.W. Brennessel, P.L. Holland, N_2 reduction and hydrogenation to ammonia by a molecular iron–potassium complex, *Science* 334 (2011) 780–783.

- [4] T. Rayment, R. Schlögl, J.M. Thomas, G. Ertl, Structure of the ammonia synthesis catalyst, *Nature* 315 (1985) 311–313.
- [5] I. Bauer, H.J. Knölker, Iron catalysis in organic synthesis, *Chem. Rev.* 115 (2015) 3170–3387.
- [6] T.B. Boit, A.S. Bulger, J.E. Dander, N.K. Garg, Activation of C–O and C–N bonds using non-precious-metal catalysis, *ACS Catal.* 10 (2020) 12109–12126.
- [7] A. Guðmundsson, J.-E. Bäckvall, On the use of iron in organic chemistry, *Molecules* 25 (2020) 1349.
- [8] Y. Lee, N.P. Mankad, J.C. Peters, Triggering N_2 uptake via redox-induced expulsion of coordinated NH_3 and N_2 silylation at trigonal bipyramidal iron, *Nat. Chem.* 2 (2010) 558–565.
- [9] P. Hu, M. Tan, L. Cheng, H. Zhao, R. Feng, W.-J. Gu, W. Han, Bio-inspired iron-catalyzed oxidation of alkylarenes enables late-stage oxidation of complex methylarenes to arylaldehydes, *Nat. Commun.* 10 (2019) 2425.
- [10] G. Jin, G.W. Werncke, Y. Escudié, S. Sabo-Etienne, S. Bontemps, Iron-catalyzed reduction of CO_2 into methylene: formation of C–N, C–O, and C–C bonds, *J. Am. Chem. Soc.* 137 (2015) 9563–9566.
- [11] S. Budweg, Z. Wei, H. Jiao, K. Junge, M. Beller, Iron–PNP–pincer-catalyzed transfer dehydrogenation of secondary alcohols, *ChemSusChem* 12 (2019) 2988–2993.
- [12] D.-S. Kim, W.-J. Park, C.-H. Jun, Metal–organic cooperative catalysis in C–H and C–C bond activation, *Chem. Rev.* 117 (2017) 8977–9015.
- [13] L. Soullart, N. Cramer, Catalytic C–C bond activations via oxidative addition to transition metals, *Chem. Rev.* 115 (2015) 9410–9464.
- [14] S.P. Morcillo, Radical-promoted C–C bond cleavage: a deconstructive approach for selective functionalization, *Angew. Chem. Int. Ed.* 58 (2019) 14044–14054.
- [15] X. Wen, X. Li, X. Luo, W. Wang, S. Song, N. Jiao, Intramolecular Csp^3 –H/C–C bond amination of alkyl azides for the selective synthesis of cyclic imines and tertiary amines, *Chem. Sci.* 11 (2020) 4482–4487.
- [16] B. Wang, M.A. Perea, R. Sarpong, Transition metal-mediated C–C single bond cleavage: making the cut in total synthesis, *Angew. Chem. Int. Ed.* 59 (2020) 18898–18919.
- [17] M. Murakami, N. Ishida, Cleavage of carbon–carbon σ -bonds of four-membered rings, *Chem. Rev.* 121 (2021) 264–299.
- [18] R. Criegee, Eine Oxydative Spaltung von Glykolen, *Ber. Dtsch. Chem. Ges. B* 64 (1931) 260.
- [19] L. Malaprade, *Bull. Soc. Chim. Fr.* 3 (1934) 833.
- [20] W. Li, W. Liu, D.K. Leonard, J. Rabeah, K. Junge, A. Brückner, M. Beller, Practical catalytic cleavage of $C(sp^3)$ – $C(sp^3)$ bonds in amines, *Angew. Chem. Int. Ed.* 58 (2019) 10693–10697.
- [21] D.K. Leonard, W. Li, K. Junge, M. Beller, Improved bimetallic cobalt–manganese catalysts for selective oxidative cleavage of morpholine derivatives, *ACS Catal.* 9 (2019) 11125–11129.
- [22] S.A. Weissman, N.G. Anderson, Design of experiments (DoE) and process optimization. A review of recent publications, *Org. Process. Res. Dev.* 19 (2015) 1605–1633.
- [23] D. Lendrem, M. Owen, S. Godbert, DOE (Design of Experiments) in development chemistry: potential obstacles, *Org. Process. Res. Dev.* 5 (2001) 324–327.
- [24] P. Anastas, N. Eghbali, Green chemistry: principles and practice, *Chem. Soc. Rev.* 39 (2010) 301–312.
- [25] V.K. Aggarwal, A.C. Staubitz, M. Owen, Optimization of the Mizoroki–heck reaction using Design of Experiments (DoE), *Org. Process. Res. Dev.* 10 (2006) 64–69.
- [26] R.A.F. Tomás, J.C.M. Bordado, J.F.P. Gomes, p -Xylene oxidation to terephthalic acid: a literature review oriented toward process optimization and development, *Chem. Rev.* 113 (2013) 7421–7469.
- [27] J. Smidt, W. Hafner, R. Jira, J. Sedlmeier, R. Sieber, R. Rüttinger, H. Kojer, Katalytische Umsetzungen von Olefinen an Platinmetall-Verbindungen Das Consortium-Verfahren zur Herstellung von Acetaldehyd, *Angew. Chem.* 71 (1959) 176–182.
- [28] A. Gavriilidis, A. Constantinou, K. Hellgardt, K.K. Hii, G.J. Hutchings, G.L. Brett, S. Kuhn, S.P. Marsden, Aerobic oxidations in flow: opportunities for the fine chemicals and pharmaceuticals industries, *React. Chem. Eng.* 1 (2016) 595–612.
- [29] P.M. Osterberg, J.K. Niemeier, C.J. Welch, J.M. Hawkins, J.R. Martinelli, T. E. Johnson, T.W. Root, S.S. Stahl, Experimental limiting oxygen concentrations for nine organic solvents at temperatures and pressures relevant to aerobic oxidations in the pharmaceutical industry, *Org. Process. Res. Dev.* 10 (2014) 1537–1543.
- [30] (a) Sigma–Aldrich Acetonitrile Safety Data Sheet. <https://www.sigmaaldrich.com/MSDS/MSDS/DisplayMSDSPage.do?country=GB&language=en&productNumber=34851&brand=SIGALD&PageToGoToURL=https%3A%2F%2Fwww.sigmaaldrich.com%2Fcatalog%2Fproduct%2Fsigald%2F34851%3Fflang%3Den> (accessed January 12, 2020); (b) INEOS Acetonitrile Safe Storage and Handling Guide. https://www.ineos.com/globalassets/ineos-group/businesses/ineos-nitriles/she/2007_acetonitrile_brochure.pdf (accessed January 12, 2020).
- [31] S.S. Stahl, Palladium-catalyzed oxidation of organic chemicals with O_2 , *Science* 309 (2005) 1824–1826.
- [32] D. Wang, A.B. Weinstein, P.B. White, S.S. Stahl, Ligand-promoted palladium-catalyzed aerobic oxidation reactions, *Chem. Rev.* 118 (2018) 2636–2679.
- [33] Minitab 19. <https://www.minitab.com> (accessed December 14, 2020).
- [34] D. Ma, Q. Cai, H. Zhang, Mild method for Ullmann coupling reaction of amines and aryl halides, *Org. Lett.* 5 (2003) 2453–2455.

5.4 A CONVENIENT AND STABLE HETEROGENEOUS NICKEL CATALYST FOR HYDRODEHALOGENATION OF ARYL HALIDES USING MOLECULAR HYDROGEN

David K. Leonard[†], Pavel Ryabchuk[†], Muhammad Anwar, Sarim Dastgir, Kathrin Junge, and Matthias Beller.

[†]These authors contributed equally to this work.

Submitted manuscript.

This manuscript was prepared in cooperation with Dr Pavel Ryabchuk, Dr Muhammed Anwar and Dr Sarim Dastgir. I performed the multivariate analysis of reaction variables, performed around half of the substrated scope and wrote the manuscript. I also assessed the analytical data and wrote the supporting information. My contribution accounts 45%.

A Convenient and Stable Heterogeneous Nickel Catalyst for Hydrodehalogenation of Aryl Halides Using Molecular Hydrogen

David K. Leonard^{1†}, Pavel Ryabchuk^{1,2†}, Muhammad Anwar³, Sarim Dastgir³, Kathrin Junge^{1*}, Matthias Beller^{1*}

[†]These authors contributed equally to this work

Supporting Information Placeholder

ABSTRACT: Hydrodehalogenation (or reductive dehalogenation) is an effective strategy for transforming persistent and potentially toxic organohalides into their more benign congeners. Common methods for this transformation utilize Pd/C or Raney Nickel as catalysts, which are either expensive or have safety concerns. Herein, we report a nickel-based catalyst supported on titania (Ni-phen@TiO₂-800), which can be used as a safe alternative to pyrophoric Raney nickel. The catalyst is prepared in a straightforward fashion via deposition of a nickel(II)/1,10-phenanthroline complex on titania, followed by pyrolysis. The catalytic material—which was characterized by means of STEM, XRD, and XPS—consists of nickel nanoparticles covered with *N*-doped carbon layers. With the aid of experimental design (DoE), this nano-structured catalyst was proficient for the facile and selective reductive dehalogenation of a diverse range of substrates bearing C–I, C–Br, and C–Cl bonds (>30 examples). Moreover, the practicality of this catalyst system has been demonstrated by the gram scale dehalogenation of environmentally hazardous and polyhalogenated substrates atrazine, tetrabromobisphenol A, tetrachlorobenzene and a polybrominated diphenyl ether (PBDE).

1. INTRODUCTION

Halogenated organic compounds are invaluable compounds with central importance in synthetic chemistry as solvents, carbon-carbon and carbon-nitrogen coupling reagents, and as protecting groups.¹ They offer diverse real-world applications as coolants,² dielectric fluids (e.g. in transformers),³ agrochemicals,⁴ and pharmaceuticals.⁵ In general, the incorporation of halogen atoms into organic compounds profoundly increases both their chemical and thermal stability. This distinguishing feature has led to the widespread adoption of organohalides (particularly organobromides) in fire retardant materials.⁶

Despite their obvious utility, organohalides can be highly damaging to animal and human health. This is especially well documented for halogenated dioxins—a broad class of compounds which have become infamous for their toxicity and environmental persistence. Notably, 2,3,7,8-tetrachlorodibenzo-p-dioxin (TCDD)—a byproduct from organic synthesis, and a component in Monsanto's Agent Orange herbicide used during the Vietnam War—has been linked to low sperm count in Vietnam veterans, as well as increased incidence of miscarriage in veterans' wives, and a wide variety of organ malformation in

their children.⁷ Moreover, dioxin-like compounds, including polychlorinated biphenyls (PCBs) and polybrominated biphenyls (PBBs) are found to be nearly impervious towards degradation, highly environmentally persistent, and have a propensity to accumulate in animal tissues. Appropriately, PCBs are now recognized as serious environmental contaminants with deleterious effects to human health, especially given their extended elimination half-lives of several years within the body.⁸

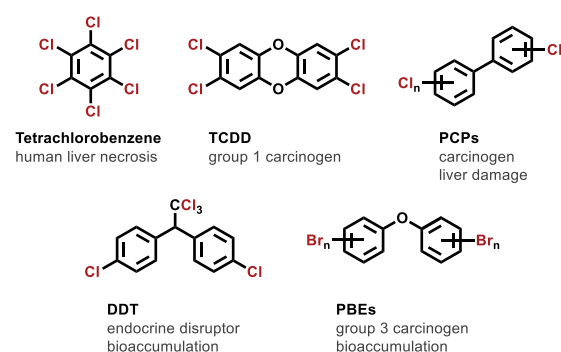


Figure 1. Examples of toxic organohalides.

Clearly, there is a real incentive to develop technologies to rid such deleterious substances from the environment. The current means for achieving this includes incineration,⁹ microbial degradation,¹⁰ chemical oxidation,¹¹ photochemical degradation,¹² ultrasonic irradiation,¹³ electrolysis,¹⁴ and catalytic hydrodehalogenation (HDH).¹⁵ Whilst incineration offers a simple solution for the treatment of chemical waste, such an approach is not appropriate in the case of (poly)halogenated organic compounds given that their high thermal stability not only makes this highly challenging but often yields products which exhibit even greater toxicity than the initial material.

HDH is the transformation whereby a carbon-halogen bond is formally substituted by a new carbon-hydrogen bond. For this reason, (hydro)dehalogenation has established itself as an effective strategy for detoxification and degradation of both anthropogenic and natural halide compounds.¹⁶

Dehalogenations of organohalides can be accomplished using (over)stoichiometric amounts of transfer hydrogenation reagents like alcohols,¹⁷ formic acid (or its salts),¹⁸ metal hydride reducing agents,¹⁹ Grignard reagents,²⁰ etc. However, molecular hydrogen is a more attractive hydrogen donor with wide

adoption in the chemical industry due to its considerably low cost and high atom efficiency.

As far as transition metal-mediated HDH goes, palladium has proven to be highly effective for C–X activation and consequently this is perhaps the most common approach for this transformation. Palladium, however, is both expensive to procure and its supply is at risk within the next 100 years. Furthermore, Pd on charcoal requires careful treatment and can ignite solvents and hydrogen if it is handled improperly. Otherwise, Raney-nickel (finely-ground nickel–aluminium alloy) has been demonstrated as a valued alternative. Nickel has some clear benefits over palladium, including its lower cost per mole and its lower supply risk in the future. On the other hand, Raney-nickel’s disadvantages are its deactivation upon use and its instability. To avoid spontaneous ignition in air, it is typically stored as an aqueous slurry. It must therefore be handled with considerable care and presents a real challenge for implementation on larger scale.

In recent decades, integrating green and sustainable practices into chemical processes has become one of the central focuses in chemistry. The 12 Principles of Green Chemistry recognizes the importance of catalysis for increasing efficiency, and selectivity, and realizing otherwise unfavorable reactions, whilst simultaneously reducing waste output.²¹ With this in mind, coupled with our interest in sustainable redox reactions, we set out to develop a non-noble based catalyst system for HDH. Herein, we report a straightforward heterogeneous nickel nano-catalyst capable of selective dehalogenation of C–I, C–Br, and C–Cl bonds.

2. RESULTS AND DISCUSSION

Identification of the active catalyst. Initially a small library of 18 heterogeneous nickel-based materials was prepared in-house following a simple procedure of i) heating Ni(OAc)₂·4H₂O and 1,10-phenanthroline monohydrate in ethanol at 60°C to yield a nickel–phenanthroline complex, (ii) adding solid supports (SiO₂, TiO₂, C, SiC, CeO₂, and Al₂O₃) to the mixture, (iii) drying the mixtures *in vacuo*, followed by, (iv) pyrolysis of the dried material at temperatures ranging from 600–1000°C. Using this method of catalyst preparation, we have previously developed several iron-, cobalt- and nickel-based catalysts.²²

Table 1. Investigation for Catalytically Active Materials^a

entry	Ni-Phen@support-pyrolysis T	conversion (%) ^b	yield (%) ^b
1	Ni-Phen@C-800	31	26
2	Ni-Phen@TiO ₂ -600	39	22
3	Ni-Phen@TiO ₂ -800	100	99
4	Ni-Phen@TiO ₂ -1000	44	32
5	Ni-Phen@Al ₂ O ₃ -1000	32	26

^aReaction conditions: 0.5 mmol **1a**, 45 mg of catalyst, Et₃N (2.0 equiv), 50 bar H₂, 25 °C, 2 mL MeOH/H₂O (1:1), 20 h.

^bConversion and yield determined by GC-FID using hexadecane as an internal standard.

With the prepared materials in hand, we examined their activities for the reductive dehalogenation of 1-

bromonaphthalene **1a** using molecular hydrogen and (excess) triethylamine as an HBr scavenger. After initial evaluation of all prepared catalysts under relatively mild conditions (60°C/50 bar H₂), we selected the five most active materials for assessing their performance at lower temperature (25°C; see SI for details). As shown in Table 1, Ni-Phen@TiO₂-800 (entry 3) was the clear front-runner, accomplishing 100% conversion of **1a** to provide a 99% yield of **1b** at ambient temperature!

Experimental design. Having identified a suitable catalyst, we set about optimization of the reaction conditions to minimize reagent and catalyst use whilst maintaining high reactivity under mild conditions. Since there are several variables which could influence the product yields of our catalytic system, we opted to utilize design of experiments (DoE) for a robust and expedient multivariate analysis of the reaction parameters. In contrast to univariate (i.e. one-factor-at-a-time) analyses, DoE can encompass a large volume of chemical space and reveal which factors—and interactions between factors—have the largest influence on the reaction outcome (e.g. yield, selectivity, etc.). We selected four different reaction parameters (T, p, catalyst loading, and base loading) to examine for the reductive dehalogenation of **1a**.

A two-level full-fractional investigation (2⁴ design) of temperature, pressure, catalyst loading, and amount of base entailed a total of 20 reaction runs, including the runs performed in the center of the design space (performed in quadruplicate). Using an analysis of variance (ANOVA), we were able to identify the reaction parameters which were statistically significant (i.e. those which had p-values below the 0.05 threshold) within the investigation range (see Table S3). Accordingly, the statistically significant parameters we observed are: (i) amount of base, (ii) catalyst loading, and (iii) temperature. Significant interactions were also detected between (iv) catalyst loading and temperature, as well as (v) catalyst loading and amount of base. The contour plots shown in Figure 2 and the Supporting Information reveal the interactions between factors and highlight the most favorable areas of chemical space. In this fashion, we were able to achieve full conversion of **1a** and 92% yield of **1b** after 18 hours at 45°C, using just 20 bar H₂ and a slight excess (1.25 equiv) of triethylamine.

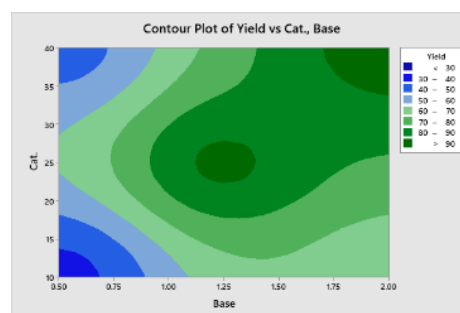


Figure 2. Contour plot from the DoE showing interaction between catalyst loading and base.

The important role of the base is not surprising in this reaction for two reasons: firstly, as the reaction progresses, a bromine atom is displaced from the substrate to form acidic HBr, and secondly, we have previously observed that NEt₃ can assist with the heterolytic cleavage of molecular hydrogen.^{22f}

Reaction scope and limitations. To examine the scope of the HDH reaction, we subjected more than 30 aryl bromides and aryl chlorides to our optimized catalyst system (Table 2). In general, we observed that the electron-rich and weakly electron-deficient substrates **1a–6a** are favored in this reaction and dehalogenation were possible under mild conditions (20 bar H₂, 45–60°C) with good to excellent yields (80 to >99%). In contrast, harsher reaction conditions were necessary for amine **7a** and electron-deficient aryl bromides **8a–16a**, as well as for all aryl chlorides. Notably, by moderating the reaction temperature, we were able to promote chemoselective dehalogenation of anisoles **2a** and **5a**, which bear more than one halide atom. At 90°C and 30 bar H₂ pressure, a decrease in HDH yield of 6% and 65% was observed for phenylmethanamines **13a–15a** upon moving the bromine atom from *para*- to *meta*-, and *meta*- to *ortho*-positions, respectively. This is likely caused by the decreased proximity between the inductively withdrawing methylmethanimine and bromine atom or due to increased steric bulk at the reaction center.

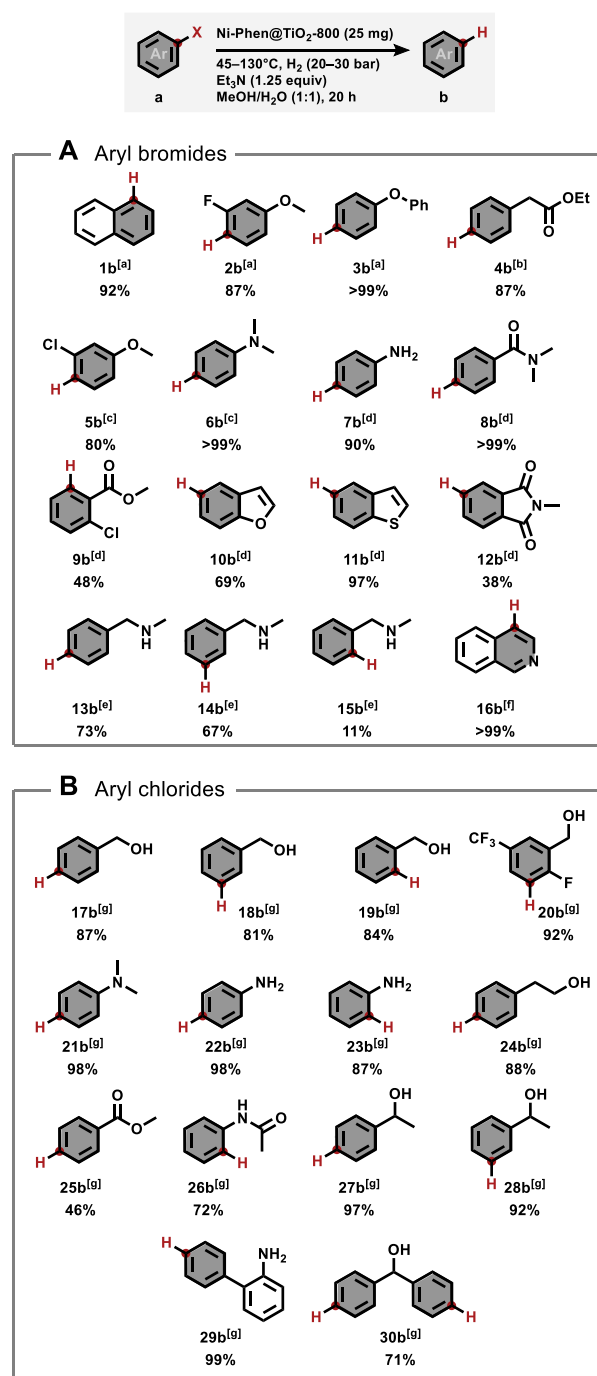
HDH of heterocyclic compounds is pertinent in the degradation of pharmaceutical and agrochemical ingredients. With this in mind, representative heterocycles 4-bromo-1-benzofuran **10a** and 4-bromobenzo-1-furanthiophene **11a** were hydrodehalogenated to the corresponding congeners in 69% and 97% yield, respectively, at 80°C and 20 bar H₂ pressure. In contrast, isoindoline **12a** proved to be more challenging under these conditions, with only a modest 38% yield of the expected product. Similarly, 4-bromoisoquinoline **16a** was found to be a particularly challenging substrate, however, an increased temperature of 120°C furnished the product in quantitative yield.

Ethyl ester **4a** was incompatible with our chosen solvent system of methanol and water (1:1), due to the incidence of transesterification to yield the corresponding methyl ester. However, upon switching to aqueous ethanol (40%), this issue was easily resolved leading to an 87% yield of **4b**. We also found that this reaction occurs smoothly in a variety of alcoholic beverages with similar alcohol content (Table S6).

Besides obtaining a low dehalogenation yield for substrate **25a** (46%), which contains an electron-withdrawing methyl ester substituent, all aryl chlorides tested were transformed in good to excellent yields (71–99%) at 130°C under 30 bar H₂.

Applications. To demonstrate the efficacy of our reaction for degradation of thermally inert substances, we subjected tetrabromobisphenol A **31a**—a widely applied fire retardant and precursor for fire-resistant polymers—to our Ni-Phen@TiO₂-800 catalyst. At 100°C full dehalogenation of all four bromine atoms was achieved giving 71% yield of the expected product **31b**. This transformation attests to this nickel catalyst's ability to take highly stable compounds, which are resistant to degradation, and transform them into substances more readily treated and disposed of. Furthermore, the upscaling of the catalytic protocol was successfully demonstrated in 5 mmol-scale reactions of the two industrially relevant compounds **32a** and **33a** (Scheme 1). Substrate **32a** represents the class of polybrominated diphenyl ethers (PBDEs) which are recognized as persistent organic pollutants that bioaccumulate in different organisms due to their low degradation.

Table 2. HDH of Aryl Halides^a

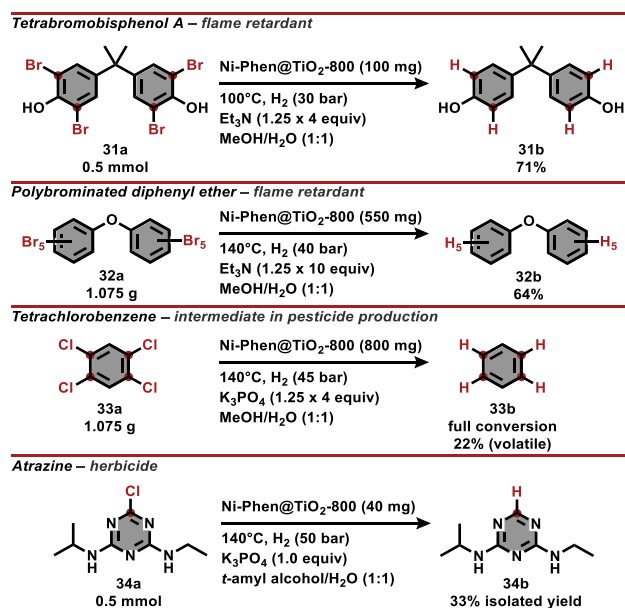


^aReaction conditions: 0.5 mmol **a**, 25 mg of Ni-Phen@TiO₂-800 (ca. 3 mol % Ni), Et₃N (1.25 equiv), 20 bar H₂, 45 °C, 2 mL MeOH/H₂O (1:1), 20 h, yields determined by GC-FID using hexadecane as an internal standard; ^b50°C, 2 mL EtOH:H₂O (1:1); ^c60°C; ^d80 °C; ^e90°C, 30 bar H₂; ^f120°C, 30 bar H₂; ^g130°C, 30 bar H₂.

1,2,4,5-Tetrachlorobenzene **33a** is a precursor which is widely used in the production of herbicides and the HDH demonstrates the catalyst's capability of activating multiple C-Cl bonds in a clean and efficient manner.

Syngenta's atrazine **34a** is a pre-emergent herbicide widely applied in the United States and Australia for broad spectrum weed control. Despite its continued operation today, it has been banned in the European Union since 2004 due to its concentrations in groundwater which exceeded regulatory limits. Moreover, this chlorinated triazole is both persistent in groundwater and in soil for up to four years.²³ Here, HDH of the C–Cl bond in **34a** was achieved using catalytic amounts of Ni-Phen@TiO₂-800 to yield the corresponding product **34b** with 33% isolated yield.

Scheme 1. HDH of tetrabromobisphenol A **31a**, PBDE **32a**, 1,2,4,5-tetrachlorobenzene, and atrazine.



Apart from catalytic HDH reactions, the required catalytic systems can be applied for similar deuterodehalogenation (DDH) transformations. Indeed, there is an ongoing interest in developing new deuteration methods, as isotope labelling plays an essential role for drug development. In detail, deuteration of active drugs can benefit their properties by significantly reducing rates of metabolism leading to less frequent dosing to achieve therapeutic effects.²⁴ Accordingly, we explored DDH for achieving deuterium incorporation. Using 5-iodo-1,2,3-trimethoxybenzene **35a**—which undergoes full dehalogenation with Ni-Phen@TiO₂-800 using just 1 bar H₂ at 80 °C—we tested various deuterium sources for selective D-labelling at the 5-position on the benzene ring. As shown in Table 3, we observed low to modest D incorporation using MeOH-d₄ and D₂O, respectively, under an atmosphere of hydrogen. Nevertheless, we found that very high D incorporation (86%) could be realized when both MeOH-d₄ and D₂O were used simultaneously. To our surprise, switching from hydrogen to deuterium gas led to no improvement in deuteration; in fact, no reactivity was observed at all and only starting material could be recovered from the reaction vessel. This observation can be explained by the increased bond strength of D–D compared to H–H, resulting in impeded bond cleavage. From these data, we infer that the D₂O is the most effective deuterium source for deuteration of **35a**. From a practical point of view, it is important to note that D₂O is relatively inexpensive (as D-sources go) and it is the parent compound of other D-sources, including D₂.

Recyclability. Catalyst stability and recyclability is undoubtedly an important consideration for heterogeneous catalysts. Accordingly, the activity of the Ni-Phen@TiO₂-800 catalyst was monitored over seven consecutive dehalogenations of **1a** using our optimized reaction conditions. From Figure 3, we see that whilst a quantitative yield of **1b** is achievable on the first run, subsequent reuse during the second run provided a significantly lower yield of 41%. Thereafter, the activity was maintained, and more consistent yields were then obtained during consecutive runs, and 19% yield of **1b** was still obtained after the seventh run.

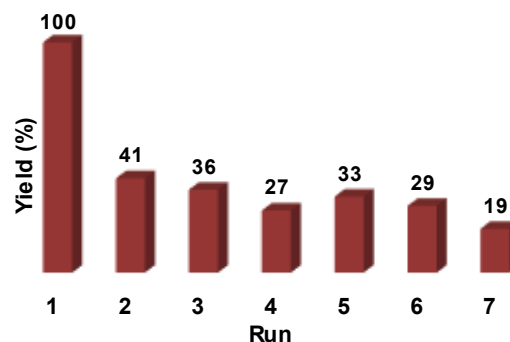
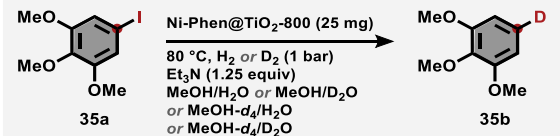


Figure 3. Recycling Ni-phen@TiO₂-800 for HDH of **1a**.

Due to the observed decrease in the catalyst's activity, we initially hypothesized that nickel may be leaching into the reaction solution. Thus, each reaction solution was analyzed by inductively coupled plasma mass spectrometry (ICP-MS) to look for the presence of any nickel. To our surprise, and despite the very low detection limit of the instrumentation, no nickel was detected. The change in reactivity therefore suggested that there were structural changes in the catalyst, most noticeably, after the first run. Thus, transmission electron microscopy (TEM) analysis for Ni-Phen@TiO₂-800 were conducted for both fresh (Figure 4) and spent catalyst samples (Figure 5). The TEM analysis showed three-dimensional nanoparticle agglomerations for the fresh catalyst. These nanoparticles have an average size in the range of 9.82–50.3 nm. The main discernible difference from the high-resolution TEM images for fresh and the spent catalyst is the randomly oriented nature of these particles with variable length thickness of the nanoparticles. Compositional analysis by energy dispersive X-ray spectroscopy (EDX)-elemental mapping reveals a widespread distribution of nickel and carbon throughout the titania matrix. It is understood that the structural changes in the catalyst are responsible for the drop in reactivity upon its reuse.

Raney nickel is well known for its ability to dehalogenate organohalides. We became interested in studying the reductive dehalogenation of **1a** and comparing our best results using Ni-Phen@TiO₂-800 with Raney nickel slurry. Using 10 mg of Raney nickel slurry proved effective for this transformation and led to an 84% yield of **1b**, with no detectable side products. But increasing amounts of Raney nickel led to a reduction in yield and drop in selectivity as hydrogenation of one aromatic ring yielded tetralin as a co-product (Section S18). Preferential selectivity for tetralin was observed, when the slurry was added in larger amounts (100–250 mg) with no detection of **1b**. Notably, even high loading (100 mg) of our Ni-Phen@TiO₂-800 catalyst completely prevented any tetralin formation.

Table 3. Deuteration of 5-Iodo-1,2,3-Trimethoxybenzene^a


entry	solv A	solv B	reductant (1 bar)	D incorp. (%)
1	D ₂ O	MeOH	H ₂	49
2	H ₂ O	MeOH-d ₄	H ₂	9
3	D ₂ O	MeOH-d ₄	H ₂	86
4	H ₂ O	MeOH	D ₂	no reactivity
5	D ₂ O	MeOH	D ₂	no reactivity
6	H ₂ O	MeOH-d ₄	D ₂	no reactivity
7	D ₂ O	MeOH-d ₄	D ₂	no reactivity

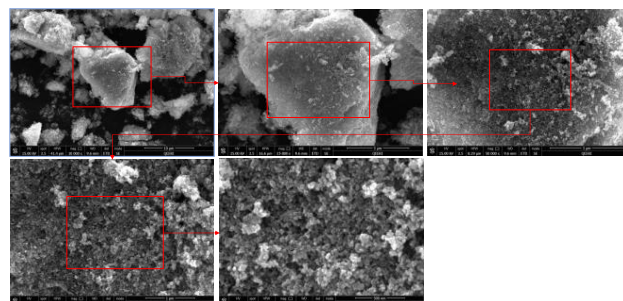
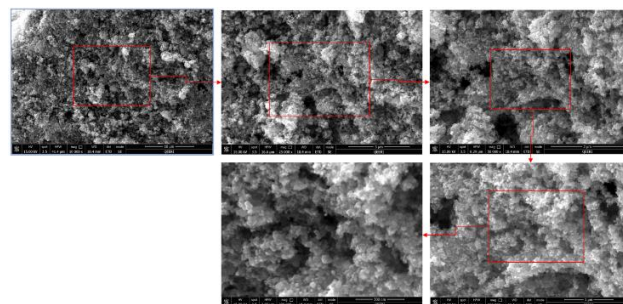
^aReaction conditions: 0.5 mmol **35a**, 25 mg of Ni-Phen@TiO₂-800 (ca. 3 mol % Ni), Et₃N (1.25 equiv), 1 bar H₂ or D₂, 80 °C, 2 mL solvent mixture (1:1), 20 h.

Characterization of the active catalyst. The Ni doped titania catalyst was characterized by means of X-ray powder diffraction (XRPD) to probe the crystallite structure of the material. Figure S2 shows the presence of mix rutile and anatase TiO₂ phases, with anatase as the dominate phase. The reflections at 2θ values of 25.31, 37.84, 48.06, 53.98, 55.12, 62.72, 68.14, 70.26, 75.14, and 82.76 are characteristic for the anatase phase matching with the standard pattern JCPDS 21-1272.²⁵ Whereas, the peaks at 2θ values 27.44, 36.06, 41.14, and 56.56 were unambiguously assigned to the rutile phase matching with JCPDS 21-1276.^{25b,26} The rutile titania phase has been reported to be predominant at a higher processing temperature and is usually obtained via high temperature calcination of anatase phase TiO₂.²⁷ The reflections at 2θ values of 44.50 and 51.84 correspond to the FCC-phase of Ni.²⁸ The crystallite size was calculated using the Scherrer equation $D = k\lambda/\beta\cos\theta$ (where D = average crystallite size, K = Scherrer coefficient, λ = wavelength of X-ray radiation, θ = diffraction angle, and β = FWHM of diffraction peak, which is reflected in the observed broad reflections in the XRD spectrum of the catalyst sample shown in Figure S2).

For further characterization, the catalyst was analyzed using X-ray photoelectron spectroscopy (XPS), scanning electron microscopy (SEM), and transmission electron microscopy (TEM). Near-surface elemental compositions and the oxidation states of the metal in fresh and spent catalysts were analyzed using XPS in the binding energy region 0 – 1400 eV. The survey spectrum for fresh catalyst shown in Figure 6a reveals the presence of Ni, O, Ti, N, and C in the Ni-Phen@TiO₂-800 matrix. The binding energy was corrected by setting the C 1s peak from adventitious hydrocarbon at 284.8 eV. The Ni 2p spectrum (Figure 6b) shows the peaks at binding energy of 855.59 eV and 873.80 eV which are characteristic peaks assigned to Ni 2p_{3/2} and Ni 2p_{1/2}, respectively. Both peaks accompanied by their satellite peaks at binding energy of 860.66 and 879.02 eV, respectively. The deconvoluted Ni 2p_{3/2} peak at 855.59 eV corresponds to NiO, and the 857.53 eV peak corresponds to Ni(OH)₂.²⁹ The peak located at 853.02 eV is attributed to Ni⁰ which indicates the presence of metallic nickel on the catalyst surface.³⁰ The atomic distribution of 1.25:1.0 for Ni²⁺: Ni⁰ was quantified using the spectral intensity of Ni 2p_{3/2} and Ni⁰ peaks of the XPS spectrum. The deconvolution of C 1s spectrum (Figure 6c) shows relevant fitting peaks with the binding energies at 284.77 eV for C(sp³)-C(sp³), 286.10 eV for C(sp³)-O, and 287.97 eV for C=O. The first peak at 284.77 eV was attributed to the adventitious elemental carbon on the surface, whereas

the other two peaks are from C–O (C–O–C) and C=O are assigned to oxidized carbon species.³¹ Moreover, the absence of a peak around 282.0 eV reveals that the substitution of oxygen in the lattice of TiO₂ as Ti–C is not formed.^{31c,31d} In the O 1s spectrum (Figure 6d), the large peak at 530.40 eV is assigned to a metal–O and peak at 531.90 eV was assigned to C–O.³² This indicates different chemical states of oxygen on the surface of catalyst. In N 1s XPS spectrum (Figure 6e), the deconvolution of the N 1s region revealed the presence of peaks at 399.20 eV and 401.30 eV attributed to pyridinic-N and graphitic-N respectively.³³ The Ti 2P spectrum indicates two photoelectron signals Ti 2p_{3/2} and Ti 2p_{1/2} with binding energies at 458.98 and 464.80 eV, respectively, and associated satellite peak at 472.51 eV.^{31d,34}

Scanning Electron Microscopy (SEM) images reveal the surface morphology of catalyst before the reaction. SEM images show presence of small spherical particles which are agglomerated together, whereas a widely dispersed spherical particles are predominantly observed for the spent catalyst samples, Figures 4 & 5. The EDS spectra for the catalyst before and after the reaction are shown in Figure S11.

**Figure 4.** SEM images of fresh Ni-phen@TiO₂-800 catalyst.**Figure 5.** SEM images of the spent Ni-phen@TiO₂-800.

3. CONCLUSIONS

In summary, we have developed safe and inexpensive Ni-Phen@TiO₂-800 as a catalyst suitable for the dehalogenation of aryl iodides, bromides, and chlorides. This catalytic system allows for HDH of various substrates possessing electron-rich, electron-poor groups, sensitive functional groups, and heterocycles. The utility of this heterogeneous nickel catalyst was demonstrated on gram-scale HDH of more challenging and industrially relevant substrates, such as environmental persistent fire retardants, toxic polybrominated diphenyl ethers (PBDE), and 1,2,4,5-tetrachlorobenzene. Furthermore, we have showcased that this catalyst system could be used for selective incorporation of deuterium labelling using D₂O/methanol-d₄ as

a deuterium source. Compared to commercial Raney nickel, our easy-to-handle nickel catalyst provides higher HDH yields than under the same conditions without byproduct formation.

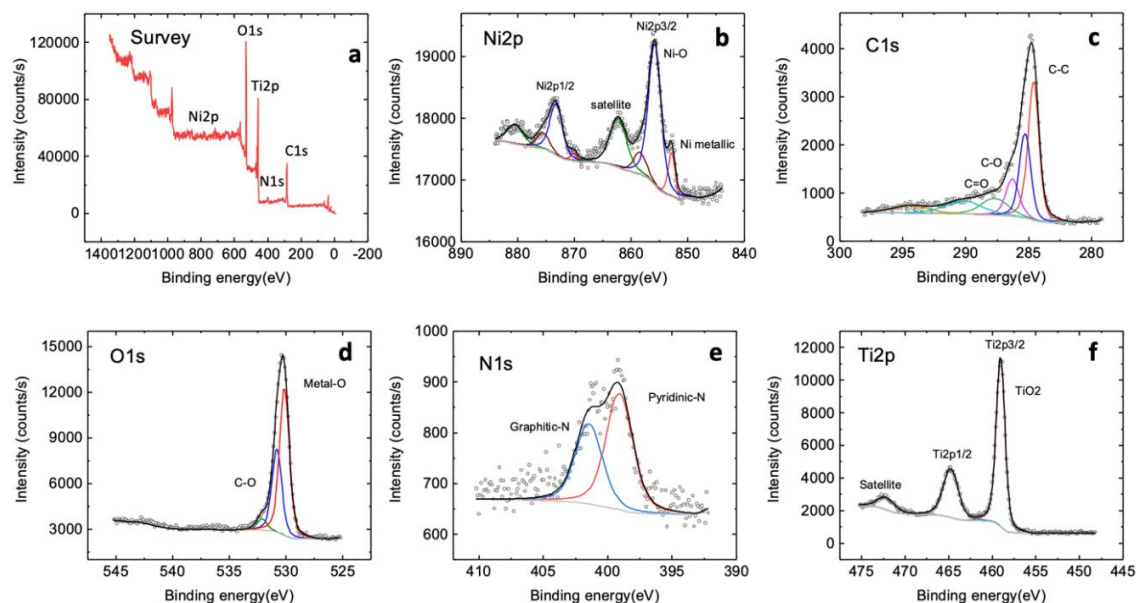


Figure 6. XPS survey spectrum of Ni-Phen@TiO₂-800 catalyst (a) and high-resolution deconvoluted XPS spectra for Ni 2p (b), C 1s (c), O 1s (d), N 1s (e) and Ti 2p (f).

ASSOCIATED CONTENT

Supporting Information

The Supporting Information is available free of charge on the ACS Publications website.

AUTHOR INFORMATION

Corresponding Authors

Matthias Beller – Leibniz-Institut für Katalyse e.V., Albert-Einstein-Straße 29a, 18059 Rostock, Germany;
Email: matthias.beller@catalysis.de

Kathrin Junge – Leibniz-Institut für Katalyse e.V., Albert-Einstein-Straße 29a, 18059 Rostock, Germany;
Email: kathrin.junge@catalysis.de

Authors

David K. Leonard – Leibniz-Institut für Katalyse e.V., Albert-Einstein-Straße 29a, 18059 Rostock, Germany;
Email: david.leonard@catalysis.de

Pavel Ryabchuk – Leibniz-Institut für Katalyse e.V., Albert-Einstein-Straße 29a, 18059 Rostock, Germany;
Current address: Galapagos NV, Generaal De Wittelaan L11 A3, 2800 Mechelen, Belgium;
Email: pavel.ryabchuk@glpg.com

Muhammad Anwar – Qatar Environment & Energy Research Institute Research, Education City, 34110, Doha;
Email: muanwar@hbku.edu.qa

Sarim Dastgir – Qatar Environment & Energy Research Institute Research, Education City, 34110, Doha;
Email: sdastgir@hbku.edu.qa

ACKNOWLEDGMENT

We gratefully acknowledge the support from the Federal Ministry of Education and Research (BMBF) and the State of Mecklenburg-Vorpommern. Financial support by Fonds der Chemischen Industrie (Kekulé-Stipendium n. 103231) for D.K.L. is also acknowledged. The authors thank Anja Simmla for ICP analyses and the analytical staff of the Leibniz Institute for Catalysis, Rostock, for their excellent service.

REFERENCES

- (a) Sahoo, B.; Surkus, A.-E.; Pohl, M.-M.; Radnik, J.; Schneider, M.; Bachmann, S.; Scalone, M.; Junge, K.; Beller, M. A Biomass-Derived Non-Noble Cobalt Catalyst for Selective Hydrodehalogenation of Alkyl and (Hetero)Aryl Halides. *Angew. Chem.* **2017**, *129*, 11394–11399. (b) Ramanathan, A.; Jimenez, L. S. Reductive Dehalogenation of Aryl Bromides and Chlorides and Their Use as Aryl Blocking Groups. *Synthesis* **2010**, *2*, 217–220.
- Thompson, R. J. Freon, a Refrigerant. *Ind. Eng. Chem.* **1932**, *24*, 620–623.
- Addison, R. F. PCB Replacements in Dielectric Fluids. *Environ. Sci. Technol.* **1983**, *17*, 486A–494A.
- (a) Blaser, H.-U. The Chiral Switch of (S)-Metolachlor: A Personal Account of an Industrial Odyssey in Asymmetric Catalysis. *Adv. Synth.*

- Catal.* **2002**, *1*, 344. (b) Kuck, K.-H.; Gisi, U. Modern Crop Protection Compounds; Kramer, W., Schirmer, U., Eds.; Wiley-VCH, 2007; Vol. 2, pp 415–432. (c) Earley, F. Modern Crop Protection Compounds; Kramer, W., Schirmer, U., Eds.; Wiley-VCH, 2007; Vol. 2, pp 433–538.
5. Wilcken, R.; Zimmermann, M. O.; Lange, A.; Joerger, A. C.; Boeckler, F. M. Principles and Applications of Halogen Bonding in Medicinal Chemistry and Chemical Biology. *J. Med. Chem.* **2013**, *56*, 1363–1388.
6. Segev, O.; Kushmaro, A.; Brenner, A. Environmental Impact of Flame Retardants (Persistence and Biodegradability). *Int. J. Environ. Res. Public Health* **2009**, *6*, 478–491.
7. (a) Stellman, J. M.; Stellman, S. D.; Christian, R.; Weber, T.; Tomasallo, C. The Extent and Patterns of Usage of Agent Orange and Other Herbicides in Vietnam. *Nature* **2003**, *422*, 681–687. (b) White, S. S.; Birnbaum, L. S. An Overview of the Effects of Dioxins and Dioxin-Like Compounds on Vertebrates, as Documented in Human and Ecological Epidemiology. *J. Environ. Sci. Health Pt C – Environ. Carcinog. Ecotoxicol. Rev.* **2009**, *27*, 197–211. (c) An extensive review regarding the health effects of Agent Orange: Institute of Medicine. 2001. Veterans and Agent Orange: Update 2000. Washington, DC: The National Academies Press, 2007.
8. Ritter, R.; Scheringer, M.; MacLeod, M.; Moeckel, C.; Jones, K. C.; Hungerbühler, K. Intrinsic Human Elimination Half-Lives of Polychlorinated Biphenyls Derived from the Temporal Evolution of Cross-Sectional Biomonitoring Data from the United Kingdom. *Environ. Health Perspect.* **2011**, *119*, 225–231.
9. Stanmore, B. R. The Formation of Dioxins in Combustion Systems. *Combust. Flame* **2004**, *136*, 398–427.
10. Gomes, H. I.; Dias-Ferreira, C.; Ribeiro, A. B. Overview of In Situ and Ex Situ Remediation Technologies for PCB-Contaminated Soils and Sediments and Obstacles for Full-Scale Application. *Sci. Total Environ.* **2013**, *445–446*, 237–260.
11. Paukshtis, E. A.; Simonova, L. G.; Zagoruiko, A. N.; Balzhinimaev, B. S. Oxidative Destruction of Chlorinated Hydrocarbons on Pt-Containing Fiber-Glass Catalysts. *Chemosphere* **2010**, *79*, 199–204.
12. Chen, X.; Ma, W.; Li, J.; Wang, Z.; Chen, C.; Ji, H.; Zhao, J. Photocatalytic Oxidation of Organic Pollutants Catalyzed by an Iron Complex at Biocompatible pH Values: Using O₂ as Main Oxidant in a Fenton-Like Reaction. *J. Phys. Chem. C* **2011**, *115*, 4089–4095.
13. Wu, Z.-L.; Ondruschka, B.; Cravotto, G. Degradation of Phend Under Combined Irradiation of Microwaves and Ultrasound. *Environ. Sci. Technol.* **2008**, *42*, 8083–8087.
14. Sun, C.; Baig, S. A.; Lou, Z.; Zhu, J.; Wang, Z.; Li, X.; Wu, J.; Zhang, Y.; Xu, X. Electrocatalytic Dechlorination of 2,4-Dichlorophenoxyacetic Acid Using Nanosized Titanium Nitride Doped Palladium/Nickel Foam Electrodes in Aqueous Solutions. *Appl. Catal. B: Environ.* **2014**, *158–159*, 38–47.
15. (a) Menini, C.; Park, C.; Shin, E.-J.; Tavoularis, G.; Keane, M. A. Catalytic Hydrodehalogenation as a Detoxification Methodology. *Catal. Today* **2000**, *62*, 355–366. (b) Léger, B.; Nowicki, A.; Roucoux, A.; Rolland, J.-P. Competitive Hydrogenation/Dehalogenation of Halogenoarenes With Surfactant-Stabilized Aqueous Suspensions of Rhodium and Palladium Colloids: A Major Effect of the Metal Nature. *J. Mol. Catal. A: Chem.* **2007**, *266*, 221–225. (c) Kopinke, F.-D.; Angeles-Wedler, D.; Fritsch, D.; Mackenzie, K. Pd-Catalyzed Hydrodechlorination of Chlorinated Aromatics in Contaminated Waters—Effects of Surfactants, Organic Matter and Catalyst Protection by Silicone Coating. *Appl. Catal. B: Environ.* **2010**, *96*, 323–328. (d) Navon, R.; Eldad, S.; Mackenzie, K.; Kopinke, F.-D. Protection of Palladium Catalysts for Hydrodechlorination of Chlorinated Organic Compounds in Wastewaters. *Appl. Catal. B: Environ.* **2012**, *119–120*, 241–247.
16. Alonso, F.; Beletskaya, I. P.; Yus, M. Metal-Mediated Reductive Hydrodehalogenation of Organic Halides. *Chem. Rev.* **2002**, *102*, 4009–4091.
17. (a) Ueno, R.; Shimizu, T.; Shirakawa, E. Reduction of Aryl Halides into Arenes with 2-Propanol Promoted by a Substoichiometric Amount of a tert-Butoxy Radical Source. *Synlett*, **2016**, *27*, 741–744. (b) Ukisu, Y.; Miyadera, T. Hydrogen-Transfer Hydrodehalogenation of Aromatic Halides With Alcohols in the Presence of Noble Metal Catalysts. *J. Mol. Catal. A-Chem.* **1997**, *125*, 135–142. (c) Zheng, H.-X.; Shan, X.-H.; Qu, J.-P.; Kang, Y.-B. Transition-Metal-Free Hydrogenation of Aryl Halides From Alcohol to Aldehyde. *Org. Lett.* **2017**, *19*, 5114–5117.
18. Larock, R. C.; Ding, S. Synthesis of Aryl-Substituted 3-Alkenamides Via Palladium-Catalyzed Cross-Coupling of Aryl Iodides and 4-Alkenyl-2-Azetidinones. *Tetrahedron Lett.* **1993**, *34*, 979–982.
19. (a) Lipshutz, B. H.; Tomioka, T.; Sato, K. Nickel-on-Charcoal-Catalyzed Reductions of Aryl Chlorides. *Synlett* **2001**, *SI*, 970–873. (b) Rettenmeier, C.; Wadepohl, H.; Gade, L. H. Stereoselective Hydrodehalogenation via a Radical-Based Mechanism Involving T-Shaped Chiral Nickel(I) Pincer Complexes. *Chem. Eur. J.* **2014**, *20*, 9657–9665. (c) Parnes, H.; Pease, J. Simple Method for the Reductive Dehalogenation of 9 α -Bromo Steroids. *J. Org. Chem.* **1979**, *44*, 151–152.
20. (a) Guo, H.; Kanno, K.-i.; Takahashi, T. Iron-Catalyzed Dechlorination of Aryl Chlorides. *Chem. Lett.* **2004**, *33*, 1356–1357. (b) Ryuichiro, H.; Wen-Hua, S.; Yasushi, N.; Tamotsu, T. Zirconocene Catalyzed Dehalogenation of Aromatic Halides by Alkylmagnesium Reagents. *Chem. Lett.* **1997**, *26*, 1251–1252. (c) Hara, R.; Sato, K.; Sun, W.-H.; Takahashi, T. Catalytic Dechlorination of Aromatic Chlorides Using Grignard Reagents in the Presence of (C₅H₅)₂TiCl₂. *Chem. Commun.* **1999**, 845–846.
21. Anastas, P. T.; Warner, J. C. Green Chemistry: Theory and Practice, Oxford University Press, 1998, p.30.
22. (a) Ryabchuk, P.; Agostini, G.; Pohl, M.-M.; Lund, H.; Agapova, A.; Junge, H.; Junge, K.; Beller, M. Intermetallic Nickel Silicide Nanocatalyst—A Non-Noble Metal-Based General Hydrogenation Catalyst. *Sci. Adv.* **2018**, *4*, eaat0761. (b) Chen, F.; Kreyenschulte, C.; Radnik, J.; Lund, H.; Surkus, A.-E.; Junge, K.; Beller, M. Selective Semihydrogenation of Alkynes with N-Graphitic-Modified Cobalt Nanoparticles Supported on Silica. *ACS Catal.* **2017**, *7*, 1526–1532. (c) Sahoo, B.; Surkus, A.-E.; Pohl, M.-M.; Radnik, J.; Schneider, M.; Bachmann, S.; Scalone, M.; Junge, K.; Beller, M. A Biomass-Derived Non-Noble Cobalt Catalyst for Selective Hydrodehalogenation of Alkyl and (Hetero)Aryl Halides. *Angew. Chem.* **2017**, *129*, 11394–11399. (d) Chen, F.; Sahoo, B.; Kreyenschulte, C.; Lund, H.; Zeng, M.; He, L.; Junge, K.; Beller, M. Selective Cobalt Nanoparticles for Catalytic Transfer Hydrogenation of N-Heterocycles. *Chem. Sci.* **2017**, *8*, 6239–6246. (e) Sahoo, B.; Formenti, D.; Topf, C.; Bachmann, S.; Scalone, M.; Junge, K.; Beller, M. Biomass-Derived Catalysts for Selective Hydrogenation of Nitroarenes. *ChemSusChem* **2017**, *10*, 3035–3039. (f) Formenti, D.; Ferretti, F.; Topf, C.; Surkus, A.-E.; Pohl, M.-M.; Radnik, J.; Schneider, M.; Junge, K.; Beller, M.; Ragaini, F. Co-Based Heterogeneous Catalysts From Well-Defined α -Diimine Complexes Discussing the Role of Nitrogen. *J. Catal.* **2017**, *351*, 79–89.
23. Jablonowski, N. D.; Schäffer, A.; Burauel, P. Still Present After All These Years: Persistence Plus Potential Toxicity Raise Questions About The Use of Atrazine. *Environ. Sci. Pollut. Res. Int.* **2011**, *18*, 328–331.
24. (a) Sanderson, K. Big Interest in Heavy Drugs. *Nature* **2009**, *458*, 269. (b) Katsnelson, A. Heavy Drugs Draw Heavy Interest From Pharma Backers. *Nat. Med.* **2013**, *19*, 656. (c) Schmidt, C. First Deuterated Drug Approved. *Nat. Biotechnol.* **2017**, *35*, 493–494.
25. (a) Li, W.; Liang, R.; Hu, A.; Huang, Z.; Zhou, Y. N. Generation of Oxygen Vacancies In Visible Light Activated One-Dimensional Iodine TiO₂ Photocatalysts. *RSC Adv.* **2014**, *4*, 36959–36966. (b) Hu, A.; Zhang, X.; Luong, D.; Oakes, K. D.; Servos, M. R.; Liang, R.; Kurdi, S.; Peng, P.; Zhou, Y. Adsorption and Photocatalytic Degradation Kinetics of Pharmaceuticals by TiO₂ Nanowires During Water Treatment. *Waste Biomass Valor.* **2012**, *3*, 443–449. (c) Meng, A.; Zhang, J.; Xu, D.; Cheng, B.; Yu, J. Enhanced Photocatalytic H₂-Production Activity of Anatase TiO₂ Nanosheet by Selectively Depositing Dual-Cocatalysts on {101} and {001} Facets. *Appl. Catal. B* **2016**, *198*, 286–294.
26. Liu, W.; Zhang, Y. Electrical characterization of TiO₂/CH₃NH₃PbI₃ Heterojunction Solar Cells. *J. Mater. Chem. A* **2014**, *2*, 10244–10249.
27. (a) Jitputti, J.; Pavaupree, S.; Suzuki, Y.; Yoshikawa, S. Synthesis of TiO₂ Nanotubes and Its Photocatalytic Activity for H₂ Evolution. *Jpn. J. Appl. Phys.* **2008**, *47*, 751–756. (b) Zhao, X.; Jin, W.; Cai, J.; Ye, J.; Li, Z.; Ma, Y.; Xie, J.; Qi, L. Shape- and Size-Controlled Synthesis of Uniform Anatase TiO₂ Nanocuboids Enclosed by Active {100} and {001} Facets. *Adv. Fun. Mater.* **2011**, *21*, 3554–3563.
28. (a) Li, J.; Li, P.; Li, J.; Tian, Z.; Yu, F. Highly-Dispersed Ni-NiO Nanoparticles Anchored on an SiO₂ Support for an Enhanced CO Methanation Performance. *Catalysts* **2019**, *9*, 506. (b) García-Cerda, L. A.; Bernal-Ramos, K. M.; Montemayor, S. M.; Quevedo-López, M. A.; Betancourt-Galindo, R.; Bueno-Báques, D. Preparation of hcp and fcc Ni and Ni/NiO Nanoparticles Using a Citric Acid Assisted Pechini-Type Method. *J. Nanomater.* **2011**, *2011*, 162495.
29. Zhang, W.; Li, B. Electrochemical Properties and XPS Analysis of Ni-B/SiC Nanocomposite Coatings. *Int. J. Electrochem. Sci.* **2018**, *13*, 3516–3526.
30. (a) Biesinger, M. C.; Payne, B. P.; Lau, L. W. M.; Gerson, A.; Smart, R. S. C. X-Ray Photoelectron Spectroscopic Chemical State

Quantification of Mixed Nickel Metal, Oxide and Hydroxide Systems. *Surf. Interface Anal.* **2009**, *41*, 324–332. (b) Hengne, A. M.; Samal, A. K.; Enakonda, L. R.; Harb, M.; Gevers, L. E.; Anjum, D. H.; Hedhili, M. N.; Saih, Y.; Huang, K.-W.; Basset, J.-M. Ni-Sn-Supported ZrO₂ Catalysts Modified by Indium for Selective CO₂ Hydrogenation to Methanol. *ACS Omega* **2018**, *3*, 3688–3701.

31. (a) Sakthivel, S.; Kisch, H. Daylight Photocatalysis by Carbon-Modified Titanium Dioxide. *Angew. Chem., Int. Ed.* **2003**, *42*, 4908–4911. (b) Wang, H.; Wu, Z.; Liu, Y. A Simple Two-Step Template Approach for Preparing Carbon-Doped Mesoporous TiO₂ Hollow Microspheres. *J. Phys. Chem. C* **2009**, *113*, 13317–13324. (c) Zhang, L.; Koka, R. V. A Study On the Oxidation and Carbon Diffusion of TiC in Alumina-Titanium Carbide Ceramics Using XPS and Raman Spectroscopy. *Mater. Chem. Phys.* **1998**, *57*, 23–32. (d) Liu, J.; Zhang, Q.; Yang, J.; Ma, H.; Tade, M. O.; Wang, S.; Liu, J. Facile Synthesis of Carbon-Doped Mesoporous Anatase TiO₂ for the Enhanced Visible-Light Driven Photocatalysis. *Chem. Commun.* **2014**, *50*, 13971–13974.

32. (a) Purbia, R.; Borah, R.; Paria, S. Carbon-Doped Mesoporous Anatase TiO₂ Multi-Tubes Nanostructures for Highly Improved Visible

Light Photocatalytic Activity. *Inorg. Chem.* **2017**, *56*, 10107–10116. (b) Koshtyal, Y.; Nazarov, D.; Ezhov, I.; Mitrofanov, I.; Kim, A.; Rymyantsev, A.; Lyutakov, O.; Popovich, A.; Maximov, M. Atomic Layer Deposition of NiO to Produce Active Material for Thin-Film Lithium-Ion Batteries. *Coatings* **2019**, *9*, 301.

33. (a) Jaouen, F.; Herranz, J.; Lefèvre, M.; Dodelet, J.-P.; Kramm, U. I.; Herrmann, I.; Bogdanoff, P.; Maruyama, J.; Nagaoka, T.; Garsuch, A.; Dahn, J. R.; Olson, T.; Pylypenko, S.; Atanassov, P.; Ustinov, E. A. Cross-Laboratory Experimental Study of Non-Noble-Metal Electrocatalysts for the Oxygen Reduction Reaction. *ACS Appl. Mater. Interfaces* **2009**, *1*, 1623–1639. (b) Matsoso, B. J.; Ranganathan, K.; Mutuma, B. K.; Leretholi, T.; Jones, G.; Coville, N. J. Time-Dependent Evolution of the Nitrogen Configurations in N-Doped Graphene Films. *RSC Adv.* **2016**, *6*, 106914–106920.

34. Wang, Y.; Li, L.; Huang, X.; Li, Q.; Li, G. New Insights Into Fluorinated TiO₂ (Brookite, Anatase and Rutile) Nanoparticles as Efficient Photocatalytic Redox Catalysts. *RSC Adv.* **2015**, *5*, 34302–34313.

APPENDIX: EXPERIMENTAL SECTION

A.1 GENERAL EXPERIMENTAL DETAILS

Most substrates were obtained from commercial sources and used as supplied; others were prepared as detailed below.

All metal catalysts were obtained from commercial sources and used as supplied.

Unless otherwise mentioned, all catalytic oxidation reactions were carried out in 2 mL glass vials, which were set in an alloy plate and placed inside a 300 mL autoclave (Parr[®] Instrument Company).

All oxidation reactions were performed in a Parr[®] Instrument Company autoclave.

Deuterated solvents were ordered from Deutero GmbH. NMR spectra were recorded using Bruker 300 Fourier, Bruker AV 300 and Bruker AV400 spectrometers. Chemical shifts are reported in ppm, relative to the deuterated solvent. Coupling constants are expressed in Hertz (Hz). The following abbreviations are used: s = singlet, d = doublet, t = triplet, and m = multiplet. The residual solvent signals were used as references for ¹H and ¹³C NMR spectra (CDCl₃: δH = 7.26 ppm, δC = 77.16 ppm; DMSO-d₆: δH = 2.50 ppm, δC = 39.52 ppm). All measurements were carried out at room temperature unless otherwise stated. GC-FID analyses were carried out using an Agilent 7890B gas chromatograph fitted with an Agilent HP5 column (30 m × 0.25 mm I.D. × 0.25 μm).

Solvents were used directly without further purification. HPLC grade MeCN was supplied by Fisher Chemical.

Scanning transmission electron microscopy (STEM) was performed with a probe aberration-corrected JEM-ARM200F (Jeol Ltd., CEOS Corrector) at 200 kV. The microscope is further equipped with an Enfinium ER (Gatan) electron energy loss spectrometer. For STEM imaging a High-Angle Annular Dark Field (HAADF) and an Annular Bright Field (ABF) detector were applied, while EELS acquisition was done with the Annular Dark Field (ADF) detector. The solid sample was dried in advance of the electron microscopy measurements and then placed without any further pretreatment on a holey carbon supported Cu-grid (mesh 300), which was then transferred to the microscope. EEL spectra were background subtracted and deconvolved.

A.2 SYNTHETIC PROCEDURES USED IN SECTION 5.1

A.2.1 *Synthesis of Morpholines and Piperazines*A.2.1.1 *General Procedure A (GP-A)*

A mixture of aryl bromide (10 mmol), morpholine or piperazine (20 mmol), K_2CO_3 (20 mmol), CuI (1.0 mmol) and L-proline (2.0 mmol) in 10 mL of DMSO was heated at 90°C and for 24 h. The cooled mixture was partitioned between water and ethyl acetate. The organic layer was separated, and the aqueous layer was extracted with ethyl acetate. The combined organic layers were dried over Na_2SO_4 , and concentrated *in vacuo*. The desired products were isolated by silica gel column chromatography (*n*-heptane/ethyl acetate mixtures). (Ma, D.; Cai, Q; Zhang, H. Mild Method for Ullmann Coupling Reaction of Amines and Aryl Halides.^[91]

A.2.2 *Synthesis of Amines*A.2.2.1 *General Procedure B (GP-B)*

To an 8 mL glass vial equipped with a magnetic stir bar, Pd/C (Palladium on activated charcoal 10 % Pd basis—purchased from Sigma–Aldrich) (40 mg), and ketone (2.0 mmol) were added. The vial was capped and pierced with a small needle before EtOH (3 mL) was added. The vial was then placed into an aluminium heating block and then sealed inside a 300 mL steel autoclave (Parr Instrument Company). The autoclave was flushed with H_2 three times and then pressurised to the desired value (50 bar). Then it was placed into an aluminium block and heated to 130°C. At the end of the reaction, the autoclave was quickly cooled to room temperature. A sample of the the reaction mixture was analysed by GC-FID. The product was purified via flash column chromatography using heptane/ethyl acetate. Solvent was removed *in vacuo* to yield the desired product.

A.2.2.2 *General Procedure C (GP-C)*

To a 100 mL round bottom flask equipped with magnetic stir bar was added amine (8.0 mmol, 1 equiv) and methanol (20 mL). Next, aldehyde (10.0 mmol, 1.25 equiv) was added, followed by $NaBH_3CN$ (10.0 mmol, 1.25 equiv). After completion, the reaction was quenched with saturated $NaHCO_3$ (20 mL) and methanol was removed *in vacuo*. The mixture was diluted with H_2O and extracted with ethyl acetate (50 mL \times 3). The extracts were combined and washed with brine and dried over anhydrous Na_2SO_4 and filtered. Lastly, the solvent was removed *in vacuo*.

A.2.2.3 General Procedure D (GP-D)

To a 100 mL round bottom flask equipped with magnetic stir bar was added dimethylformamide (20 mL), bromide (20.0 mmol, 1 equiv) and amine (30.0 mmol, 2.0 equiv). The reaction mixture was heated to 100°C. After completion the reaction mixture was filtered to remove K₂CO₃. The mixture was diluted with H₂O and extracted with ethyl acetate (50 mL × 3). The extracts were combined and washed with brine and dried over anhydrous Na₂SO₄ and then filtered. Lastly, solvent and amine was removed *in vacuo*.

A.2.3 Copper-Catalysed Oxidations

A.2.3.1 General Procedure E (GP-E) – Cleavage of Amines

To a 4 mL vial equipped with a magnetic stir bar, CuCl (2.5 mg, 0.025 mmol) was added. The vial was capped and pierced with a small needle. HPLC grade acetonitrile (2 mL), pyridine (80 µg) and tertiary amine (0.5 mmol) were added, independently. The vial was then placed into an aluminium heating block and then sealed inside a 300 mL steel autoclave (Parr Instrument Company). The autoclave was flushed with air twice and then pressurised to the desired value (30 bar). Then it was placed into an aluminium block and heated to 100°C. At the end of the reaction, the autoclave was quickly cooled to room temperature. A sample of the the reaction mixture was analysed by GC-FID. The product was purified via flash column chromatography using heptane/ethyl acetate. Solvent was removed *in vacuo* to yield the desired product.

A.2.3.2 General Procedure F (GP-F) – Cleavage of Morpholines and Piperazines

To a 4 mL vial equipped with a magnetic stir bar, Cu(OTf)₂ (6.0 mg) was added. The vial was capped and pierced with a small needle. HPLC grade acetonitrile (2 mL), pyridine (80 µL) and morpholine or piperazine (0.5 mmol) were added, independently. The vial was then placed into an aluminium heating block and then sealed inside a 300 mL steel autoclave (Parr Instrument Company). The autoclave was flushed with air twice and then pressurised to the desired value (20 bar). Then it was placed into an aluminium block and heated to 80°C. At the end of the reaction, the autoclave was quickly cooled to room temperature. A sample of the the reaction mixture was analysed by GC-FID. The product was purified via flash column chromatography using heptane/ethyl acetate. Solvent was removed *in vacuo* to yield the desired product.

A.3 SYNTHETIC PROCEDURES USED IN SECTION 5.2

Morpholines were synthesised according to GP-A, Section A.2.1.1.

A.3.1 Cobalt–Manganese-Catalysed Oxidations

A.3.1.1 General Procedure G (GP-G) – Cleavage of Morpholines

To a 4 mL glass vial equipped with a magnetic stir bar, aryl morpholine (0.5 mmol), $\text{Mn}(\text{OAc})_2 \cdot 4\text{H}_2\text{O}$ (6.1 mg; 5 mol %) and CoBr_2 (10.9 mg; 10 mol %) were added. The vial was capped and pierced with a small needle. HPLC grade acetonitrile (2 mL) was added via a 2 mL syringe. Pyridine (8 μL ; 20 mol %) was added via a glass microsyringe. The vial was then placed into an aluminium heating block and then sealed inside an autoclave (Parr Instrument Company). The autoclave was then pressurised with air (20–30 bar). The reaction mixture was stirred for 24 hours at 60–120°C. Next, the reaction was cooled to room temperature. A sample of the reaction mixture was analysed by GC-FID and using TLC. The product was purified via flash column chromatography (RediSep Rf+ automatic column) using heptane/ethyl acetate. Solvent was removed *in vacuo* to yield the desired product.

A.4 SYNTHETIC PROCEDURES USED IN SECTION 5.3

Morpholines and piperazines were synthesised according to GP-A, [Section A.2.1.1](#).

A.4.1 Iron-Catalysed Oxidations

A.4.1.1 General Procedure H (GP-H) – Cleavage of Morpholines

A 4 mL glass vial equipped with a magnetic stir bar was charged with aryl morpholine (0.5 mmol) and FeCl_3 (8.1 mg; 10 mol %). The vial was capped, and the septum was pierced with a small needle. HPLC grade acetonitrile (2 mL) was added via a 2 mL syringe. Pyridine (80 μL ; 2.0 equiv) was added via a glass microsyringe. The vial was then placed into an aluminium heating block and then sealed inside an autoclave (Parr[®] Instrument Company). The autoclave was then pressurised with air (30 bar). The reaction mixture was stirred for 24 h at 100°C. Next, the reaction was cooled to room temperature. A sample of the reaction mixture was analysed by GC-FID and TLC. The product was purified via flash column chromatography (RediSep[®] Rf+ automatic column) using heptane/ethyl acetate. Solvent was removed *in vacuo* to yield the desired product.

A.4.1.2 General Procedure I (GP-I) – Design of Experiments

A 4 mL glass vial equipped with a magnetic stir bar was charged with 1,4-diphenylpiperazine (59.6 mg; 0.25 mmol), TEMPO (3.9–11.7 mg; 10–30 mol %) and FeCl_3 (2.0–6.1 mg; 3–15 mol %) in that order. The vial was capped, and the septum was pierced with a small needle. HPLC grade acetonitrile (1 mL) was added via a 2 mL syringe. Pyridine (2.0–6.0 μL ; 10–30 mol %) was added via a glass microsyringe. The vial was then placed into an aluminium heating block and then sealed inside an autoclave (Parr[®] Instrument Company). The autoclave was

then pressurised with air (10–30 bar). The reaction mixture was stirred for 24 h at 80–120°C. Next, the reaction was cooled to room temperature. A sample of the reaction mixture was analysed by GC-FID and yield was determined using *n*-hexadecane as an internal standard. Product isolation was achieved via flash column chromatography (RediSep[®] Rf+ automatic column) using a suitable mixture of heptane/ethyl acetate determined by TLC. Solvent was removed in vacuo to yield the desired product.

A.5 SYNTHETIC PROCEDURES USED IN SECTION 5.4

A.5.1 *Synthesis of the Ni-Phen@TiO₂-800 Catalyst*

A 250 mL oven-dried single-necked round-bottom flask equipped with an Allihn reflux condenser and a teflon-coated, egg shaped magnetic stir bar (40 × 18 mm) was charged with Ni(OAc)₂ · 4H₂O (373.3 mg, 1.5 mmol, 1.0 equiv), 1,10-phenanthroline monohydrate (594 mg, 3.0 mmol, 2.0 equiv) and dissolved in ethanol (60 mL). After stirring for 5 min at 25°C, the flask was immersed in a preheated oil bath and heated at 60°C for 2 h. To the reaction mixture, TiO₂ (2.10 g) was added via a glass funnel and the resulting heterogeneous mixture was stirred at 750 rpm for 2 h at 60°C. Next, the flask was taken out from the bath and cooled to ambient temperature. The solvent was then removed *in vacuo* (ca. 180 mbar, T_{bath}=40°C, 200 rpm) before being completely dried under oil pump vacuum (ca. 1.0 mmHg, ca. 22°C) for 14 h to yield a light blue–green solid. Using a mortar and pestle, the sample was ground to a very fine powder and then transferred to a ceramic crucible (height – 20 mm, top Ø – 40 mm) and placed in an oven. The latter was evacuated to ca. 5 mbar and then flushed with argon three times. The furnace was heated to 800°C at a rate of 25°C min⁻¹ and held at 800°C for 2 h under an atmosphere of argon.* After the heating was switched off, the oven was allowed to reach room temperature. The Ni-phen@TiO₂-800 catalyst was obtained as a dark blue–black powder.

*Argon was constantly passed through the oven during the whole pyrolysis process.

Elemental analysis: 3.23% Ni, 1.56% N, 12.70% C.

A.5.1.1 *General Procedure K (GP-K)–Design of Experiments*

An 8 mL glass vial (Ø – 14 mm, height 50 mm) equipped with a Teflon-coated oval magnetic stirring bar (8 × 5 mm) was charged with Ni-Phen@TiO₂-800 (10–40 mg) before the vessel was sealed a plastic screw capbearing a silicone septum. The septum was then punctured with a 26-gauge syringe needle (0.45 × 12 mm). 1-Bromonaphthalene (70 µL, 0.5 mmol) and triethylamine (35–140 µL, 0.25–2.0 mmol, 0.5–2.0 equiv) were then added via a microsyringe. Deionised water (1 mL) and methanol (1 mL) were then added before the vial was placed into a small aluminium plate and then transferred into a 300 mL steel autoclave (Parr[®] Instrument

Company). Once sealed, the autoclave was placed into a large aluminium heating block and purged three times with hydrogen (at 5–10 bar). Next, the autoclave was pressurised with hydrogen (10–30 bar) and heated (30–60°C) with thorough stirring (700 rpm). After 18 h, the autoclave was removed from the large aluminium block and cooled to room temperature in a water bath. The remaining hydrogen was then discharged and the vials containing reaction products were removed from the autoclave. Hexadecane (100 µL, internal standard) was then added to the crude reaction mixture, followed by the addition of ethyl acetate (6 mL). The resulting mixture was then stirred intensively for a minute and then the solid catalyst was separated by centrifugation and the supernatant was analysed by GC-FID to quantify the yield of naphthalene.

BIBLIOGRAPHY

- (1) Greenberg, A., *From Alchemy to Chemistry in Picture and Story*; John Wiley & Sons, Inc.: Hoboken, 2007, p 10.
- (2) Anastas, P. T.; Warner, J. C., *Green Chemistry: Theory and Practice*; Oxford University Press: Oxford, 1998.
- (3) Vogel, A.; May, O., *Industrial Enzyme Applications*; Wiley-VCH Verlag GmbH & Co. KGaA: Weinheim, 2019.
- (4) McGovern, P. E.; Zhang, J.; Tang, J., et al. *Proc. Natl. Acad. Sci. U.S.A.* **2004**, *101*, 17593–17598.
- (5) Samuel, D. *Science* **1996**, *273*, 488–490.
- (6) Possehl, G. L., *Oxford Companion to Archaeology*; Oxford University Press: Oxford, 1996.
- (7) Beller, M.; Renken, A.; van Santen, R., *Catalysis: From Principles to Applications*; Wiley-VCH Verlag GmbH & Co. KGaA: Weinheim, 2012.
- (8) Honkala, K.; Hellman, A.; Remediakis, I. N.; Logadottir, A.; Carlsson, A.; Dahl, S.; Christensen, C. H.; Nørskov, J. K. *Science* **2005**, *307*, 555–558.
- (9) Erisman, J. W.; Sutton, M. A.; Galloway, J.; Klimont, Z.; Winiwarter, W. *Nat. Geosci.* **2008**, *1*, 636–639.
- (10) Smil, V. *Nature* **1999**, *400*, 415.
- (11) Nowlin, T. E.; Mink, R. I.; Kissin, Y. V., *Handbook of Transition Metal Polymerization Catalysts*; John Wiley & Sons, Inc.: Hoboken, 2010, pp 131–155.
- (12) The Nobel Prize in Chemistry 2010, <https://www.nobelprize.org/prizes/chemistry/2010/summary/>, Accessed April 2020.
- (13) IUPAC Compendium of Chemical Terminology, <https://goldbook.iupac.org>, Accessed April 2021.
- (14) Hapke, M.; Hilt, G., *Cobalt Catalysis in Organic Synthesis*; Wiley-VCH Verlag GmbH & Co. KGaA: Weinheim, 2020.
- (15) Qiao, B.; Wang, A.; Yang, X.; Allard, L. F.; Jiang, Z.; Cui, Y.; Liu, J.; Li, J.; Zhang, T. *Nat. Chem.* **2011**, *3*, 634–641.
- (16) Wang, A.; Li, J.; Zhang, T. *Nat. Rev. Chem.* **2018**, *2*, 65–81.
- (17) Mitchell, S.; Pérez-Ramírez, J. *Nat. Commun.* **2020**, *11*, 4302.
- (18) Shang, Y.; Xu, X.; Gao, B.; Wang, S.; Duan, X. *Chem. Soc. Rev.* **2021**, *50*, 5281–5322.
- (19) Liu, J. *Curr. Opin. Green Sustain. Chem.* **2020**, *22*, 54–64.

- (20) Cheng, N.; Zhang, L.; Doyle-Davis, K.; Sun, X. *Electrochem. Energy R.* **2019**, *2*, 539–573.
- (21) Liang, S.; Hao, C.; Shi, Y. *ChemCatChem* **2015**, *7*, 2559–2567.
- (22) Bornscheuer, U. T.; Huisman, G. W.; Kazlauskas, R. J.; Lutz, S.; Moore, J. C.; Robins, K. *Nature* **2012**, *485*, 185–194.
- (23) Yi, D.; Bayer, T.; Badenhorst, C. P. S.; Wu, S.; Boerr, M.; Höhne, M.; Bornscheuer, U. T. *Chem. Soc. Rev.* **2021**, *50*, 8003–8049.
- (24) Rosenthaler, L. *Biochem. Z.* **1908**, *14*, 238–253.
- (25) Savile, C. K. et al. *Science* **2010**, *329*, 305–309.
- (26) Flemming, C. A.; Trevors, J. T. *Water Air Soil Pollut.* **1989**, *44*, 143–158.
- (27) Tishchenko, K. I.; Beloglazkina, E. K.; Mazhunga, A. G.; Zyk, N. V. *Rev. J. Chem.* **2016**, *6*, 49–82.
- (28) Costa, L. G.; Aschner, M., *Manganese in Health and Disease*; The Royal Society of Chemistry: Cambridge, 2014.
- (29) Kemmitt, R. D. W., *The Chemistry of Manganese, Technetium and Rhenium*; Pergamon Press: Oxford, 1973.
- (30) Banci, L., *Metallomics and the Cell*; Springer: Dordrecht, 2012, pp 169–201.
- (31) Williams, M.; Todd, G. D.; Roney, G. D.; Crawford, J.; Coles, C.; McClure, P. R.; Garey, J. D.; Zaccaria, K.; Citra, M., *Toxicological Profile for Manganese*; U.S. Agency for Toxic Substances and Disease Registry: Atlanta, 2012.
- (32) Trumbo, P.; Yates, A. A.; Schlicker, S.; Poos, M. J. *Am. Diet. Assoc.* **2001**, *3*, 294–301.
- (33) Nicholls, D., *The Chemistry of Iron, Cobalt and Nickel*; Pergamon Press: Exeter, 1973.
- (34) Fürstner, A. *ACS Cent. Sci.* **2016**, *2*, 778–789.
- (35) Wilkinson, G.; Rosenblum, M.; Whiting, M. C.; Woodward, R. B. *J. Am. Chem. Soc.* **1952**, *74*, 2125–2126.
- (36) Woodward, R. B.; Rosenblum, M.; Whiting, M. C. *J. Am. Chem. Soc.* **1952**, *74*, 3458–3459.
- (37) Fischer, E. O.; Pfab, W. Z. *Naturforsch.* **1952**, *7B*, 377–379.
- (38) Crundwell, F. K.; Moats, M. S.; Ramachandran, V.; Robinson, T. G.; Davenport, W. G., *Extractive Metallurgy of Nickel, Cobalt and Platinum-Group Metals*; Elsevier Ltd.: Oxford, 2011.
- (39) Baumann-Pauly, D., *Making Mining Safe and Fair: Artisanal cobalt extraction in the Democratic Republic of the Congo [White paper]*; World Economic Forum: Geneva, 2020.
- (40) Bennett, B.; Holz, R. C. *J. Am. Chem. Soc.* **1997**, *119*, 1923–1933.
- (41) Wang, J.; Cui, W.; Liu, Q.; Xing, Z.; Asiri, A. M.; Sun, X. *Adv. Mater.* **2016**, *28*, 215–230.
- (42) Gao, S.; Lin, Y.; Jiao, X.; Sun, Y.; Luo, Q.; Zhang, W.; Li, D.; Yang, J.; Xie, Y. *Nature* **2016**, *529*, 68–71.

- (43) Gavriilidis, A.; Constantinou, A.; Hellgardt, K.; Hii, K. K. M.; Hutchings, G. J.; Brett, G. L.; Kuhn, S.; Marsden, S. P. *React. Chem. Eng.* **2016**, *1*, 595–612.
- (44) Osterberg, P. M.; Niemeier, J. K.; Welch, C. J.; Hawkins, J. M.; Martinelli, J. R.; Johnson, T. E.; Root, T. W.; Stahl, S. S. *Org. Process Res. Dev.* **2015**, *19*, 1537–1543.
- (45) Lewis, B.; von Elbe, G., *Combustion, Flames and Explosions of Gases*, 3rd ed.; Academic Press: New York, 1987, p 339.
- (46) Brooks, M. R.; Crawl, D. A. *J. Loss. Prev. Process Ind.* **2007**, *20*, 144–150.
- (47) Zabetakis, M. G., *Flammability Characteristics of Combustible Gases and Vapors*; U.S. Department of the Interior, Bureau of Mines: Washington, 1965.
- (48) Tomás, R. A.; Bordado, J. C.; Gomes, J. F. *Chem. Rev.* **2013**, *113*, 7421–7469.
- (49) Brill, W. *Ind. Eng. Chem.* **1960**, *52*, 837–840.
- (50) Murai, M.; Kakiuchi, F.; Sekine, S.; Tanaka, Y.; Kamatani, A.; Sonoda, M.; Chatani, N. *Nature* **1993**, *366*, 13759–13769.
- (51) Crabtree, R. H.; Lei, A. *Chem. Rev.* **2017**, *117*, 8481–8482.
- (52) Labinger, J. A. *Chem. Rev.* **2017**, *117*, 8483–8496.
- (53) Roque, J. B.; Kuroda, Y.; Göttemann, L. T.; Sarpong, R. *Science* **2018**, *361*, 171–174.
- (54) Sattler, A.; Parkin, P. *Nature* **2010**, *463*, 523–526.
- (55) Crabtree, R. H., *The Organometallic Chemistry of the Transition Metals*, 7th; John Wiley & Sons, Inc.: Hoboken, 2019.
- (56) Murakami, M.; Ishida, N. *J. Am. Chem. Soc.* **2016**, *42*, 13759–13769.
- (57) Saliu, F.; Orlandi, M.; Bruschi, M. *ISRN Org. Chem.* **2012**, *2012*, 1–5.
- (58) Suarez-Bertoa, R.; Saliu, F.; Bruschi, M.; Rindone, B. *Tetrahedron* **2012**, *68*, 8267–8275.
- (59) Binder, C. M.; Dixon, D. D.; Almaraz, E.; Tius, M. A.; Singaram, B. *Tetrahedron Lett.* **2008**, *48*, 2764–2767.
- (60) Criegee, R. *Berichte der Dtsch. Chem. Gesellschaft* **1931**, *64*, 260–266.
- (61) Melro, E.; Filipe, A.; Sousa, D.; Medronho, B.; Romano, A. *New J. Chem.* **2021**, *45*, 6986–7013.
- (62) Ganewatta, M. S.; Lokupitiya, H. N.; Tang, C. *Polymers* **2019**, *11*, 1176.
- (63) Malaprade, L. *Bull. Soc. Chim. Fr.* **1934**, *3*, 833.
- (64) Zhou, W.; Fan, W.; Jiang, Q.; Liang, Y.-F.; Jiao, N. *Org. Lett.* **2015**, *17*, 2542–2545.
- (65) Qin, C.; Su, Y.; Shen, T.; Shi, X.; Jiao, N. *Angew. Chem., Int. Ed.* **2016**, *55*, 350–354.
- (66) Liu, J.; Wen, X.; Qin, C.; Li, X.; Luo, X.; Sun, A.; Zhu, B.; Song, S.; Jiao, N. *Angew. Chem., Int. Ed.* **2017**, *56*, 11940–11944.
- (67) Liang, Y.-F.; Jiao, N. *Acc. Chem. Res.* **2017**, *50*, 1640–1653.

- (68) Zhao, B.; Tan, H.; Chen, C.; Jiao, N.; Shi, Z. *Chin. J. Chem.* **2018**, *36*, 995–999.
- (69) Liu, J. et al. *Nat. Chem.* **2019**, *11*, 71–77.
- (70) Adeli, Y.; Huang, K.; Liang, Y.; Jiang, Y.; Liu, J.; Song, S.; Zheng, C.-C.; Jiao, N. *ACS Catal.* **2019**, *9*, 2063–2067.
- (71) Tsang, A. S.-K.; Kapat, A.; Schoenebeck, F. J. *Am. Chem. Soc.* **2016**, *138*, 518–526.
- (72) Dalvi, V. H.; Rosicky, P. J. *PNAS* **2010**, *107*, 13603–13607.
- (73) Morimoto, Y.; Bunno, S.; Fujieda, N.; Sugimoto, H.; Itoh, S. *J. Am. Chem. Soc.* **2015**, *137*, 5867–5870.
- (74) Zhu, F.; Johnson, J. A.; Ablin, D. W.; Ernst, G. A., *Efficient Petrochemical Processes: Technology, Design and Operation*, 1st ed.; John Wiley & Sons, Inc.: Hoboken, 2019, pp 21–22.
- (75) Yan, J.; Meng, Q.; Shen, X.; Chen, B.; Sun, Y.; Xiang, J.; Liu, H.; Han, B. *Sci. Adv.* **2020**, *6*, eabd1951.
- (76) Wang, Y.; Wang, N.; Zhao, J.; Sun, M.; You, H.; Fang, F.; Liu, Z.-Q. *ACS Catal.* **2020**, *10*, 6603–6612.
- (77) Zhao, J.; Shen, T.; Sun, Z.; Wang, N.; Yang, L.; Wu, J.; You, H.; Liu, Z.-Q. *Org. Lett.* **2021**, *23*, 4057–4061.
- (78) Zhou, J.; Wang, S.; Duan, W.; Lian, Q.; Wei, W. *Green Chem.* **2021**, *23*, 3261–3267.
- (79) Li, W.; Liu, W.; Leonard, D. K.; Rabeah, J.; Brückner, A.; Junge, K.; Beller, M. *Angew. Chem., Int. Ed.* **2019**, *58*, 10693–10697.
- (80) Leonard, D. K.; Li, W.; Junge, K.; Beller, M. *ACS Catal.* **2019**, *9*, 11125–11129.
- (81) Weissman, S. A.; Anderson, N. G. *Org. Process Res. Dev.* **2015**, *19*, 1605–1633.
- (82) Lendrem, D.; Owen, M.; Godbert, S. *Org. Process Res. Dev.* **2001**, *5*, 324–327.
- (83) Anastas, P.; Eghbali, N. *Chem. Soc. Rev.* **2010**, *39*, 301–312.
- (84) Taber, G. P.; Pfisterer, D. M.; Colberg, J. C. *Org. Process Res. Dev.* **2004**, *8*, 385–388.
- (85) Laird, T. *Org. Process Res. Dev.* **2002**, *6*, 337.
- (86) Stahl, S. S. *Science* **2005**, *309*, 1824–1826.
- (87) Eppedgui, J.; Neumann, R. *J. Am. Chem. Soc.* **2009**, *131*, 4–5.
- (88) Harris, C. E.; Chrisman, W.; Bickford, S. A.; Lee, L. Y.; Torreblanca, A. E.; Singaram, B. *Tetrahedron Lett.* **1997**, *38*, 981–984.
- (89) Sahoo, B.; Surkus, A.-E.; Pohl, M.-M.; Radnik, J.; Schneider, M.; Bachmann, S.; Scalone, M.; Junge, K.; Beller, M. *Angew. Chem., Int. Ed.* **2017**, *129*, 11394–11399.
- (90) Formenti, D.; Ferretti, F.; Topf, C.; Surkus, A.-E.; Pohl, M.-M.; Radnik, J.; Schneider, M.; Junge, K.; Beller, M.; Ragaini, F. *J. Catal.* **2017**, *351*, 79–89.
- (91) Ma, D.; Cai, Q.; Zhang, H. *Org. Lett.* **2003**, *5*, 2453–2455.